FORCED CONVECTION FILM BOILING OF SUBCOOLED WATER AROUND A SPHERE

Thesis by

Richard Norman Jacobson

In Partial Fulfillment of the Requirements

For the Degree of

Doctor of Philosphy

California Institute of Technology

Pasadena, California

1970

(Submitted May 11, 1970)

ACKNOWLEDGMENTS

I wish to express my appreciation to my research advisor, Dr. F. H. Shair, for the assistance, encouragement, and guidance which he gave me during the course of this investigation.

In addition, I would like to thank George Griffith and his staff for the many hours they spent helping design, construct, and maintain the experimental apparatus. I would like to thank Margo Jenner and her staff for the secretarial assistance given me during my years at Caltech. I also would like to thank Christopher England and J. Edwin Blakemore for their advice and suggestions concerning gas chromatography.

I would like to express my gratitude to the following for my personal financial support during my study at Caltech: John Stauffer, California Institute of Technology, National Science Foundation, State of California, and Standard Oil of California.

Finally, I owe much to my wife, Elaine, for her help and encouragement, and especially, for the help she gave me editing and typing this thesis.

ABSTRACT

An experimental investigation was made of forced convection film boiling of subcooled water around a sphere at atmospheric pressure. The water was sufficiently cool that the vapor condensed before leaving the film with the result that no vapor bubbles left the film. The experimental runs were made using inductively heated spheres at temperatures above 740°C. and using inlet water temperatures between 15°C. and 27°C. The spheres used had diameters of 1/2 inch, 9/16 inch, and 3/8 inch and were supported by the liquid flow. Reynolds numbers between 60 and 700 were used.

Analysis of the collected non-condensables indicated that oxygen and nitrogen dissolved in the water accumulated within the vapor film and that hetrogeneous chemical reactions occurred at the sphere surface. An iron-steam reaction resulted in more than 20% by volume hydrogen in the film at wall temperatures above 900°C. At temperatures near 1100°C. more than 80% by volume of the film was composed of hydrogen. It was found that gold plating of the sphere could eliminate this reaction.

Material and energy balances were used to derive equations which may be used to predict the overall average heat transfer coefficients

for subcooled film boiling around a sphere. These equations include the effect of dissolved gases in the water. Equations also were derived which may be used to predict the composition of the film for cases in which an equilibrium exists between the dissolved gases and the gases in the film.

The derived equations were compared to the experimental results. It was found that a correlation existed between the Nusselt number for heat transfer from the vapor-liquid interface into the liquid and the Reynolds number, liquid Prandtl number product. In addition, it was found that the percentage of dissolved oxygen removed during the film boiling could be predicted to within 10%.

TABLE OF CONTENTS

LIST OF FIGURES

LIST OF TABLES

INTRODUCTION

Boiling is the rapid vaporization of a liquid which occurs when a liquid is heated to a temperature such that its vapor pressure is above that of the surroundings. Boiling, however, occurs in three characteristic forms which are nucleate, transition, and film boiling. Figure 1 is an illustration of the location of the three regimes (67).

Nucleate boiling is the most common type of boiling and it is represented by the region A - B of Figure 1. It is characterized by bubbles which rise from discrete points on a surface whose temperature is only slightly above the liquid's saturation temperature. The nucleate boiling regime has been described as consisting of four subregions (25). The first of these is the discrete bubble region in which the vapor rises in distinct bubbles. The second is a region in which the bubbles leave the nucleation site rapidly enough to join vertically into vapor columns. The third is a region in which the vapor columns become numerous enough to join horizontally into vapor mushrooms. The last subregion is characterized by small vapor patches beginning to appear on the heated surface.

In general, the number of nucleation sites are increased by an increasing surface temperature. When the surface temperature reaches a maximum value, the critical superheat, vapor begins to

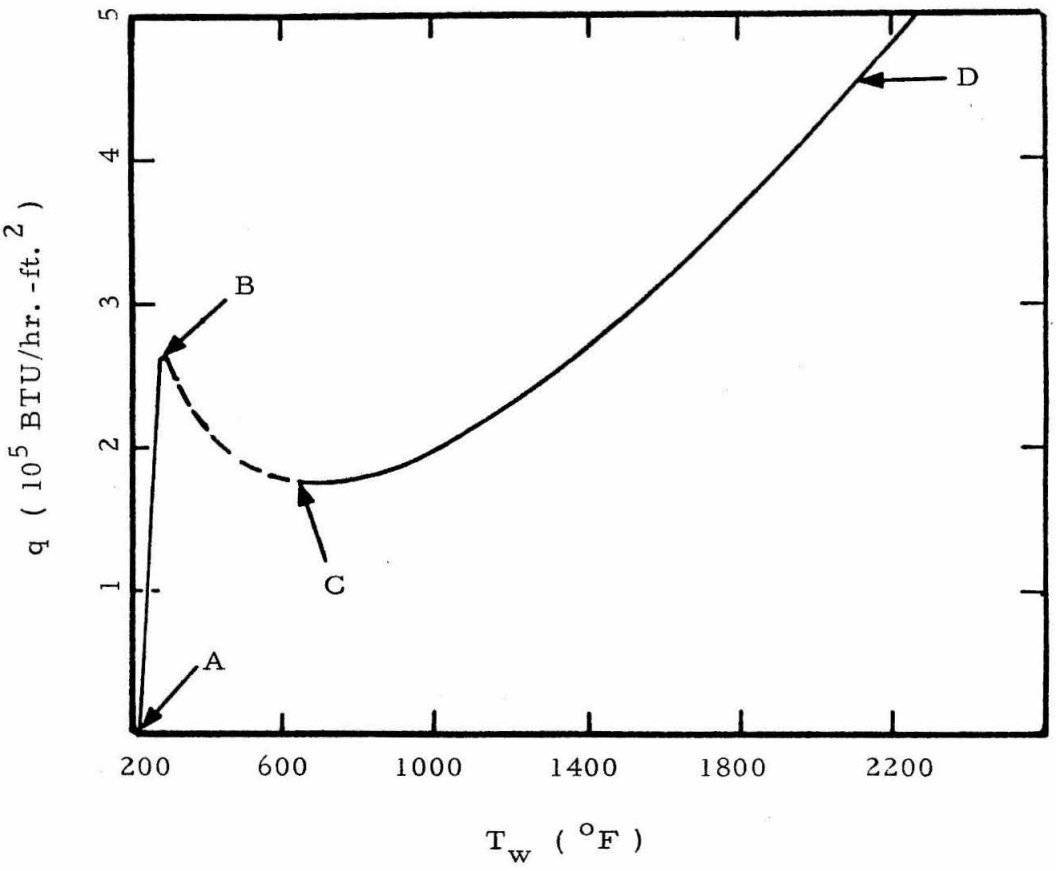

Figure 1. --The first boiling curve which was obtained by Nukiyama in 1934 (67).

form at a more rapid rate than the rate at which the liquid can reach the surface. Thus, the heated surface suddenly becomes covered with a vapor layer. Because of its lower thermal conductivity, this vapor layer insulates the surface. This condition of a vapor film insulating the surface from the liquid characterizes film boiling which is represented by region C - D in Figure 1.

Region B - C in Figure 1 is the transition region. Transition boiling may be defined as the unstable boiling which occurs at surface temperatures between the maximum attainable in nucleate boiling and the minimum attainable in film boiling. A characteristic of this regime is that an increase in temperature difference between the heated surface and the liquid results in a decrease in heat flux.

Since nucleate boiling occurs in most applications, it has been studied in great detail. However, since the bubbles randomly leave the surface, nucleate boiling is by nature complex and may not be described by simple analytical expressions. Experimental research has shown that the surface characteristics are extremely important in nucleate boiling. Because of this, analytical investigations have been primarily concerned with the dynamics of single bubbles in the vicinity of nucleation sites (65).

In contrast, extremely little experimental work has been done on transition boiling, because it cannot be maintained on an electrically

or combustion heated surface. No practical applications have been found for transition boiling.

Film boiling was first described by Leidenfrost in 1756 (44). However, it was not until 1934 that Nukiyama (67) described the three regimes of boiling as shown in Figure 1. The first analytical investigation of film boiling was published by Bromley in 1950 (9). Since that time, many experimental and analytical investigations of film boiling have been made.

In contrast to nucleate boiling, the surface characteristics have been found to have little effect on film boiling. The analytical investigations of film boiling have been based on heat transfer through a continuous vapor film. A comprehensive survey of the analytical and experimental investigations of film boiling has been made and is presented in Appendix A.

The previous studies of film boiling have not considered the effect of dissolved gases and the effect of heterogeneous chemical reactions on the solid surface.

Film boiling may be accompanied by deaeration and chemical reactions. During film boiling of a liquid containing small amounts of a dissolved gas, the dissolved gas will diffuse into the vapor film. Thus, the film boiling of water containing small amounts of dissolved air will result in a partial deaeration of the water. A common

commercial method of deaeration of water involves exposing the water to steam and permitting the air to diffuse into the steam until an equilibrium is established (38). A similar situation will occur during the film boiling of aerated water. The vapor film will contain a much higher percentage of oxygen and nitrogen than the liquid originally contained.

If the material being film boiled decomposes at the temperature of the hot wall, thermal cracking may occur. Since the liquid is vaporized rapidly and remains in the vapor briefly, a condition of rapid heating and quenching results (9). If the vapor film is rich in air from a deaeration of the liquid, the oxygen present may result in a partial oxidation of the vapor. In other words, if small quantities of oxygen are present in the liquid, sufficiently large quantities may be present in the vapor film to cause partial oxidation to occur in addition to the thermal cracking.

A second type of chemical reaction is possible. If the solid surface on which the film boiling takes place reacts chemically with the gases in the film, a heterogeneous reaction may occur on the surface (53). Reactions of this type possibly may be used for catalytic reactions in which rapid quenching occurs.

Since there has been no previous investigation of the effects of gases dissolved in the liquid being boiled and since there has been

no previous investigation of the effect of a heterogeneous chemical reaction on the solid surface, these problems were chosen for an investigation of film boiling. It was anticipated that these effects should greatly influence the rate of heat transfer during film boiling.

The decision was made to use subcooled film boiling around a sphere because by using sufficient subcooling the vapor could be made to condense as it left the film. This would greatly facilitate the measurement of heat transfer rates. In addition, the sphere could be supported by the liquid flow and could be heated inductively. Since, in this case, no solid object would touch the sphere, a constant surface temperature should be maintained.

A previous investigation of subcooled film boiling on a sphere was made by Witte et al. (70) (71). However, they preheated the spheres prior to the film boiling, and consequently, the spheres did not have a constant surface temperature. In one of their typical experimental runs, the sphere surface temperature dropped from 1400°C to 800°C. in 0.15 seconds.

It was decided to study the film boiling of water for the following four reasons. First, the concentration of dissolved gases could be determined easily. Secondly, water is widely used for electrical power generation. Thirdly, water is used in nuclear reactors. Lastly,

when stainless steel spheres were used, the water could be expected to react heterogeneously with the sphere surface. Thus, the film boiling of subcooled water around a sphere should serve perfectly to investigate the effects of dissolved gases and heterogeneous reactions on heat transfer.

CHAPTER I

DESCRIPTION OF APPARATUS

Taylor (45) (64) noted that when a denser fluid is positioned above a lighter fluid, the interface will be unstable. As a result of this instability, bubbles of a less dense fluid will rise into a more dense fluid; the instability is commonly called the Rayleigh-Taylor instability (29). The film boiling of a saturated liquid around a sphere demonstrates this phenomena. Frederking and Daniels (22) considered the Rayleigh-Taylor instability while examining the film boiling of a saturated liquid around a sphere and noted that the frequency at which the bubbles leave the film is inversely proportional to the square root of the diameter of the bubbles. Hendricks and Baumeister (30) noted that as a result of the Rayleigh-Taylor instability, bubbles leave the film from either a single dome on a small sphere or from several domes on larger spheres.

However, if the liquid is subcooled below its boiling point and is forced to flow upward past the sphere, the bubbles can be made to condense as they are about to leave the interface, as reported by Jacobson and Shair (35). Thus, the cool liquid tends to stabilize the interface with respect to the Rayleigh-Taylor instability. As a result, no net formation of vapor occurs in the vapor film.

Figure 2 illustrates the apparatus used to achieve these conditions experimentally. The sphere was supported by the upward flow of the liquid through the funnel shaped tube.

An additional advantage of using conditions under which no net formation of vapor occurs was that the downstream liquid flow consisted of only one phase. Thus, the rate of heat transfer from the sphere to the liquid was determined by measuring the downstream and the upstream temperatures and the liquid flow rate. The temperature of the sphere was measured optically with the result that no contact existed between the sphere and any other solid object. Therefore, the sphere surface possessed a uniform temperature over the entire surface.

Non-condensables may enter the vapor film in any of three ways: (1) gases dissolved in the liquid may diffuse into the vapor film, (2) the vapor itself may be thermally decomposed, and (3) the vapor may react with the solid surface. As the vapor condensed in the upper region of the vapor film, these non-condensables present were not absorbed into the liquid phase in the short period required for the condensation of the vapor. The non-condensables then appeared as small bubbles in the downstream liquid flow.

The apparatus constructed for the experimental investigation of the preceeding phenomena consisted of a constant head tank to force

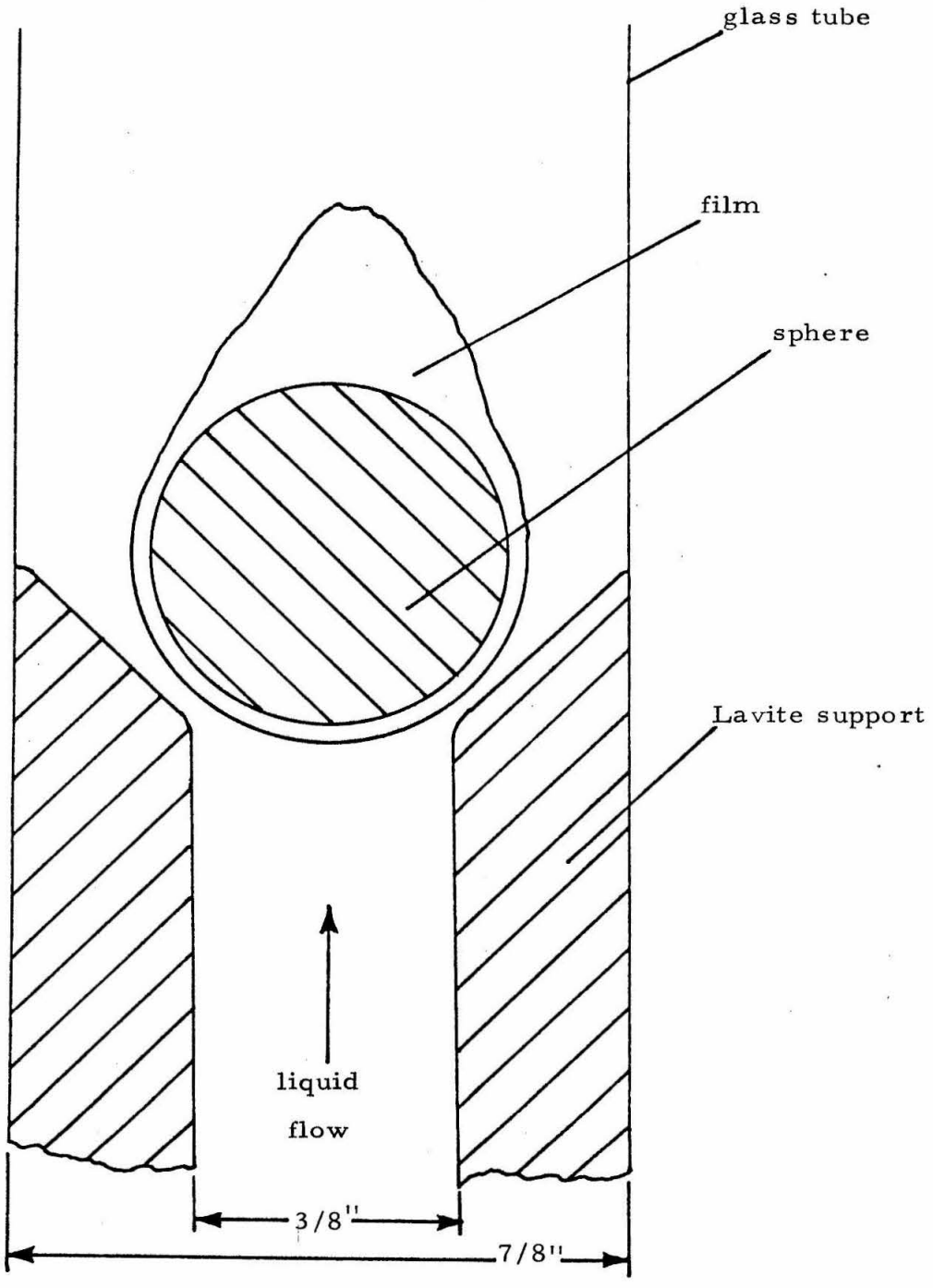

Figure 2. --Geometry used in experimental investigation.

liquid through the test section, a test section to contain the sphere, an induction heating unit to heat the sphere, a temperature recorder and an optical pyrometer to measure temperatures, a gas chromatograph to determine the composition of the non-condensables, and an oxygen analyzer to determine the dissolved oxygen concentration. Table 1 lists in detail the basic components used to construct this apparatus which is shown in Figure 3.

Reservoir and Constant Head Tank

To maintain a constant liquid pressure into the test section, a constant head tank was used, as shown in Figure 4. The liquid to be boiled was stored in a reservoir which consisted of a three liter flask from which the liquid was continuously pumped through the constant head tank. The constant head tank was constructed from a 500 milliliter boiling flask and was located to maintain a liquid head of 5.5 feet. Pressure oscillations introduced by the pump were not of sufficient magnitude to cause variations in the flow through the test section. The various components were connected by 0.5 inch O.D. Tygon tubing.

The constant temperature bath used to heat or cool the reservoir was not temperature controlled, but was of sufficient size to remain within one Centigrade degree during an experimental run. In general,

TABLE 1

DESCRIPTION OF EQUIPMENT USED

Equipment	Model	Manufacturer
Pump	Model D - 6 (motor model 9404)	Eastern Industries Hamden, Conn.
Heat exchanger	Two concentric tube glass condensers	---
Rotameter	Precision bore flowrator. Tube number 2-F 1/4 - 20 - S/70 Bead float	Fischer and Porter Co. Warminster, Pa.
Steel sphere	Type 440 stainless steel ball bearing	---
Gold sphere	Steel sphere plated with 0.0003 - 0.0005 inch of nickel and 0.00010 inch of gold	Anchor Plating Co. South El Monte, Calif.
Induction heating unit	Model T-5-3-MC-E-S high frequency induction heating unit with saturable reactor power control and 5 kw. output from 6960 oscillator tube	Lepel High Frequency Laboratories, Inc. 55th St. & 37th St. Woodside, N. Y.
Temperature recorder	Model 7460	Wheelco Instrument Division Barber - Colman Co. Rockford, Ill.

TABLE 1 (Continued)

Equipment	Model	Manufacturer
Optical pyrometer	Pyro micro-optical pyrometer	The Pyrometer Instrument Co. Bergenfield, N. J.
Oxygen analyzer	Fieldlab	Beckman Instruments, Inc. Fullerton, Calif.
Chromatograph	Basic	Carle Instrument, Inc. 1141 East Ash Avenue Fullerton, Calif.
Sample valve	---	Loenco, Inc. Altadena, Calif.
Recorder	Mosely model 681 strip chart	Hewlett Packard 1501 Page Mill Road Palo Alto, Calif.

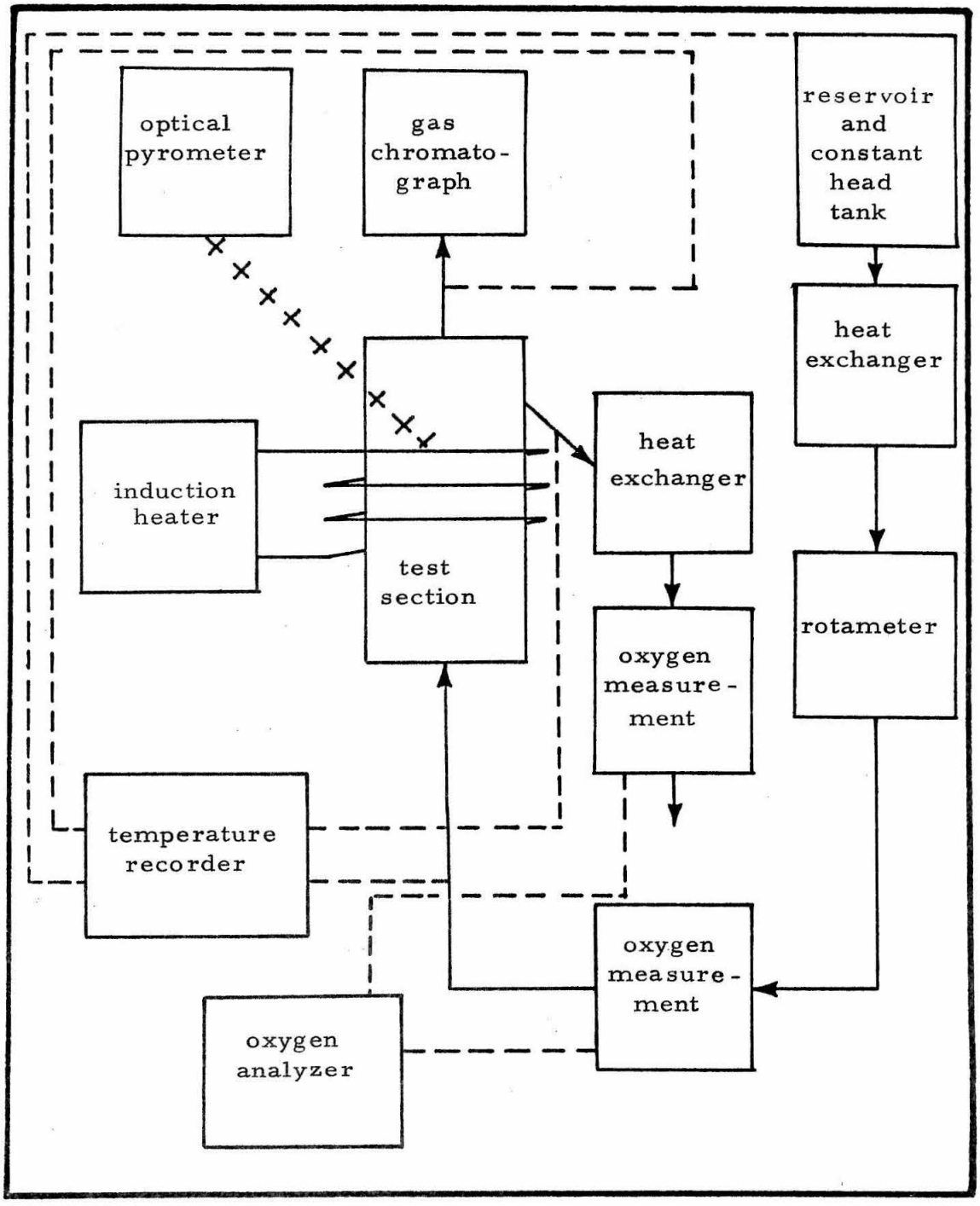

Figure 3. --Components of experimental apparatus.

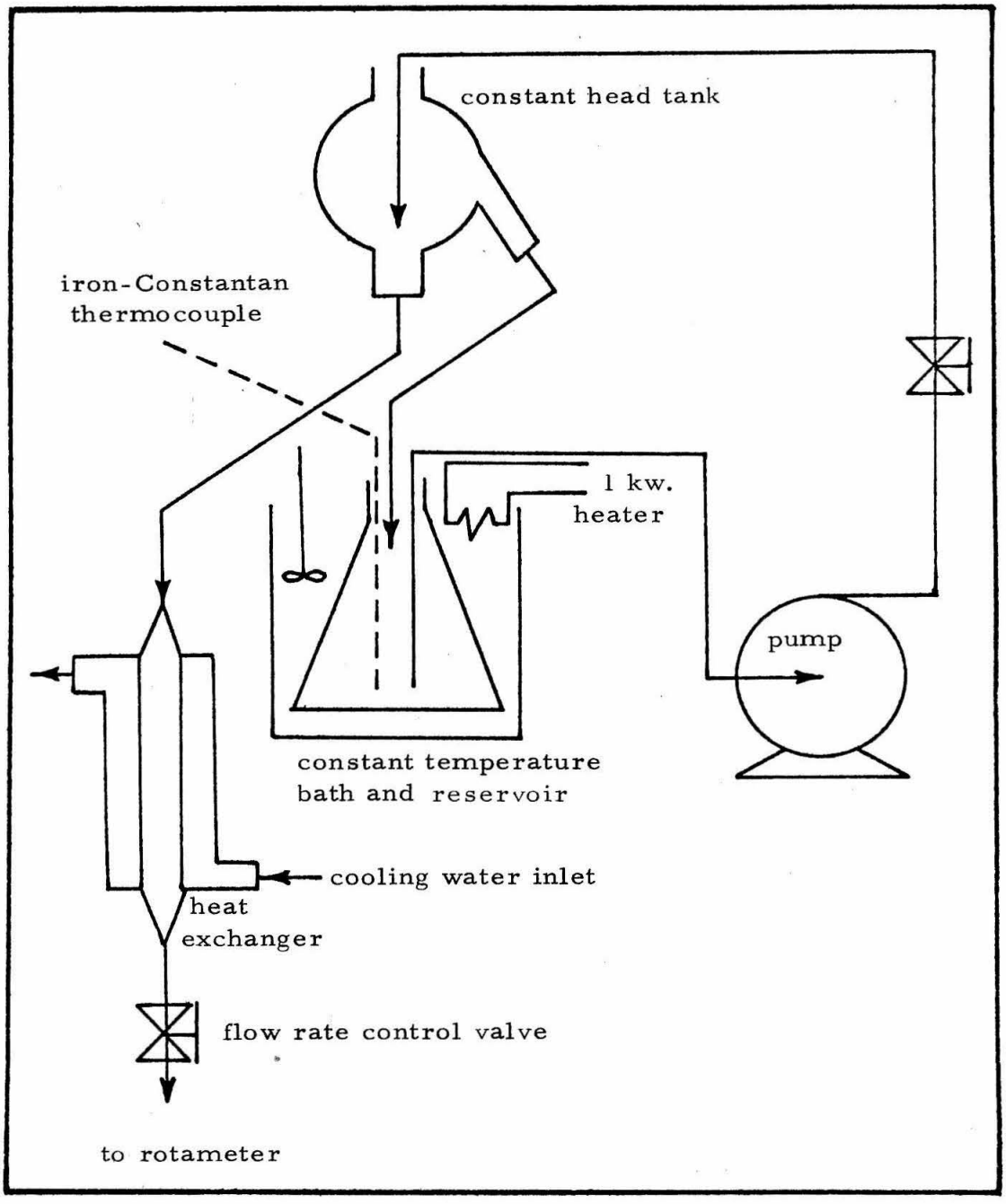

Figure 4. --Diagram of constant head tank and reservoir.

the temperature at the inlet to the test section was not determined by the temperature in the constant temperature bath, but by a heat exchanger on the inlet to the test section. The purpose of the constant temperature was to allow the liquid to reach an equilibrium with the atmosphere. In other words, the dissolved oxygen and nitrogen were at equilibrium with the atmosphere at the temperature in the reservoir. By varying the temperature in the reservoir, the concentrations of the dissolved oxygen and nitrogen in the liquid could be varied.

The concentration of dissolved oxygen was measured analytically because it was not certain that an equilibrium existed in the reservoir. The temperature in the reservoir was measured as a check on the accuracy of the analytical measurement. The constant temperature bath was stirred constantly and was heated by a 0 to 1.0 kilowatt heater. If cooling was desired, ice was added to the constant temperature bath. The temperature in the reservoir was measured with an iron-Constantan thermocouple in a glass well.

The heat exchanger was used to determine the temperature at the inlet of the test section. The water to be boiled flowed through the inner tube and the cooling or heating water flowed through the outer tube of the heat exchanger. A valve was located downstream from the

heat exchanger and was used to vary the flow rate through the test section.

The flow rate of water through the test section was measured by a rotameter. The rotameter was located downstream from the valve used to vary the flow rate. The rotameter had been calibrated by using the constant head tank to pass water through it. The flow had been diverted into a graduated cylinder and timed with a stop watch at various flow rates. Figure 5 is a plot of the rotameter scale reading versus the flow rate in grams per second. It was noted during the calibration of the rotameter with water that the error introduced by varying the temperature of the water was negligible.

Test Section

After leaving the rotameter, the liquid to be boiled flowed into the test section diagramed in Figure 6. The test section consisted of a 7/8 inch I. D. glass tube with a Lavite support for the sphere as shown in Figure 2. Lavite was used to support the sphere because it is an insulator and, therefore, not effected by the induction heater. Lavite has an additional advantage of being insensative to thermal shock which may result from sudden contact between the sphere and the support. The Lavite support was one inch in height and had an internal diameter of 3/8 inch and an external diameter of 7/8 inch.

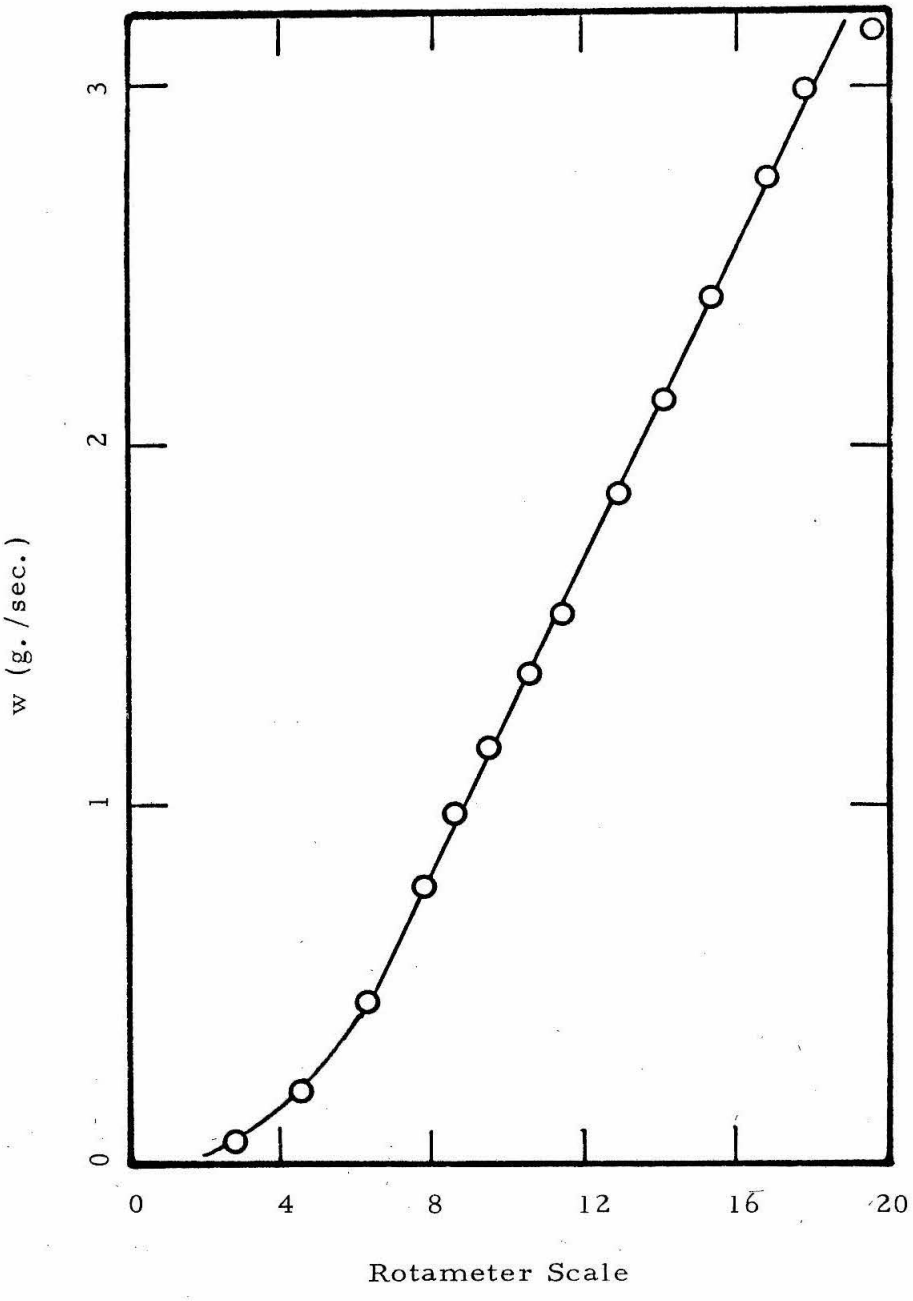

Figure 5.--Rotameter calibration for water at 20°C.

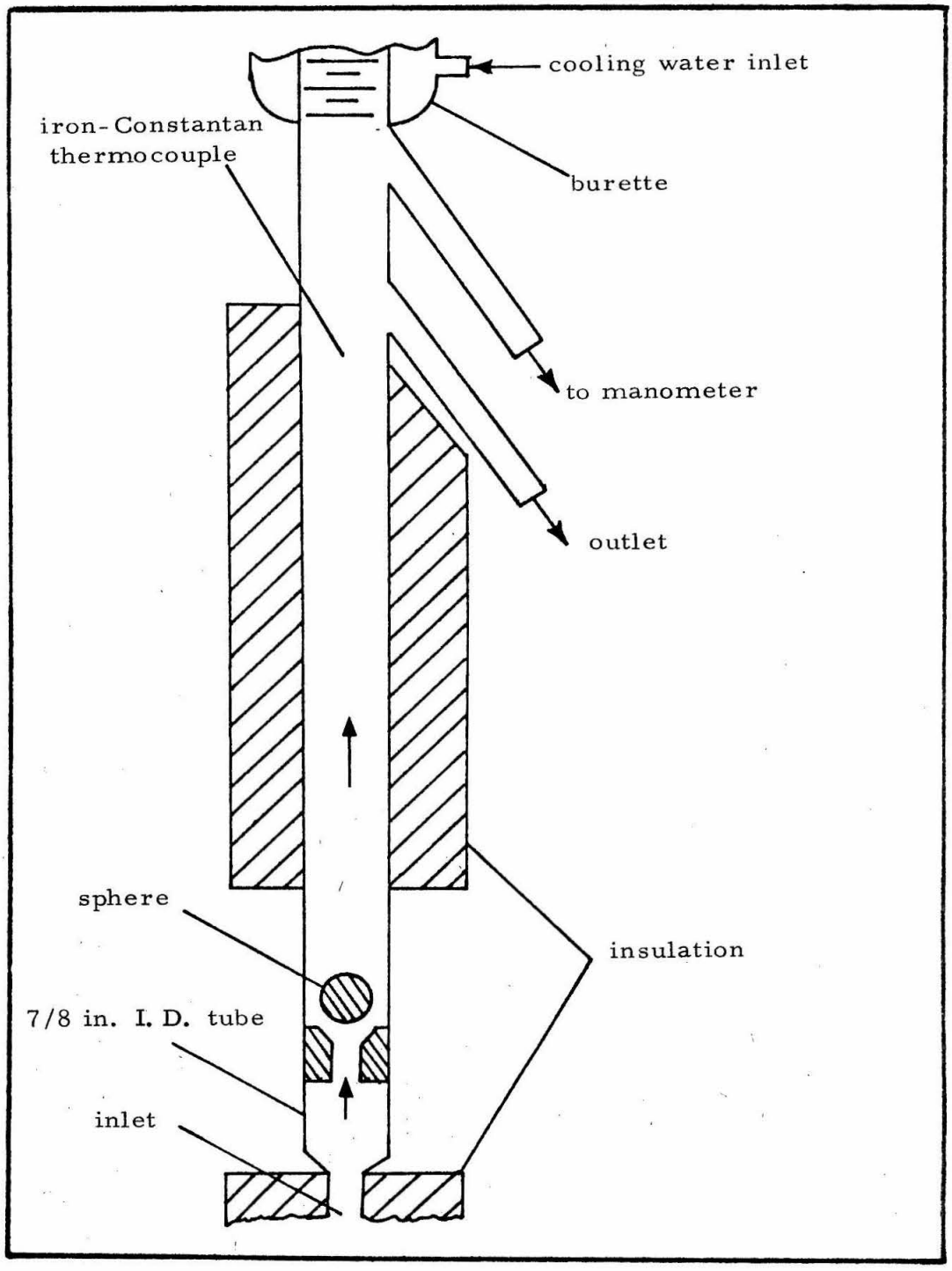

Figure 6. --Diagram of test section.

Above the sphere the liquid flowed through a six inch long equilibrium section before reaching the outlet tube and the downstream thermocouple. The equilibrium section was insulated with Armstrong Armaflex insulation to prevent heat losses to the atmosphere. The entrance section upstream from the sphere also was insulated to prevent heat losses and errors in the measurement of the inlet temperature.

The outlet tube was inclined downward as shown in Figure 6 preventing the non-condensables from being entrained in the outlet stream. The non-condensables were allowed to rise as bubbles into an inverted 50 milliliter burette located above the equilibrium section. At the beginning of an experimental run the burette was filled with water and as the run progressed the burette would fill with non-condensables. These non-condensables later were analyzed with a gas chromatograph to determine their composition. An iron-Constantan thermocouple located in the upper end of the burette was used to measure the temperature of the collected gases. The burette was used to measure the volume of gases collected over a given period of time. The burette was surrounded with a cooling jacket which maintained the collected gases at a constant temperature.

A downward inclined pressure tap was located above the outlet. This pressure tap was connected by a water filled line to a mercury

manometer. The pressure of the collected gases in the burette was determined by measuring the height of the mercury column and the height of the water column.

Heat transfer measurements were made by the previously mentioned upstream and downstream thermocouples. The thermocouples were both iron-Constantan and were painted with Glyptol insulating varnish to prevent corrosion of the junction. They were located far enough from the induction heating coil to prevent inductive heating of the thermocouples. To allow visual observation of the sphere and to allow its temperature measurement by an optical pyrometer, the test section was not insulated near the sphere.

The spheres used in the various experimental runs were ball bearings of several diameters. The bulk of the spheres was type 440 stainless steel which is corrosion resistant and is easily heated inductively. The Handbook of Chemistry and Physics (32) reports that type 440 stainless steel is composed of 0.6% to 0.75% carbon, 16% to 18% chromium, 0.75% molybdenum, less than 0.04% phosphorus, less than 0.03% sulfur, and the remaining portion iron.

Several additional spheres were used consisting of gold plated on a layer of nickel which in turn was plated on stainless steel spheres of the above type. The nickel retarded diffusion of the gold into the stainless steel.

Induction Heating Unit

The sphere was heated inductively with a high frequency induction heating unit which was used with an appropriate coil to operate at frequencies between 2.5 and 5.0 MHz. The manufacturer recommends a load coil of approximately 1.5 μh. when operating in the 2.5 to 5.0 Mhz. range.

The load coil was wound from 3/16 inch O.D. copper tubing. The coil had 5 1/2 turns, had a length of 1 3/8 inches, and had a diameter of 1 7/8 inches. A coil of these dimensions had a calculated inductance of 1.07 μh. The connection of the coil to the induction heating unit was made with two 30 inch lengths of copper tubing spaced one inch apart. The load coil was positioned directly around the sphere being heated.

Temperature Measurement

The temperature at the inlet and outlet of the test section, in the reservoir, and of the collected gas were measured with iron-Constantan thermocouples and a temperature recorder. This recorder was equipped with a meter and a strip chart to measure temperatures over the range of 0-400^{o}F. Because it was more accurate, the meter rather than the strip chart was used. The instrument read six temperatures automatically and switched from one to another every

thirty seconds; in three minutes all six thermocouples were read. In addition to the four thermocouples mentioned above, a fifth thermocouple was used in a water bath with a mercury thermometer to calibrate the recorder. The sixth thermocouple position was not used during the experimental runs. All thermocouples were made from the same spool of thermocouple wire.

The temperature of the surface was measured with an optical pyrometer which measured the brightness of emitted red light. The pyrometer was located 13 inches from the surface of the sphere which was viewed by looking into the induction heating coil at an angle of approximately 45° from horizontal. The optical pyrometer measured the black body temperature. An error in the temperature measurement may have been introduced because of variations in the emissivity of the sphere's surface.

A test was run which indicated that the error introduced by absorbtion of red light by the water was negligible. A type T-24 tungsten strip lamp was viewed directly and through various depths of water. It was found that the error introduced was approximately 4° C. per inch of water. The depth of water through which the sphere was viewed during the experimental runs was less than one inch; therefore, this correction was ignored.

Gas Chromatograph

To determine quantitatively the composition of the gas removed during the film boiling, a gas chromatograph was used. Figure 7 is an illustration of the gas analyzing system. The gas collection burette of the film boiling apparatus was connected by five feet of 1/8 inch O. D. copper tubing to a sampling valve.

At the completion of a test run, the collected gas was forced from the burette by opening the exit stopcock and pressurizing the collected gas. The gas was pressurized by closing the liquid exit from the film boiling apparatus and opening the valve between the constant head tank and the film boiling apparatus. The increased water pressure then pressurized the collected gas and forced it through the stopcock and the copper tube into the sampling valve. This valve then was used to inject a gas sample into an argon carrier. The volume of the gas sample injected during test runs was 0. 525 milliliters.

This sample injected into the carrier by the sampling valve passed through a packed column which separated the sample plug into three plugs of hydrogen, oxygen, and nitrogen. These three plugs then flowed into the chromatograph detector. The column used was maintained at room temperature and the flow rate through it was measured by a bubble-tube flowmeter. The column was constructed by packing

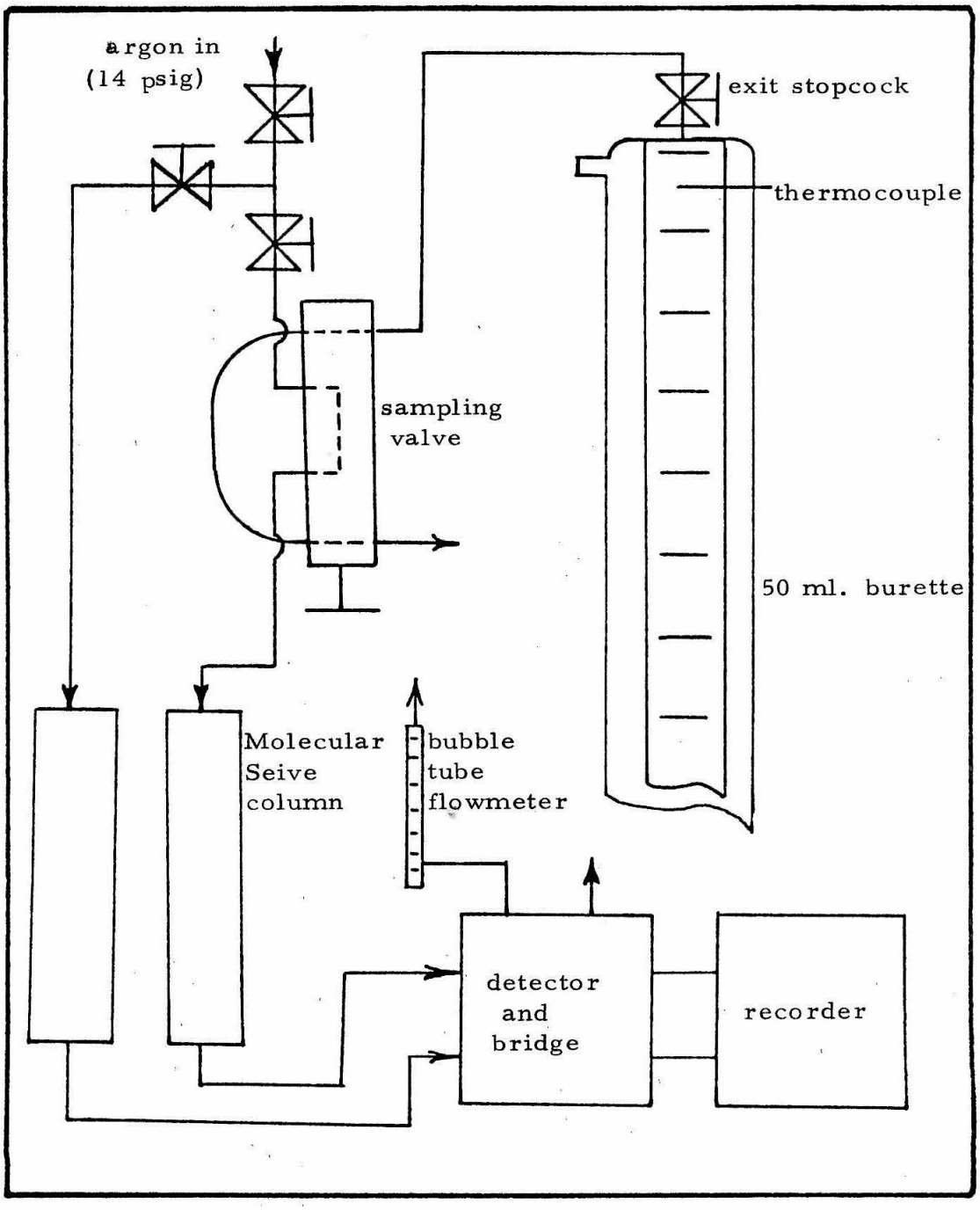

Figure 7. --Gas chromatograph used to analyze non-condensables.

a tube (8 feet 9 inches long, 1/8 inch O. D., 30 gage, 303 stainless steel) with 13 X Molecular Sieve of 30/60 mesh. Prior to its use, the column was conditioned by heating it for 16 hours at 345° C. while passing helium through it to remove contaminates.

The chromatograph used consisted of a bridge circuit and two thermistor detectors. The carrier gas was constantly fed through one detector while carrier gas and sample were fed through the other. The bridge then measured the unbalance between the two detectors which responded to gases of varying thermal conductivity. Since it was necessary to know the hydrogen concentration accurately, and since the thermal conductivity of argon is considerably higher than that of hydrogen, argon was chosen as the carrier gas.

The unbalance of the bridge was measured with a strip chart recorder set to the 5 millivolt range. The output of the recorder was related to the concentration of the injected sample. The chromatograph had been calibrated for the integrated areas under the recorder trace as described in Appendix E.

Dissolved Oxygen Measurement

A 125 milliliter flask was located upstream from the inlet of the test section at the point labled "Oxygen Measurement" in Figure 3. As an experimental run progressed, the incoming water flowed

through this flask and at the conclusion of the run, the flask contained a representative sample of the incoming fluid. During an experimental run approximately 2 liters of water flowed through the sample flask. This was enough volume to purge the 125 milliliter flask of its original contents. At the outlet of the test section the liquid flowed through a heat exchanger composed of two concentric tube glass condensers which lowered the temperature of the outlet flow below 50° C. The liquid then flowed through a second 125 milliliter flask which provided a sample of the outlet flow. The outflow of this flask was discarded. During an experimental run the 125 milliliter flasks were sealed with rubber stoppers and at the completion of the runs the stoppers were removed and the oxygen analyzer was used to determine the concentration of dissolved oxygen in each flask.

The oxygen analyzer used detected the oxygen partial pressure by the diffusion of oxygen through a Teflon membrane. The oxygen was then reduced electrochemically at a rhodium electrode when a potential of 0.53 volts was applied between the rhodium cathode and a silver anode. The resulting current was proportional to the oxygen partial pressure in the sample.

The oxygen analyzer was calibrated to compensate for the temperature of the sample in the range of 0-50° C. The temperature of the sample was read with a mercury thermometer. Prior to each experimental run the analyzer was calibrated against a standard solution of oxygen in water. This standard solution was prepared by constantly bubbling air through water for at least 24 hours. After this period of time it safely could be assumed that the dissolved oxygen was at equilibrium with the atmosphere.

CHAPTER II

PROCEDURE USED FOR EXPERIMENTAL RUNS

Three different series of data were taken during various stages of completion of the apparatus. The first taken was a series of preliminary data in which dissolved gases were not collected. The main purpose of the first series was to investigate the heat transfer relationships. However, during the experimental runs, it became apparent that dissolved gases might have an effect on the heat transfer relationships. Therefore, a second series of data was obtained from experimental runs during which the non-condensables were collected and the inlet and outlet oxygen concentrations were measured. Upon analysis of these data, it became apparent that a heterogeneous chemical reaction may have occurred at the wall. Therefore, a third and final series of data was obtained in which a gas chromatograph was used to measure the concentrations of the gases in the collected non-condensables. The apparatus used for the final series of data is that described in Chapter I, "Description of Apparatus".

The experimental procedure for the first and second series of runs was identical to that for the third series with the exception that measurements of the volume and composition of the non-condensables

were omitted. Therefore, only a description of the procedure used to obtain the final series of data will be presented.

Prior to each run, the entire flow system was filled with water and the water was pumped continuously through the constant head tank. The pumping permitted the dissolved gases in the water to reach an equilibrium with the atmosphere at the temperature of the reservoir. To obtain the desired temperature, the constant temperature bath was either heated electrically or cooled with ice. The pumping process was continued for a minimum of one hour to allow equilibrium to be reached. After pumping for one half hour at a given temperature, no further change in oxygen concentration occurred as determined by the oxygen analyzer. Thus, the concentration of oxygen and nitrogen in the reservoir was set by the temperature in the constant temperature bath.

The detector heaters of the gas chromatograph were turned on several hours prior to each run. After a two hour warm up, no noticeable drift of the recorder took place. The induction heater's cooling water and the filament power were turned on one half hour prior to each run with the warm up period allowing complete vaporization of the mercury in the rectifier tubes. The atmospheric pressure was measured with a mercury barometer.

Immediately prior to each run, the temperature recorder was zeroed by placing a mercury thermometer and an extra thermocouple in a water bath. The zero control on the recorder was varied to adjust the recorder temperature to equal the temperature shown on the mercury thermometer.

The oxygen analyzer was calibrated by placing the probe in a standard solution of oxygen in water. This standard solution was prepared by bubbling air through distilled water for at least 24 hours which allowed the atmospheric oxygen to be at equilibrium with the water. The concentration of oxygen in the water was obtained from equilibrium data (2) for an atmospheric pressure of 740 millimeters of mercury and for the temperature of the water. The apparatus was calibrated for 740 millimeters because it is the approximate atmospheric pressure in the laboratory. The atmospheric pressure variations in the laboratory were less than 2% of the 740 millimeters. The temperature of the standard solution was measured by the mercury thermometer, and the oxygen analyzer temperature compensation control was set accordingly.

The cooling water for the heat exchanger and the burette next was turned on. The temperature of the collected non-condensables was approximately the temperature of the cooling water.

Each run was begun with the system completely filled with water. Initially, there was no water flow in the test section. The induction heater was turned on and a small amount of power was applied to the sphere. After a minute, film boiling began on the upper portion of the sphere and within ten seconds the film covered the entire sphere. There was no difficulty in starting film boiling on the sphere when sufficient power was used. Next, the flow control valve was opened and adjusted to give the desired rotameter reading. The power control of the induction heater was advanced to produce the desired surface temperature. The grid control of the induction heater was adjusted simultaneously to keep the grid current within the limits prescribed for the induction heater (0.4 amperes to 0.6 amperes).

The surface temperature of the sphere was measured several times during each run. The surface temperature recorded was an average of readings taken. The rotameter reading was observed during the experiment to ascertain that it remained constant. At the lower flow rates oscillations in the flow rate were noted, and if these oscillations were present, an average flow rate was recorded. These oscillations were approximately 0.1 milliliter per second from the average flow rate.

When approximately five milliliters of the non-condensables had been collected in the burette, the exact volume was recorded. Also, the pressure on the manometer was recorded and the stopwatch was started. Approximately half-way through each run, the temperatures were recorded. These temperature measurements were taken at the inlet and outlet of the test section, inside the burette, and in the reservoir.

Prior to the termination of each run, the volume of non-condensables collected was recorded along with the manometer pressure. Simultaneously, the stopwatch was stopped. Next, the induction heater was shut off. The volume collected in the burette was recorded. After a ten minute period this volume again was recorded. During the run, the non-condensables could not be expected to be at equilibrium with the water vapor within the burette, therefore, the ten minute wait was used to allow excess vapor present within the burette to condense and equilibrium to occur. The volume difference was subtracted from the recorded volume obtained when the stopwatch was stopped. This correction was generally less than 1% of the total volume.

The oxygen analysis and the chromatographic analysis were made after the run. The oxygen analysis was begun by blocking the Tygon tubing with clamps at the inlet and outlet of the outlet oxygen sample

collection flask. The valve controlling the flow through the test section also was closed. The rubber stopper of the oxygen collection flask at the inlet of the test section was removed. The oxygen analyzer probe and a mercury thermometer were placed in the flask, and the oxygen concentration was measured. The oxygen concentration in the sample collection flask at the outlet of the test section was determined by the same method.

The non-condensables were analyzed by the gas chromatograph. The recorder chart paper was set to advance at 4.0 inches per minute. The valve used to control the flow of liquid from the constant head tank through the test section was cracked which pressurized the gas sample in the burette. The stopcock at the top of the burette was opened and the collected non-condensables were forced through the sample valve. After the lines were purged with at least 10 milliliters of gas, the sample valve was pushed to inject a 0.525 milliliter sample into the chromatograph. The pen of the recorder was then lowered into position and the trace recorded. This procedure was repeated a second time to provide a duplicate trace. The area under the chromatogram was determined by counting the squares under the curves, and the average for the two traces was recorded. In most cases, the differences in the chromatogram areas were less than 3%

of the average. The error was largely a result of inaccurate counting of the squares.

The above procedure resulted in nineteen measured values which are listed in Table 2. This table also includes the range of these values and an estimation of the error in the recorded value.

TABLE 2

VARIABLES MEASURED DURING AN EXPERIMENTAL RUN

Variable Measured	Symbol	Range	Approximate Maximum Error
1. Temperature at inlet to test section	T_{in}	60-82°F	1%
2. Temperature at outlet of test section	T_o	187-212°F	1%
3. Temperature of collected non-condensables	T_{air}	73-80°F	1%
4. Temperature of water in reservoir	T_{res}	41-99°F	1%
5. Temperature of sphere wall	T_w	743-1143°C	2%
6. Liquid flow rate	w	0.45-3.37g./sec.	0.1g./sec.
7. Inlet oxygen concentration	$m_{O_2, in}$	6.87-11.6p.p.m.	0.1p.p.m.
8. Outlet oxygen concentration	$m_{O_2, o}$	0.81-4p.p.m.	0.1p.p.m.
9. Initial volume of collected non-condensables	V_c	2 - 6cc.	0.1cc.
10. Final volume of collected non-condensables	V_f	19 - 46cc.	0.1cc.
11. Initial pressure of collected non-condensables	ξ_i	-0.6 to 0cm.	0.1cm.

TABLE 2 (Continued)

Variable Measured	Symbol	Range	Approximate Maximum Error
12. Final pressure of collected non-condensables	ξ_f	-0.6 to 0 cm.	0.1cm.
13. Atmospheric pressure	P_{atm}	74.0-75.3cm.	0.1cm.
14. Time during which non-condensables were collected	t	.75 - 36 min.	0.02 min.
15. Volume of non-condensables immediately following run	V_h	---	0.1 cm.
16. Volume of non-condensables 10 minutes following run	V_{cool}	---	0.1 cm.
17. Relative area under hydrogen chromatogram	A_{H_2}	0 - 8600	3%
18. Relative area under oxygen chromatogram	A_{O_2}	1-68	3%
19. Relative area under nitrogen chromatogram	A_{N_2}	3-133	3%

CHAPTER III

DERIVATION OF HEAT TRANSFER RELATIONSHIPS

The physical situation investigated experimentally has been described in Chapter I and shown in Figure 2. By simple energy and material balances, equations were derived which can be used to predict the rates of heat transfer and the composition of the vapor film which were encountered in the experiments. Equations (A-27) and (A-31) of Appendix A which were derived by Kobayasi (39) (31) (40) and Witte (69) do not take into account the effects of subcooling of the liquid, mass transfer of a dissolved gas into the film, and chemical reactions at the wall. However, these effects were present during the experimental runs.

Energy Balance

The physical situation was modeled as shown in Figure 8. On the lower half of the sphere, vaporization occurred and heat was transferred to the liquid. Half of the way up the sphere, the average temperature of the liquid was T_3 and the liquid mass flow rate was w_3. At this position, the vapor flow rate was w_2. The numerical subscripts refer to positions in Figure 8. Diffusion of dissolved gases into the film occurred on the lower half of the sphere. On the upper half of the sphere, the vapor condensed and caused further heating

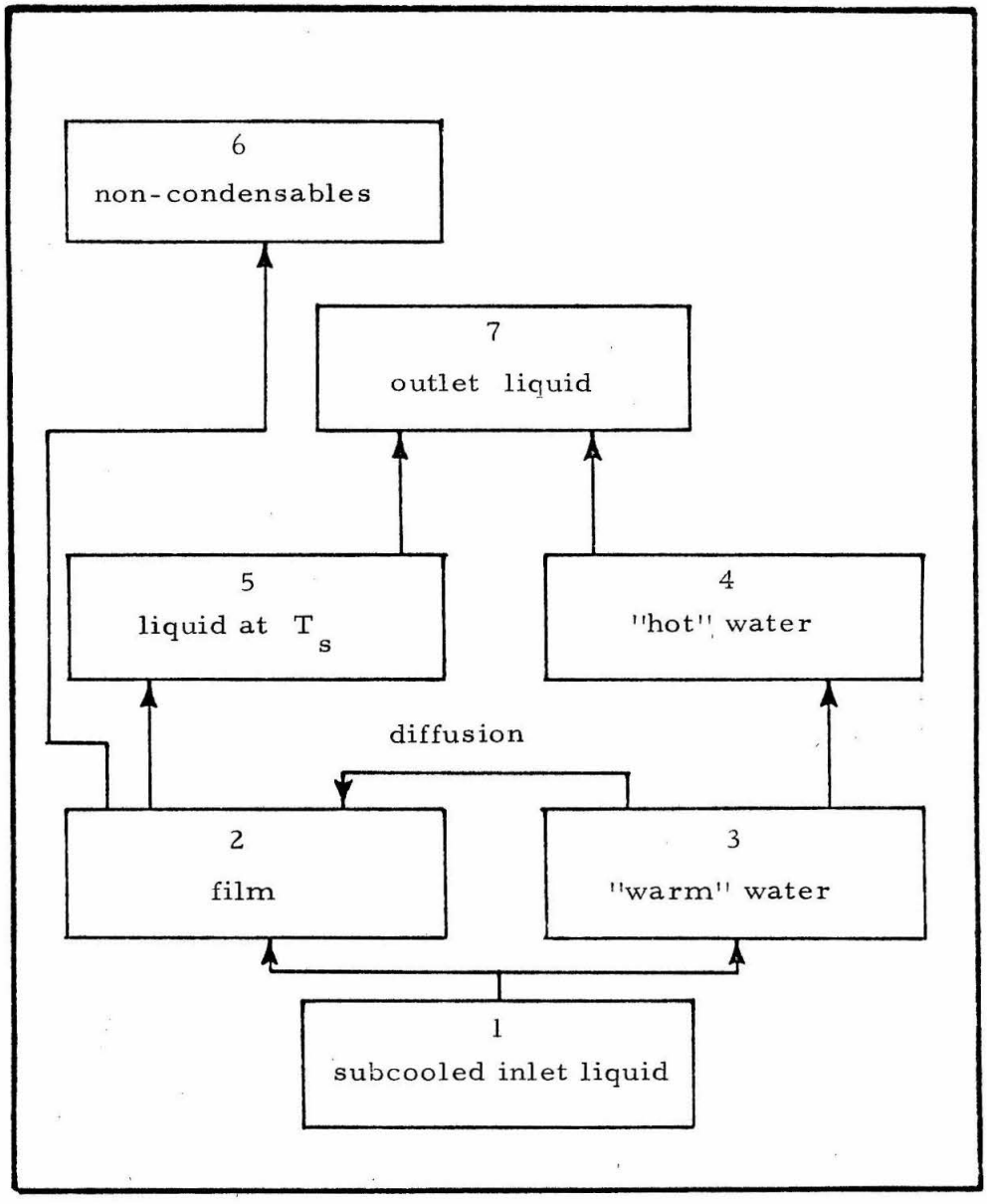

Figure 8. --Model of subcooled film boiling with no vapor leaving the film.

of the liquid. At Point Number 7 the condensed vapor and the "hot" liquid from Point Number 4 mixed. However, the non-condensables were collected and did not redissolve into the liquid.

Two energy balances were made; the first was made between Points 2 and 3 and Points 4 and 5, and the second was made between Points 4 and 5 and Point 7. The following equation is a general statement of an energy balance between Point A and Point B(33) :

$$E_A + y_A + \frac{u_A^2}{2g} + P_A V_A + q - W = E_B + y_B + \frac{u_B^2}{2g} + P_B V_B \qquad (3-1)$$

where W represents mechanical work. Since very little change in elevation occurred in going from Point Number 2 to Point Number 7 in the apparatus the y_A term may be neglected. The velocities involved were small enough that the kinetic energy term also may be neglected. The pressure and the density remained constant, and no mechanical work was done on the system. It was previously assumed that no heat transfer from the sphere occurred above Point Number 2 and it may be assumed that the system was adiabatic; therefore, "q" is zero in the above equation. The above equation then may be re-written as

$$E_A = E_B \qquad (3-2)$$

If Point A represents Points 4 and 5 in the model, and if Point B represents Point Number 7, Equation (3-2) may be written for the mixing as

$$w_5 c_{p,1} (T_5 - T_7) + w_4 c_{p,1} (T_4 - T_7) = 0 \qquad (3-3)$$

since w_7 equals w_5 and w_4. The heat capacities were assumed to be constant in the above equation and there was assumed to be no phase change.

Before mixing, the condensed liquid was at its saturation temperature, there fore Equation (3-3) may be rewritten as

$$w_5 (T_s - T_7) = w_4 (T_7 - T_4) \qquad (3-4)$$

which may be rearranged as

$$T_4 = \frac{w_5}{w_4} (T_7 - T_s) + T_7 \qquad (3-5)$$

The above equation relates the outlet temperature to that at Point 4.

If the dissolved gases are present in the liquid in dilute concentrations, then

$$w_3 = w_4 \tag{3-6}$$

In the film,

$$w_5 = m_k w_2 \tag{3-7}$$

where m_k is the mass fraction of water vapor present in the film. Then,

$$\frac{w_5}{w_4} = \frac{w_2 m_k}{w_3} \tag{3-8}$$

and by combining Equations (3-5) and (3-8)

$$T_4 = \frac{w_2 m_k}{w_3} (T_7 - T_s) + T_7 \tag{3-9}$$

An energy balance may be written for the condensation process occurring in the upper half of the sphere as follows:

$$w_2 T_2 \sum_{i=k}^{j} m_i c_{p,v,i} - w_2 T_s \sum_{i=k}^{j} m_i c_{p,v,i} + m_k w_2 \lambda$$

$$= w_3 c_{p,l} T_4 - w_3 c_{p,l} T_3 \tag{3-10}$$

where the subscripts $i = k+1$ to j refer to the species of non-condensables and λ is the latent heat of vaporization at the saturation temperature. The above equation may be rewritten as

$$\frac{w_2}{w_3}\left[\sum_{i=k}^{j} m_i\, c_{p,v,i}\,(T_2 - T_s) + \lambda m_k\right] = c_{p,l}\,(T_4 - T_3) \qquad (3\text{-}11)$$

By combining Equations (3-9) and (3-11)

$$\frac{w_2}{w_3}\left[\sum_{i=k}^{j} m_i\, c_{p,v,i}\,(T_2 - T_s) + \lambda m_k\right]$$

$$= c_{p,l}\left[\frac{m_k\, w_2}{w_3}\,(T_7 - T_s) + T_7 - T_3\right] \qquad (3\text{-}12)$$

This may be rewritten as

$$\frac{w_2}{w_3} = \frac{c_{p,l}\,(T_7 - T_3)}{\left[\sum_{i=k}^{j} c_{p,v,i}\, m_i\,(T_2 - T_s) + m_k\, c_{p,l}\,(T_7 - T_s) + m_k\lambda\right]} \qquad (3\text{-}13)$$

Now, χ'' is defined as

$$\chi'' = \sum_{i=k}^{j} c_{p,v,i}\, m_i\,(T_2 - T_s) / m_k + c_{p,l}\,(T_7 - T_s) + \lambda \qquad (3\text{-}14)$$

The λ'' used in the above equation is similar to the λ' used by Bromley (9) in Equation (A-3). However, the above λ'' contains an additional term to account for the subcooling of the liquid. The other terms used above and also used in Bromley's λ' account for the heat of vaporization and for the superheating of the vapor.

By combining Equations (3-13) and (3-14),

$$m_k \frac{w_2}{w_3} = \frac{c_{p,1}(T_7 - T_3)}{\lambda''} \qquad (3\text{-}15)$$

The density in the film was assumed to be constant at the average temperature of the film and assumed to be defined by

$$\rho_v = \sum_{i=k}^{j} x_{i,v} \quad \rho_{i,v} \qquad (3\text{-}16)$$

where $x_{i,v}$ is the mole fraction of the species "i" in the film.

The heat transfer coefficient was derived by using the coordinates shown in Figure 9. It was assumed that vaporization occurred in the region $\theta \leq \pi/2$ and that condensation occurred in the region $\pi/2 \leq \theta \leq \pi$. It also was assumed that the film thickness, δ, was constant on the lower half of the sphere and was much less than the diameter of the sphere. At $\theta = \pi/2$ the following assumption was made

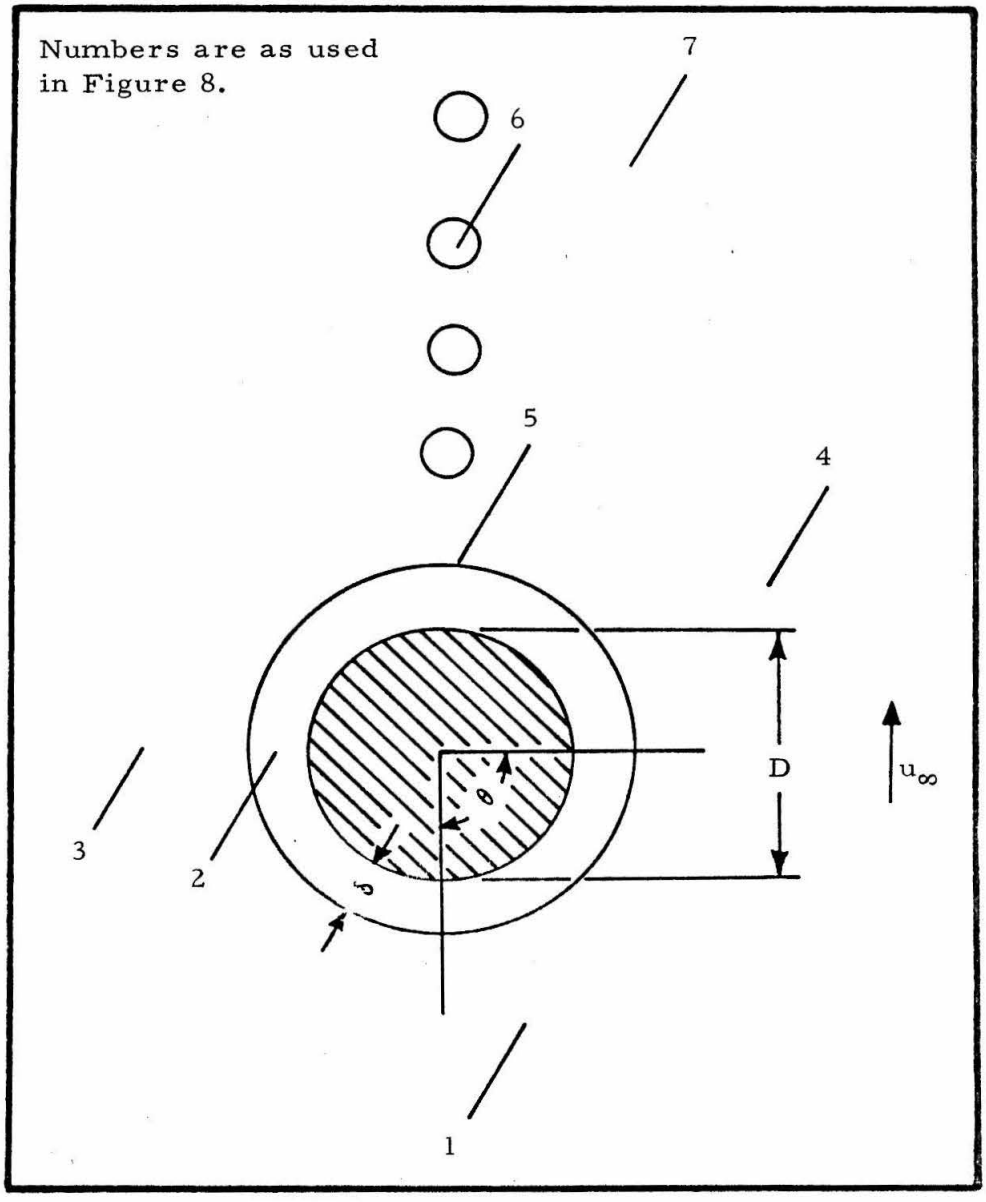

Figure 9. --Coordinate system used for obtaining heat transfer coefficient for subcooled film boiling on a sphere.

$$\bar{u} = 1/2\ u_\infty \tag{3-17}$$

where $\bar{u}$ was the average vapor flow velocity. This assumption was based on the film thickness being much less than the diameter of the sphere; therefore, at $\pi/2$ the vapor flow was similar to the flow between two parallel plates, one of which was made in such a way that there were no free convection effects present. Now,

$$w_2 = \bar{u}\ \pi\ D\ \delta\ \rho_v \tag{3-18}$$

and

$$\delta = \frac{2w_2}{\pi D\ \rho_v\ u_\infty} \tag{3-19}$$

If by definition

$$\tau = \frac{T_7 - T_3}{T_7 - T_1} \tag{3-20}$$

then Equation (3-15) becomes

$$\frac{w_2}{w_3} = \frac{c_{p,1}\ \tau\ (T_7 - T_1)}{m_k \lambda''} \tag{3-21}$$

By substituting Equation (3-21) into (3-19),

$$\delta = \frac{2 w_3 c_{p,l} (T_7 - T_3)}{\pi \lambda'' D \rho_v u_\infty m_k} \tag{3-22}$$

or

$$\delta = \frac{2 q A r}{\pi \lambda'' D \rho_v u_\infty m_k} \tag{3-23}$$

As an approximation,

$$k_v = \sum_{i=k}^{j} k_{i,v} x_{i,v} \tag{3-24}$$

where $k_{i,v}$ is evaluated at the average temperature of the film and

$$h = k_v/\delta \tag{3-25}$$

where "h" is the local heat transfer coefficient at $\theta = \pi/2$. Since it has been assumed that the film thickness is constant over the lower half of the sphere, then

$$\bar{h} = k_v/\delta \tag{3-26}$$

where $\bar{h}$ is the average heat transfer coefficient, and

$$q = \bar{h}\, \Delta T \tag{3-27}$$

where

$$\Delta T = T_2 - T_s \tag{3-28}$$

The area of the sphere is determined by

$$A = \pi D^2 \tag{3-29}$$

Substituting Equations (3-23), (3-27), and (3-29) into Equation (3-26) yields

$$\bar{h} = \frac{1}{\sqrt{2}} \left(\frac{k_v \rho_v \chi'' u_\infty m_k}{D \Delta T \tau} \right)^{1/2} \tag{3-30}$$

In terms of the average Nusselt number, this is

$$\frac{\overline{Nu_D}}{\sqrt{Re_D}} \frac{\mu_v}{\mu_1} = \frac{1}{\sqrt{2}} \left(\frac{(\rho \mu)_v Pr_v \chi'' m_k}{(\rho \mu)_1 c_{p,v} \Delta T \tau} \right)^{1/2} \tag{3-31}$$

The above equation is similar to the equation obtained by Kobayasi (39) (31) (40) and Witte (69), Equation (A-31). However, the above equation contains the subcooling parameter, τ, and the water concentration in the film, m_k. The constant in the above differs slightly from that of Equation (A-31), because of the assumption that the film

thickness is constant over the lower half of the sphere. Based on Bromley's data for forced convection film boiling around horizontal cylinders, Witte suggested a constant of 2.7. Because of the subcooling, λ'' in the above equation also is slightly different from the λ suggested by Witte.

From Equation (3-21)

$$w_2 \lambda'' = q A \tau / m_k \tag{3-32}$$

Then,

$$\tau = m_k w_2 \lambda'' / q A \tag{3-33}$$

or

$$\tau = \frac{q - q_1}{q} \tag{3-34}$$

where q_1 is the heat transferred from the liquid-vapor interface into the liquid. By rearranging Equation (3-34),

$$q_1 = (1 - \tau) q \tag{3-35}$$

If $\overline{h_1}$ is defined as

$$\overline{h_l} = q_l / \Delta T_l \tag{3-36}$$

where

$$\Delta T_l = T_s - T_\infty \tag{3-37}$$

then

$$\overline{h_l} = 2 (1 - \tau) q / \Delta T_l \tag{3-38}$$

The factor of 2 is the result of the assumption that the heat transfer to the liquid occurred only on the lower half of the sphere; whereas, "q" was evaluated for the entire sphere. In terms of the average Nusselt number this becomes:

$$\overline{Nu_{D,l}} = \frac{2 (1 - \tau) q D}{k_l \Delta T_l} \tag{3-39}$$

or

$$\tau = 1 - \frac{\overline{Nu_{D,l}} k_l \Delta T_l}{2 D \overline{h} \Delta T} \tag{3-40}$$

The transfer of heat into the liquid from the liquid-vapor interface was independent of the vapor properties and the wall temperature.

Therefore, the following could be expected:

$$\overline{Nu_{D,1}} = f(Re_D, Pr_1) \tag{3-41}$$

The form of the functional relationship would be

$$\overline{Nu_{D,1}} = c\, Re_D^{\,m} Pr_1^{\,n} \tag{3-42}$$

for a situation in which the liquid extends to infinity in all directions as described by Garner et al. (26). The letters c, m, and n designate constants in the above expression.

In the case investigated experimentally, the functional relationship of the Reynolds and Nusselt numbers may not have been this simple. The addition of a geometric factor may be necessary.

Equation (3-40) may be rearranged as

$$\tau = 1 - \left[\frac{f(Re_D, Pr_1)}{\overline{Nu_D}}\right]\left[\frac{c_{p,1}\,\Delta T_1\, Pr_v}{c_{p,v}\,\Delta T\, Pr_1}\right]\left[\frac{\mu_v}{\mu_1}\right] \tag{3-43}$$

Equation (3-43) expresses τ as a function of $\overline{Nu_D}$, and Equation (3-31) expresses $\overline{Nu_D}$ as a function of τ. If these two equations are solved simultaneously, either $\overline{Nu_D}$ or τ may be found as a function of the following variables:

$$Re_D, \quad \frac{\mu_v}{\mu_l}, \quad \frac{(\rho\mu)_v}{(\rho\mu)_l}, \quad Pr_v, \quad \frac{\chi'' m_k}{c_{p,l}\,\Delta T}, \quad Pr_l,$$

$$\frac{c_{p,l}\,\Delta T_l\,Pr_v}{c_{p,v}\,\Delta T\,Pr_l}$$

These are the same parameters used by Cess and Sparrow (14) to describe subcooled forced convection film boiling on a flat plate. An exception to this similarity is that the effect of dissolved gases are taken into account by the presence of m_k.

If the degree of subcooling of the liquid is very large, then

$$0 \leq \gamma << 1 \tag{3-44}$$

and

$$0 = 1 - \frac{f(Re_{D,l}, Pr_l)\, k_l\, \Delta T_l}{2\, h\, \Delta T\, D} \tag{3-45}$$

By rearranging,

$$\bar{h} = \frac{f(Re_{D,l}, Pr_l)\, k_l\, \Delta T_l}{2\, D\, \Delta T} \tag{3-46}$$

In other words, heat transfer is governed by the liquid parameters and the liquid temperature difference, although a film may be present.

Material Balance

A material balance may be used in determining the concentration of the vapor film, if the assumption is made that the gases within the film are at equilibrium with the liquid. If the liquid is bounded as it was in the apparatus, an equilibrium may exist. If the liquid extends to infinity, the time required for diffusion of the dissolved gases to the liquid - vapor interface will be much greater than the time required for the liquid to move past the sphere. In this case, an imaginary boundary layer thickness may be used. For the purpose of this discussion, it will be assumed that an equilibrium exists between the gases in the film and their average concentrations in the liquid.

If Henry's law applies to this equilibrium, then

$$P_j = x_j H_j \tag{3-47}$$

where P_j is the vapor pressure of the dissolved gas and H_j is a proportionality constant. The subscript "j" refers to the gases other than the solvent, water.

If

$$P_{atm} = \sum_{i=k}^{j} P_i \tag{3-48}$$

and if the mole fractions in the film are proportional to the partial pressures, then

$$x_{j,3} = x_{j,2} P_{atm} / H_j \tag{3-49}$$

where the numerical subscripts refer to points in Figure 8.

If none of the non-condensables in the film are redissolved into the liquid, then

$$x_{j,5} = 0 \tag{3-50}$$

and

$$N_4 x_{j,4} = N_7 x_{j,7} \tag{3-51}$$

where N is the molar flow rate. Since

$$N_6 << N_7 \tag{3-52}$$

then

$$N_7 = N_2 + N_3 \tag{3-53}$$

Substituting Equation (3-53) into (3-51) yields

$$x_{j,4} = \left(\frac{N_2}{N_3} + 1 \right) x_{j,7} \tag{3-54}$$

If at this point there are no chemical reactions in the film or at the wall, then the following will be true:

$$N_1 x_{j,1} = N_2 x_{j,2} + N_3 x_{j,3} \tag{3-55}$$

and

$$N_1 = N_2 + N_3 \tag{3-56}$$

By substituting Equations (3-49) and (3-56) into (3-55),

$$\frac{x_{j,2}}{x_{j,1}} = \frac{1 - N_3 / N_2}{1 + \frac{N_3 P_{atm}}{N_2 H_j}} \tag{3-57}$$

By combining Equations (3-49) and (3-57), the following is obtained:

$$\frac{x_{j,3}}{x_{j,1}} = \frac{(1 + N_3 / N_2)}{(N_3 / N_2 + H_j / P_{atm})} \tag{3-58}$$

If the equilibrium is reached on the lower half of the sphere, then

$$x_{j,3} = x_{j,4} \tag{3-59}$$

If Equations (3-54) and (3-59) are substituted into (3-58), then

$$\frac{x_{j,7}}{x_{j,1}} = \frac{(1 + N_3 / N_2)}{(N_2 / N_3 + 1)\ (N_3 / N_2 + H_j / P_{atm})} \tag{3-60}$$

Since

$$N_2 << N_3 \tag{3-61}$$

the following results

$$\frac{x_{j,7}}{x_{j,1}} = \frac{1}{1 + \frac{N_2 H_j}{N_3 P_{atm}}} \tag{3-62}$$

The above equation relates the inlet and outlet concentrations of a dissolved gas with the ratio of the molar flow rates in the vapor and the liquid. It has been assumed that the diffusion of dissolved gases is instantaneous; therefore, the gases in the vapor are in equilibrium with the dissolved gases in the liquid. It also has been assumed that no chemical reactions took place anywhere in the system.

The Henry's law constant in Equation (3-62) depends upon the saturation temperature, which in turn depends upon the vapor pressure of the water vapor in the film. Since gases other than water vapor may be present, the saturation temperature could be lowered. The total pressure is related to the partial pressures by

$$P_{atm} = \sum_{i=k}^{j} P_i \tag{3-48}$$

If the Clausius - Clapeyron equation applies, then

$$\frac{d \ln P_k}{d 1 / T_s} = - \frac{\lambda}{R} \tag{3-63}$$

or

$$\ln \left[P_k / (1 \text{ atm.}) \right] = \frac{\lambda}{R} \left(\frac{1}{T_{BP}} - \frac{1}{T_s} \right) \tag{3-64}$$

where T_{BP} is the normal boiling point. If the total pressure in the film is one atmosphere and the mole fraction equals the partial pressure, then

$$x_{k,2} = P_k / (1 \text{ atm.}) \tag{3-65}$$

and

$$T_s = \frac{1}{\frac{1}{T_{BP}} - \frac{R \ln x_{k,2}}{\lambda}} \tag{3-66}$$

Because

$$H_j = f(T_s) \tag{3-67}$$

Equations (3-48), (3-62), (3-66), and (3-67) must be solved simultaneously.

Chemical Reactions

Chemical reactions may occur either homogeneously within the film or heterogeneously at the wall. During the experimental runs, only the latter was apparent, and therefore, only the heterogeneous reactions will be discussed.

Partridge and Hall (53) suggested that a steam-iron reaction may occur in boilers, if film boiling occurred. The reaction which they suggested could take place is

$$3\,Fe + 4H_2O \longrightarrow Fe_3O_4 + 4H_2$$

Therefore, hydrogen could be produced at the wall during film boiling on an iron surface.

Additional reactions could occur when large amounts of oxygen are present in the film. A possible reaction is

$$3Fe + 2O_2 \longrightarrow Fe_3O_4$$

Other iron-oxygen reactions also could be present.

The reaction of a gas with a sphere in a similar geometry was investigated by Campagne (11). He suggested a system similar to that used here, as a reactor with rapid heating and quenching. However, his experiments dealt only with a single gas phase and not a two phase boiling situation.

The rates at which the reactions occur may be determined by

$$N_{R,i} \simeq k_o \left(e^{- \Delta E/RT_w} \right) f(x_i) \qquad (3\text{-}68)$$

where N_R is the molar quantity of component "i" reacted. One method of incorporating the chemical reactions into the material balances is by assuming that the reactions occur in a narrow boundary layer at the wall and that the reaction does not effect the Henry's law equilibrium. The following will govern the rate of collection of the non-condensables:

$$N_6 x_{j,6} = N_1 x_{j,1} - N_7 x_{j,7} - N_{R,j} A \qquad (3\text{-}69)$$

By substituting Equation (3-62) into (3-69),

$$N_6 x_{j,6} = N_1 x_{j,1} \left(1 - \frac{1}{1 + \frac{N_2 \; H_j}{N_3 \; P_{atm}}} \right) - N_{R,j} A \qquad (3\text{-}70)$$

The preceeding energy and material balances must be combined with the kinetic expression to predict the outcome of the experimental runs.

CHAPTER IV

RESULTS OF THE EXPERIMENTAL INVESTIGATION

Nineteen parameters were measured during each test run of the final series of runs. The data were reduced to determine whether or not the theory outlined in Chapter III adequately described the phenomena. The raw experimental data for the final series of runs are tabulated in Appendix F. The results of the first series of runs have been published elsewhere (35) and are presented in Appendix J. The reduced final data are tabulated in Appendix G; for convenience, these results are also presented graphically in this chapter.

There were ninety - one experimental runs in the final series. Table 3 lists the size spheres used and other miscellaneous information regarding these runs.

The data were reduced in three steps. First, the volume of the collected non-condensables was determined. Secondly, the composition of the non-condensables was determined. Lastly, the overall heat transfer coefficient was determined. Because gases other than water vapor were present in the film, the composition of the gases in the film had to be known as a prerequisite to determining the heat transfer coefficient.

TABLE 3

OUTLINE OF FINAL SERIES OF RUNS

Run No.	Sphere Diameter (inches)	Comments
1-34 & 45-68	1/2	Runs were made at various conditions using stainless steel spheres.
34-44	1/2	Runs were made at high temperatures using gold plated spheres. See Appendix D.
69-76	9/16	Runs were made at various conditions using stainless steel spheres.
77-90	5/8	Runs were made at various conditions using stainless steel spheres.
91	1/2	Run was made using a gold plated sphere to determine the effect of gold on eliminating the hydrogen generation. See Appendix C.

Collected Non-Condensables

The reduction of the data was begun by determining the final and initial volumes of the gases in the burette. The burette was calibrated and the burette scale was found to be accurate when the burette reading was increased by 2.1 milliliters.

The final burette reading was determined by subtracting the following correction for non-equilibrium. Since the gases in the burette at the end of the run may have been supersaturated with water vapor, a volume reading was made at the end of the run, V_H, and another was made 10 minutes folowing the run, V_{cool}. This 10 minute waiting period was used to allow the excess water vapor present to condense. The volume difference resulting from condensation was subtracted from the volume recorded when the stopwatch was stopped. In all cases, this correction was less than 2% of the final volume. The corrected initial and final volumes are tabulated in Table 12 as V_i^* and V_f^*.

The final and initial pressures of the gases in the burette were determined from the height of the water and mercury columns and from the atmospheric pressure in the laboratory. Figure 10 illustrates the relative positions of the burette and the mercury manometer. The burette scale read in both milliliters and centimeters.

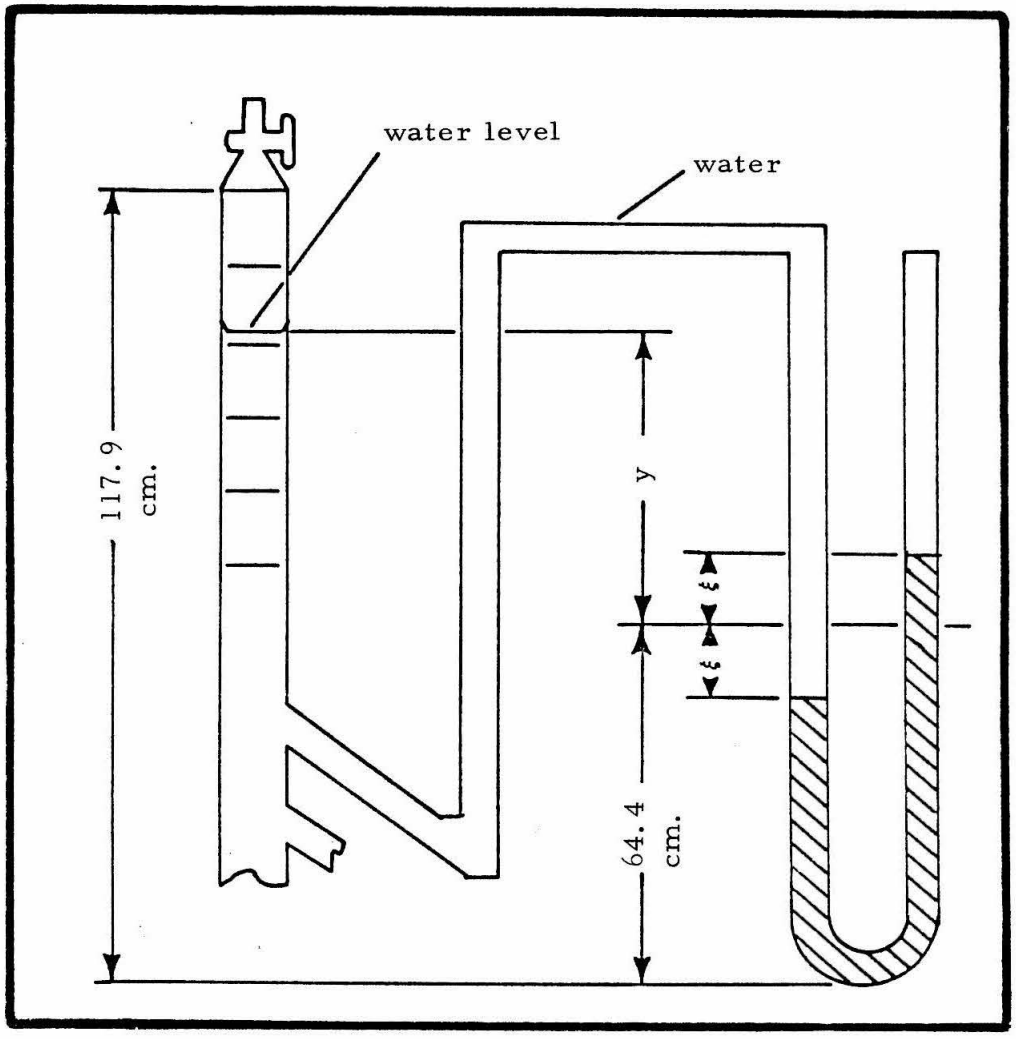

Figure 10. --Relative positions of burette and mercury manometer.

Thus, the same scale was used for the determination of the volume and the water column height.

The pressure in the burette was equal to the atmospheric pressure, plus the height of the mercury column, minus the height of the water column divided by the specific gravity of mercury. The height of the water column was $y + \xi$ and the height of the mercury column was 2ξ . The total pressure inside the burette can be expressed by

$$P = P_{atm} + \frac{2\xi - (y + \xi)\left(\rho_{H_2O} / \rho_{Hg}\right)}{76 \text{ cm.}} \qquad (4\text{-}1)$$

where

$$y = (53.5 \text{ cm.} - \text{burette reading in centimeters}) \qquad (4\text{-}2)$$

The pressure, P, is atmospheres and the manometer reading, ξ , is in centimeters of mercury and is listed in the data. The above formula was used to calculate the initial and final pressures ranging from 0.917 atmospheres to 0.966 atmospheres which are tabulated in Table 12.

The collected non-condensables contained water vapor. Assuming that the gases were saturated with water vapor, the partial pressure of the water vapor depended on the temperature of the collected gases.

These vapor pressures were obtained from the Handbook of Chemistry and Physics (32) and are listed in Table 12. The water vapor pressures were in all cases approximately 3% of the total pressure.

Because it was necessary to know the rate of collection of non-condensables per kilogram of water boiled, the rotameter readings were converted to grams per second by using Figure 5. The total volume of water boiled was found by multiplying the flow rate by the time. The rotameter reading ranging from 0.43 grams per second to 3.37 grams per second and total volumes boiled are tabulated in Table 12.

The volumes were converted to a standard temperature and pressure (0°C and 1 atmosphere). The volume difference, final minus initial, was then divided by the total water flow and multiplied by the fraction of dry air. The resulting collected volume per kilogram of water boiled is listed in Table 12. These collected volumes per kilogram of water boiled ranged from 6.84 milliliters to 1230. milliliters.

Composition of Non-Condensables

Since the oxygen analyzer was calibrated for an atmospheric pressure of 740 millimeters of mercury, a correction of the measured oxygen concentration was made. The measured values were

multiplied by the atmospheric pressure and divided by 740 milliliters of mercury. Because the analyzer meter reading was directly proportional to the oxygen partial pressure and the oxygen partial pressure was directly proportional to the atmospheric pressure, the correction could be expected to yield an accurate measurement of the oxygen concentration.

The concentration of dissolved air was determined by finding an equilibrium reservoir temperature using the inlet oxygen concentration. The measured reservoir temperature was not used since temperature variations between the reservoir and the constant head tank may have resulted in an equilibrium at a temperature other than that in the reservoir. The equilibrium temperature was found by using the original inlet oxygen concentration and Figure 11 (2). This equilibrium temperature was compared to the reservoir temperature to check for gross errors in oxygen concentration measurement. In all cases, these temperatures were within 5 C^{o}. The equilibrium temperature was used with Figure 12 (32) to find the concentration of dissolved air. The concentration of dissolved air was multiplied by the atmospheric pressure and divided by 740 millimeters of mercury to compensate for atmospheric pressure variations as was done with the oxygen measurements. The corrected air and oxygen concentrations are tabulated in Table 13. In all cases, the dissolved air

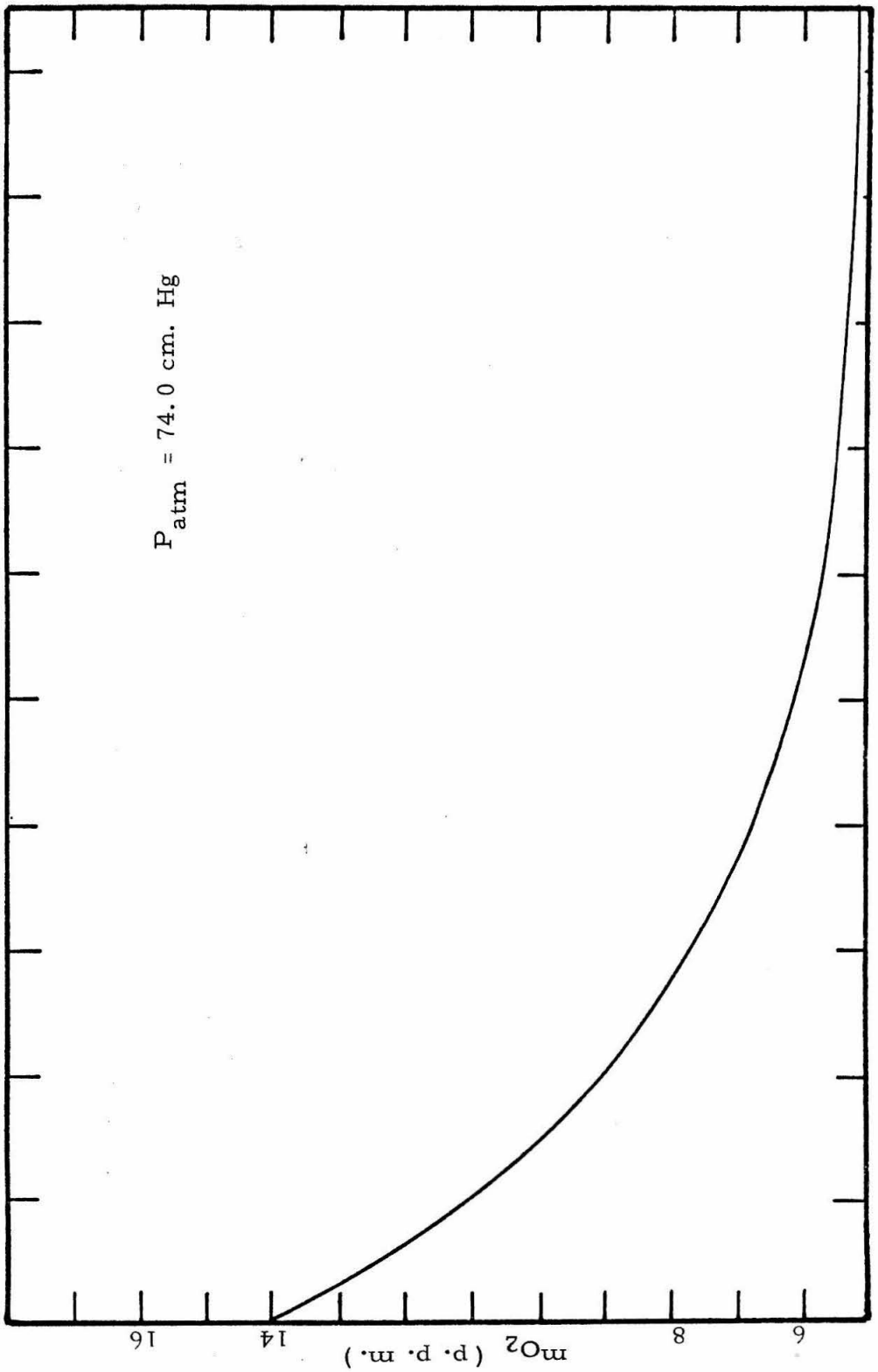

Figure 11. -- Solubility of oxygen in water. (2)

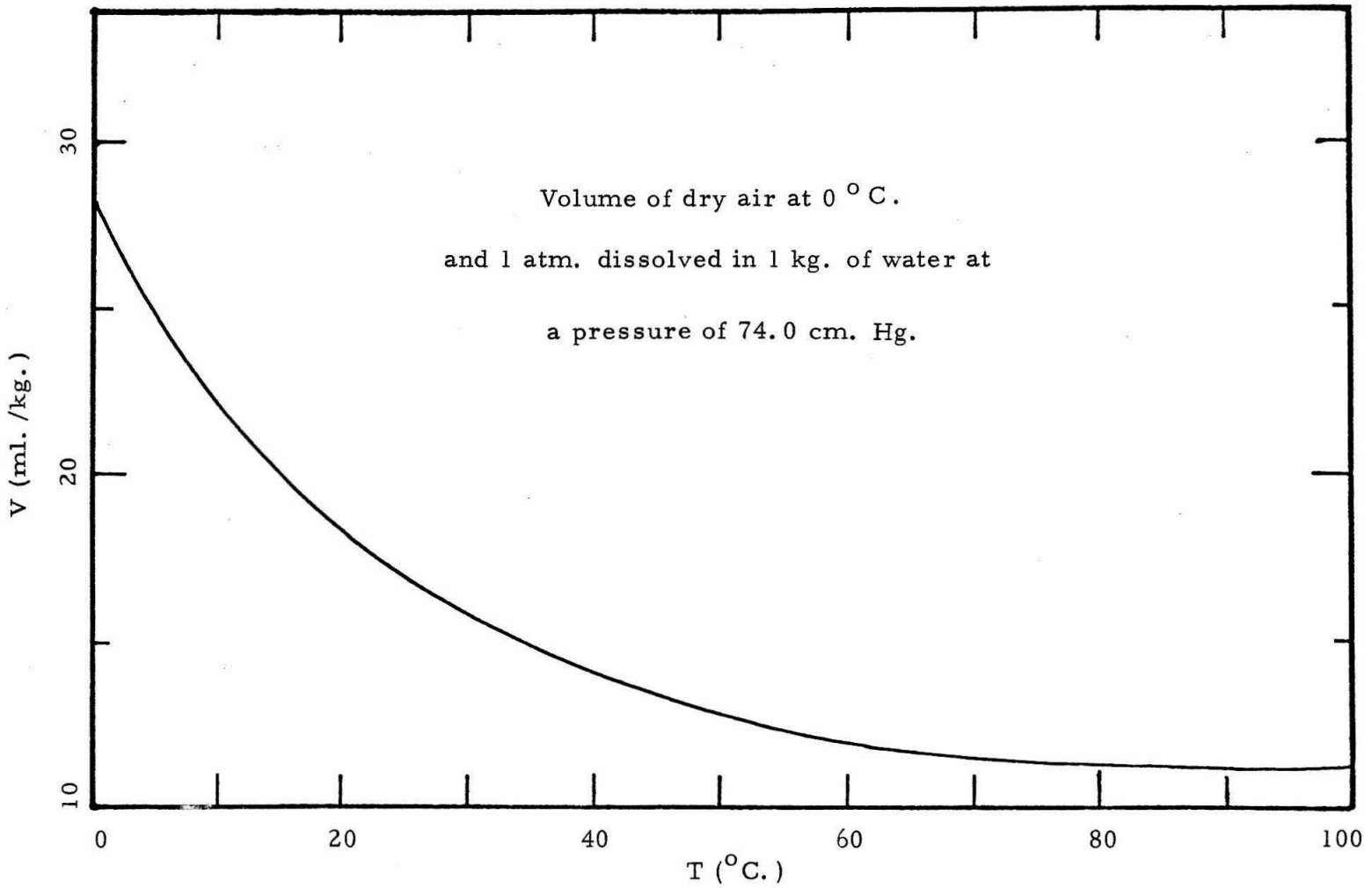

Figure 12. -- Solubility of air in water. (32)

consisted of approximately 1/3 oxygen by volume.

The ratio of the molar flow rate in the film to the molar flow rate in the liquid was determined by

$$\frac{x_{j,7}}{x_{j,1}} = \frac{1}{1 + \frac{N_2 \; H_j}{N_3 \; P_{atm}}} \qquad (3\text{-}62)$$

The use of the inlet and outlet oxygen concentrations implies that any chemical reaction of oxygen at the wall did not effect the equilibrium at the vapor liquid interface. The Henry's law constant was evaluated at the normal boiling point and was found to be 70, 100 atmospheres (54). The lowering of the boiling point did not effect the value of the Henry's law constant, because the constants for oxygen, nitrogen and hydrogen are approximately constant over the range of 70°C. - 100°C. This is evident for oxygen by examining Figure 12.

The inlet oxygen and air concentrations and the outlet oxygen concentrations were converted to mole fractions. The inlet nitrogen mole fraction was found by subtracting the inlet oxygen mole fraction from the inlet air mole fraction. Thus, the nitrogen mole fraction actually is the mole fraction of "atmospheric nitrogen", since it includes dissolved inerts. Next, the outlet nitrogen concentration was found by Equation (3-62).

The oxygen and "atmospheric nitrogen" concentrations in the film were found by

$$x_{j,3} = x_{j,2} P_{atm} / H_j \qquad (3\text{-}49)$$

A value of 126,000 atmospheres was used for H_{N_2} (54). The determination of the hydrogen concentration in the film required reduction of the chromatographic data.

The composition of the collected non-condensables was calculated from the gas chromatogram areas using the calibration constants given in Appendix E.

The number of moles of oxygen and nitrogen collected per mole of water which flowed through the test section during each run was calculated using the ideal gas law. An oxygen balance was made by subtracting the mole fraction of oxygen at the outlet and the number of moles of oxygen collected per mole of water which passed through the test section from the mole fraction of oxygen at the inlet. The difference found was the number of moles reacted per mole of water. It is listed in Table 14 as the number of moles reacted per mole of oxygen in the film.

The molar ratio of oxygen to nitrogen in the collected non-condensables was calculated for each run using the chromatographic results. This ratio also was calculated using the film concentrations

obtained from Equation (3-49). These values are tabulated in Table 14 as O_2/N_2 (exp.) and O_2/N_2 (th.) respectively. In most cases, these two values were within 15% of each other.

The mole fraction of hydrogen in the film was calculated by assuming that the ratio of the mole fraction of hydrogen to the mole fraction of nitrogen in the film was equal to the ratio of the mole fraction of hydrogen to mole fraction of nitrogen in the collected non-condensables. The mole fractions of nitrogen and oxygen in the film calculated by Equation (3-49) and the mole fraction hydrogen in the film are listed in Table 13. The remaining mole fraction was water vapor; in most cases, this mole fraction was between 0.5 and 0.8.

The percentage of oxygen removed by the boiling was calculated by

$$\%O_2 \text{ removed} = \left(1 - \frac{x_{O_2,o}}{x_{O_2,in}}\right) x\ 100\% \qquad (4-3)$$

The above equation considers that any reaction of oxygen occurs after the equilibrium takes place.

The rate of hydrogen production at the wall was calculated by assuming that the water at the outlet of the test section was at equilibrium with the hydrogen in the film. This differs from the assumption made regarding oxygen reaction at the wall. The oxygen reaction

was assumed to have no effect on the Henry's law equilibrium. Since the hydrogen generation reaction appeared to be faster than the oxygen reaction, since the hydrogen diffusivity is higher than the oxygen diffusivity, and since the diffusion driving force is greater for hydrogen, the hydrogen was assumed to be at equilibrium with the liquid phase.

The Henry's law constant used for hydrogen was 75,000 atmospheres (54). The rate of production of hydrogen per mole of water passing through the test section is given by the following:

$$N_{R,H_2} = \frac{N_3}{A}\left(\frac{N_2\, x_{2,H_2}}{N_3} + \frac{x_{2,H_2}}{H_{H_2}}\right) \qquad (4\text{-}4)$$

where the subscripts "2" and "3" refer to the vapor and liquid phases respectively. The natural logarithm of the rate of hydrogen generation was calculated and is listed in Table 14 along with the percentage of oxygen removed and the percentage of oxygen reacted. The range of oxygen removed was between 33% and 90%. The natural logarithm of the hydrogen generation rate which ranged up to -10.6 also is plotted for various conditions in Figures 13 through 17 as a function of the reciprocal of the absolute wall temperature. The wall temperature ranged between 743°C and 1143°C. These figures illustrate that the logarithm of the hydrogen generation rate increases

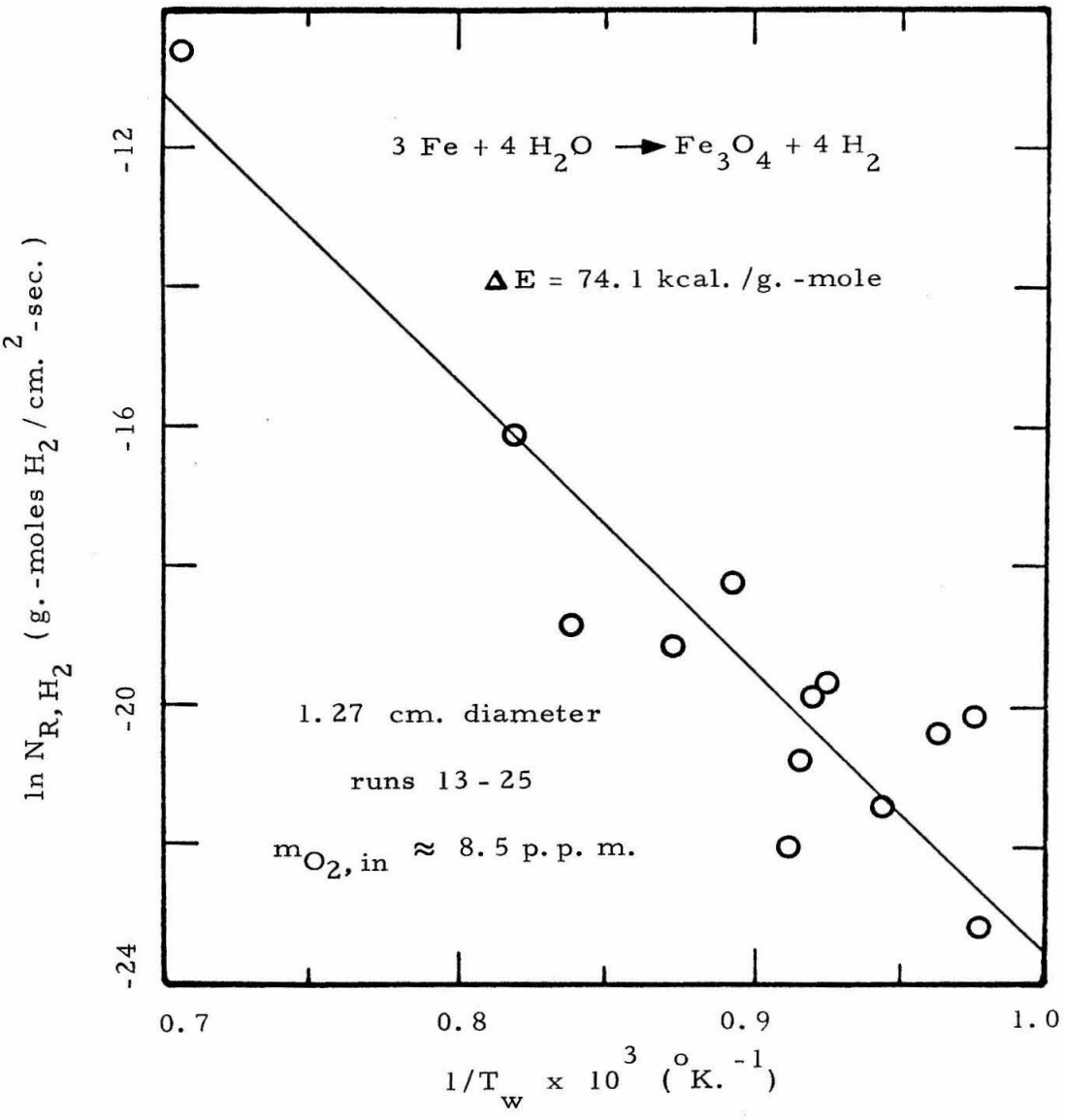

Figure 13. -- Rate of hydrogen generation as a function of temperature.

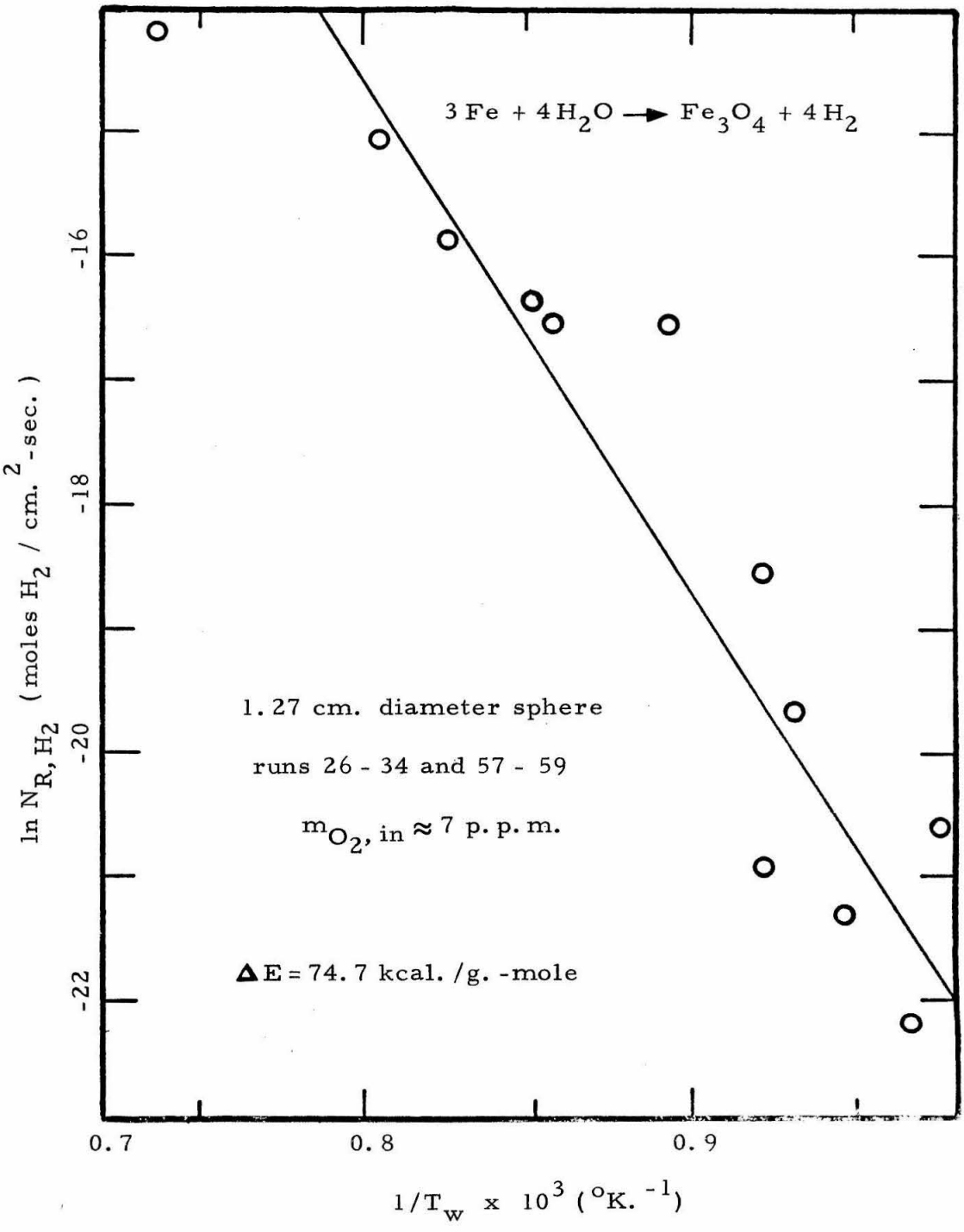

Figure 14. -- Rate of hydrogen generation as a function of temperature.

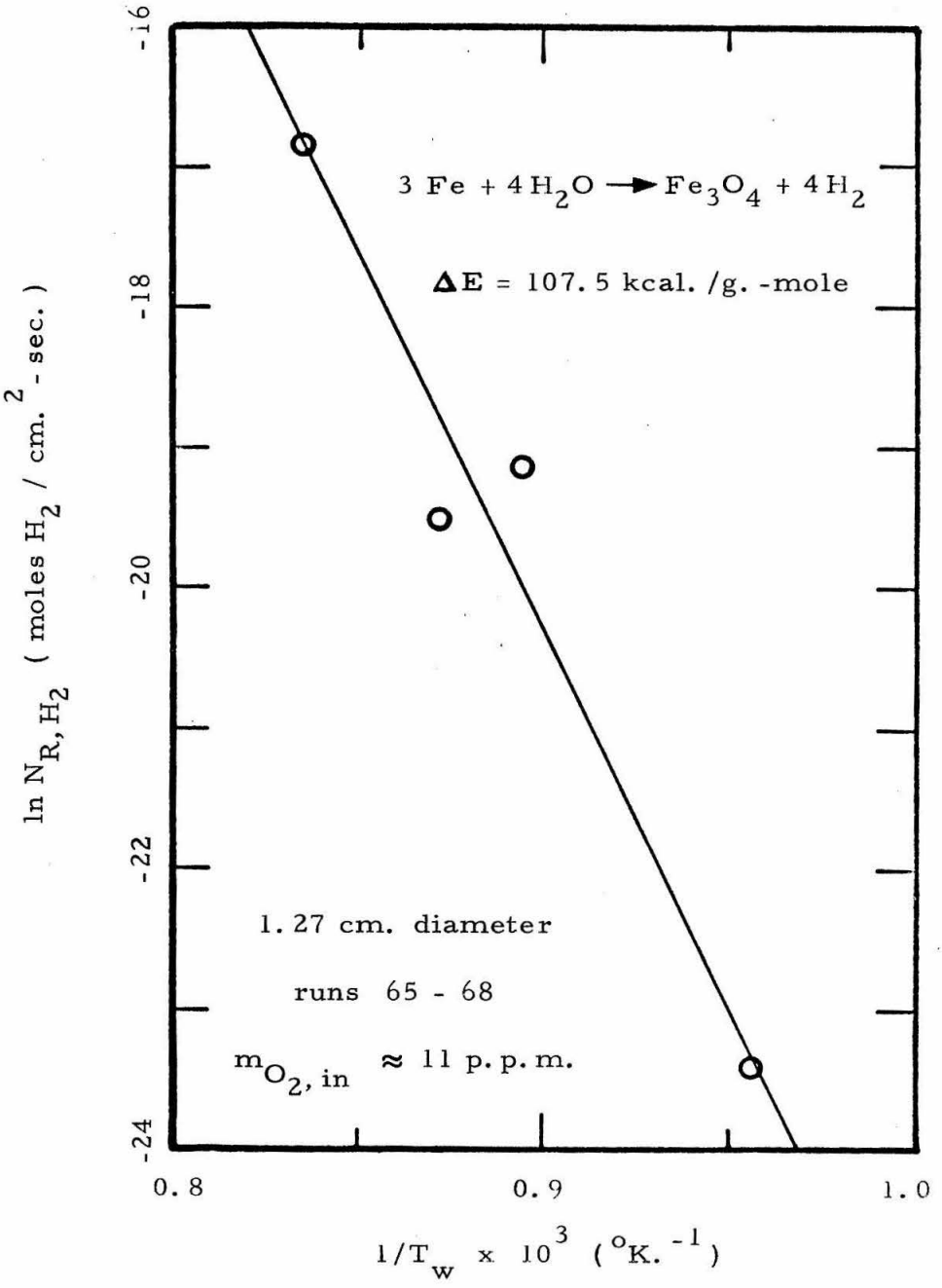

Figure 15. --Rate of hydrogen generation as a function of temperature.

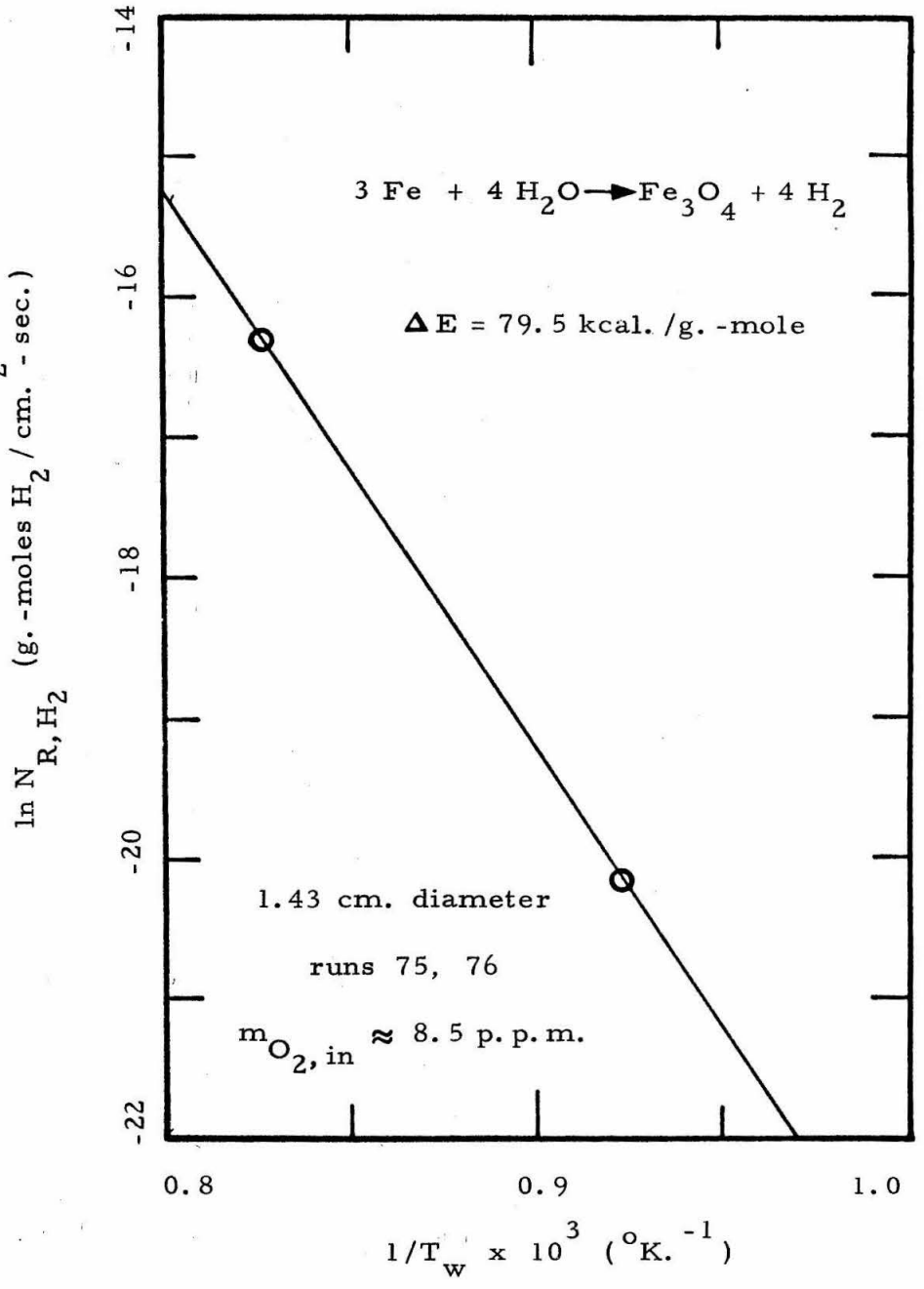

Figure 16. --Rate of hydrogen generation as a function of temperature.

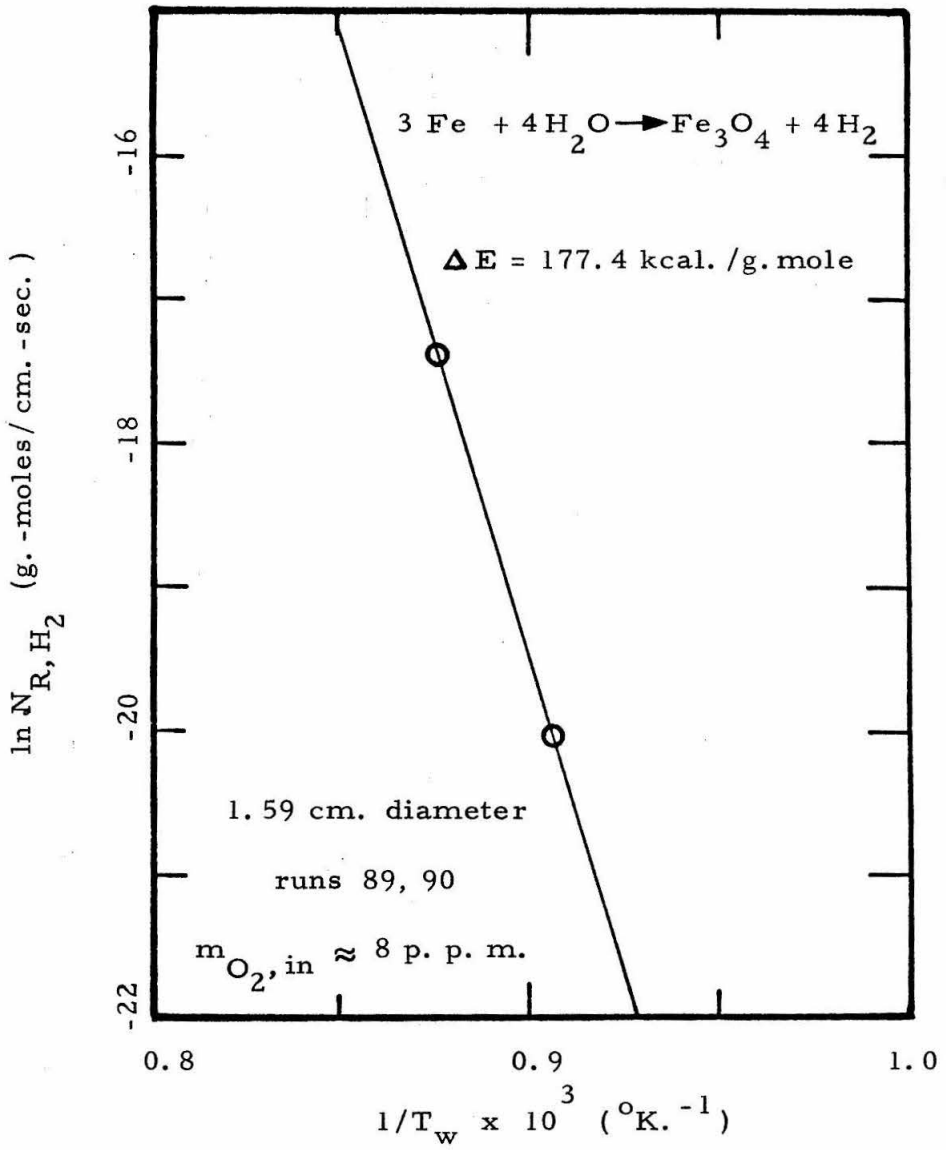

Figure 17. -- Rate of hydrogen generation as a function of temperature.

linearly with increasing temperatures. The scatter in the data is discussed in Appendix B, "Error Analysis", and in Chapter V, "Conclusions of Investigation". The results of the rate of hydrogen generation on gold plated spheres are discussed in detail in Appendix D.

Data for a steam-carbon steel reaction have been published by Potter et al. (56). Their results showed that the reaction has an activation energy of 23.2 kilocalories per gram-mole. Their reaction rates have been plotted as a function of the reciprocal absolute temperature in Figure 18. In their experiments the temperature varied between 800°F and 1200°F.

Data for an oxygen-mild steel reaction have been published by Potter et al. (57). These reaction rates were plotted as a function of reciprocal absolute temperatures in Figure 19. The temperatures used in this investigation ranged from 500°C to 1200°C. These results indicate that this reaction has an activation energy of 22.9 kilocalories per gram-mole.

Heat Transfer Coefficient

The overall heat transfer rate convective and conductive heat transfer was determined by the following:

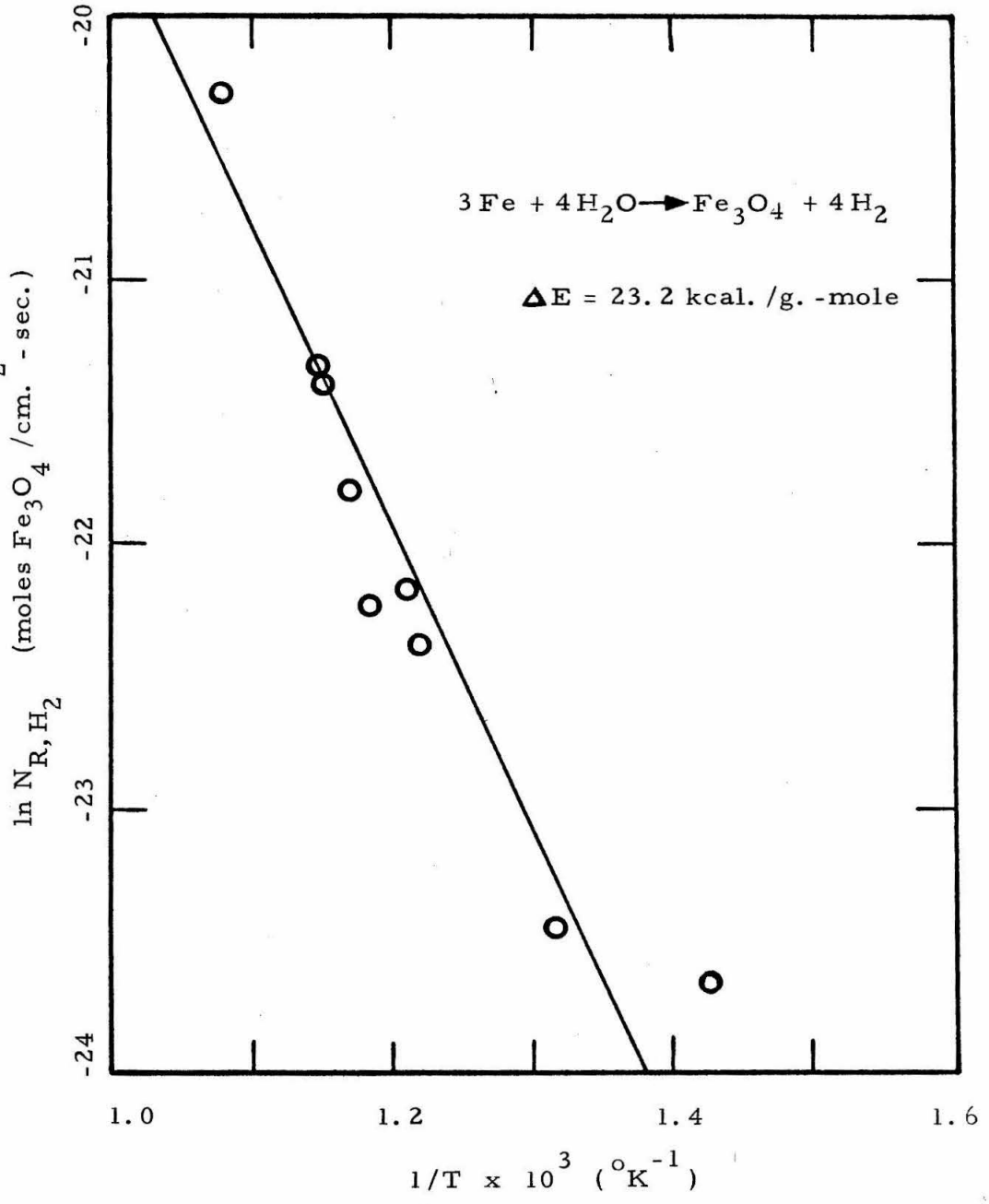

Figure 18. -- Published data for the reaction of steam with carbon steel. (56)

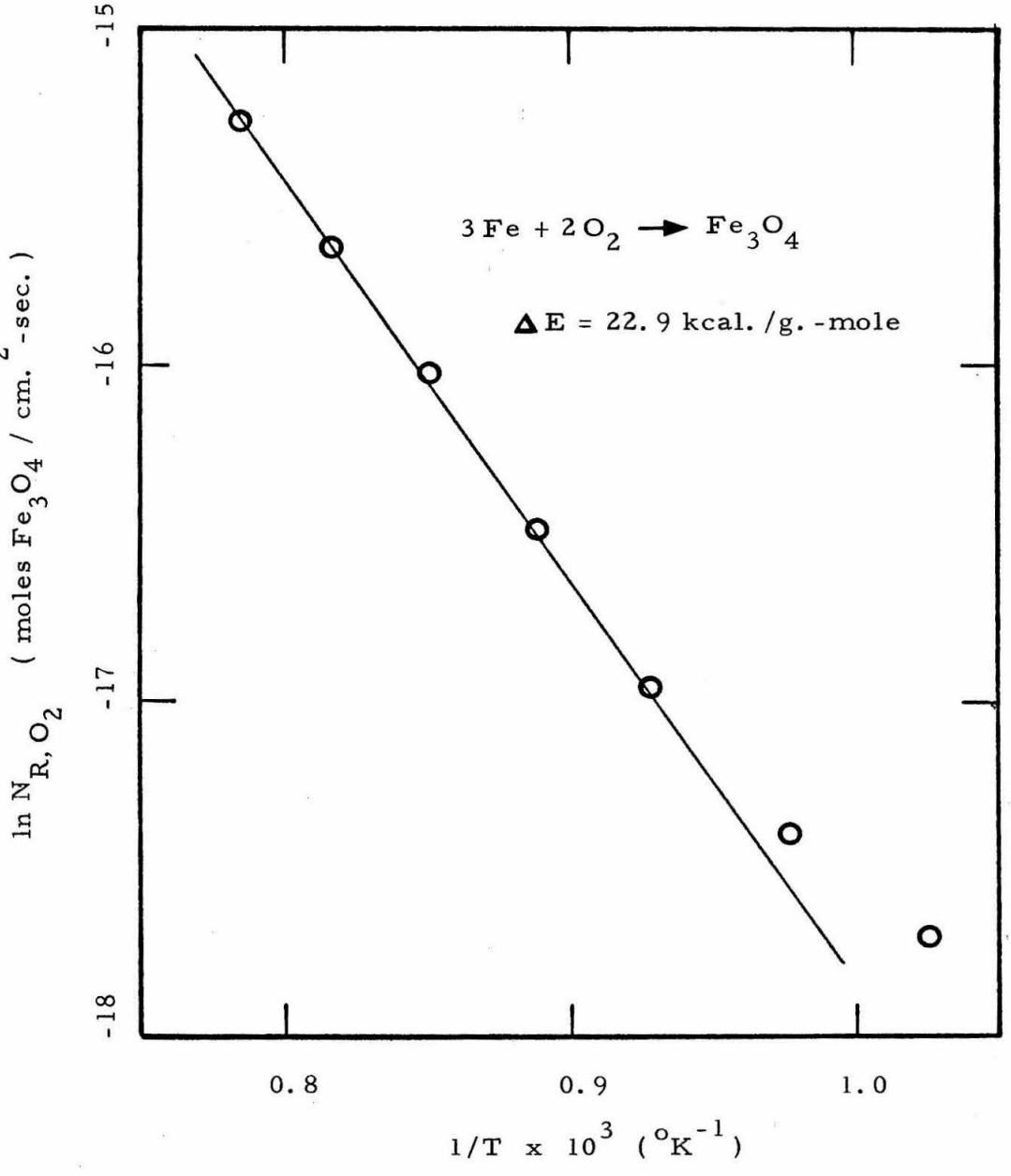

Figure 19. -- Published data for the reaction of oxygen with mild steel (57).

$$q_c = \left(\frac{w\, c_{p,l} (T_o - T_{in})}{A} \right) - q_r \qquad (4\text{-}5)$$

To find an approximation of the rate of radiative heat transfer, the following equation was used:

$$q_r = \sigma_{SB} (T_w^4 - T_s^4) \qquad (4\text{-}6)$$

The above formula is valid if the wall of the sphere and the liquid are black bodies.

The overall heat transfer coefficient for convective and conductive heat transfer was calculated by

$$\bar{h} = \frac{q_c}{T_w - T_s} \qquad (4\text{-}7)$$

The above heat transfer rate and heat transfer coefficient are tabulated for Runs Number 1 - 90 in Table 15 of Appendix G; the heat transfer rate for Run Number 91 is discussed in Appendix C. The heat transfer coefficients were found to vary from 0.26 to 5.3 calories per square centimeter-second-^{o}C.

Next, r was found from Equation (3-30),

$$\bar{h} = 2.7 \left[\frac{k_v \ \rho_v \ \lambda'' u_\infty \ m_k}{D \ \Delta T \ r} \right]^{1/2} \qquad (3\text{-}30)$$

where

$$k_v = \sum_{i=k}^{j} k_{i,v} \, x_{i,v} \qquad (3\text{-}24)$$

and

$$\rho_v = \sum_{i=k}^{j} x_{i,v} \ \rho_{i,v} \qquad (3\text{-}16)$$

and

$$\lambda'' = \sum_{i=k}^{j} c_{p,v,i} \, m_i \, (T_2 - T_s) / m_k - c_{p,l} \, (T_7 - T_s) + \lambda \qquad (3\text{-}14)$$

The constant used in Equation (3-30) was 2.7 as suggested by Witte (69).

The values of $k_{i,v}$ were obtained from the following:

$$k_{i,v} = k_i^* \left\{ 1 + \alpha_i \left[\left(\frac{T_2 - 100^\circ C}{2} \right) + 100^\circ C \right] \right\} \qquad (4\text{-}8)$$

The values of k_i^* and α_i were obtained from the International Critical Tables (51) and are listed in Table 4. The values of $\rho_{i,v}$ were obtained from the ideal gas law using an average film

TABLE 4

PHYSICAL PROPERTIES USED IN HEAT TRANSFER ANALYSIS (51) (33)

Component	$k_i^* \times 10^5$ (cal/cm^2 - sec - ^oC)	α_i ($^oC^{-1}$)	$c_{p,v,i}$ (cal/g - mole - ^oC)
H_2O	5.63	0.00359	8.82
H_2	3.80	0.00277	7.07
N_2	5.45	0.00291	7.30
O_2	5.57	0.00310	7.71

temperature. The values of $c_{p,v,i}$ used also are listed in Table 4. The value of u_∞ was obtained from the following:

$$u_\infty = \frac{w}{\frac{\pi}{4}\left(D_t^2 - D^2\right)\rho_1} \tag{4-9}$$

where D_t is the diameter of the test section.

The saturation temperature was calculated from

$$T_s = \frac{1}{\frac{1}{T_{BP}} - \frac{R \ln x_{k,2}}{\lambda}} \tag{3-66}$$

The values of the experimentally obtained heat transfer coefficient, the saturation temperature, the percentage heat transer by radiation, and the subcooling parameter, r, are tabulated in Table 15. The subcooling parameter ranged from 6×10^{-4} to 3×10^{-2}.

The Reynolds number for the liquid flow was calculated by using the following approximation for the liquid viscosity (66):

$$\mu_1 = (0.814 - 0.0053\ T_s)\ \text{cp.} \tag{4-10}$$

The values of the subcooling parameter, r, have been plotted as a function of the Reynolds number in Figures 20 through 23. The points plotted are those at which the sphere surface temperature was

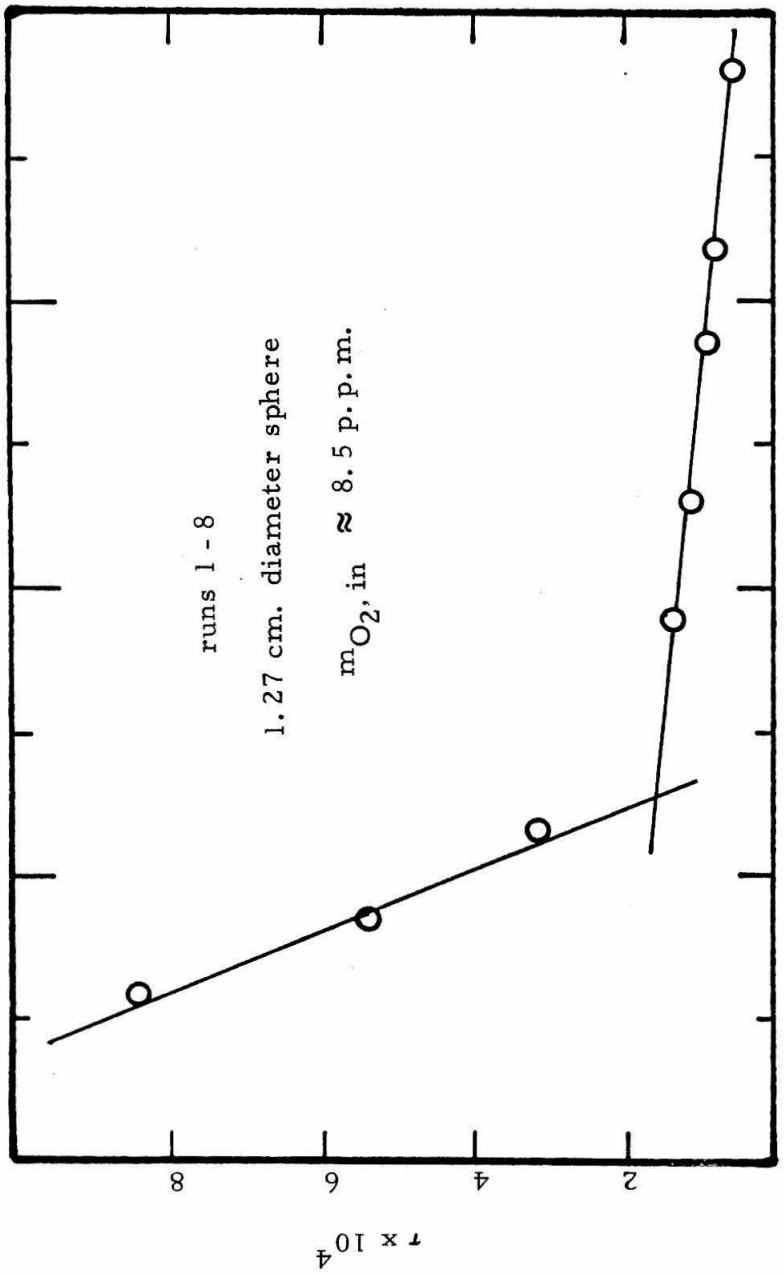

Figure 20.--Subcooling parameter versus Reynolds number.

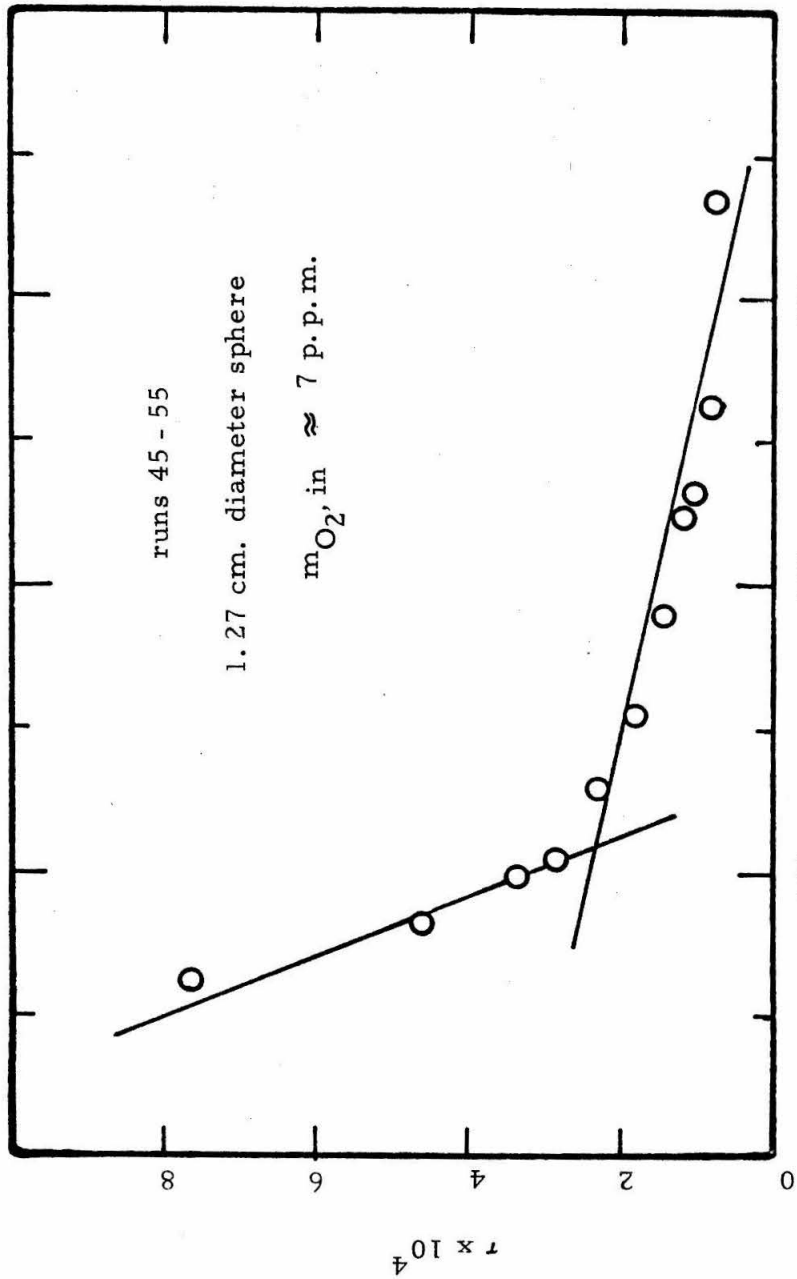

Figure 21.--Subcooling parameter versus Reynolds number.

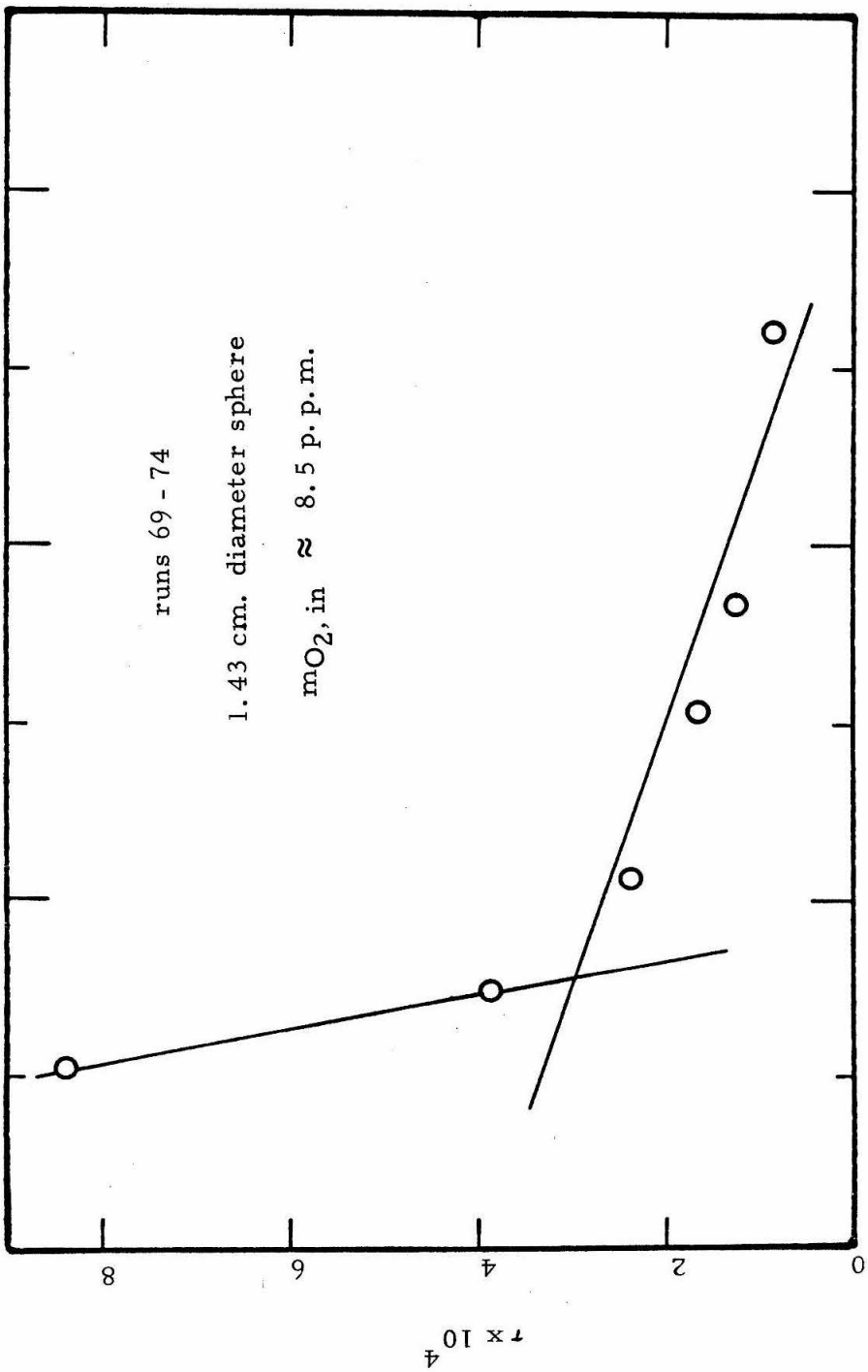

Figure 22. --Subcooling parameter versus Reynolds number.

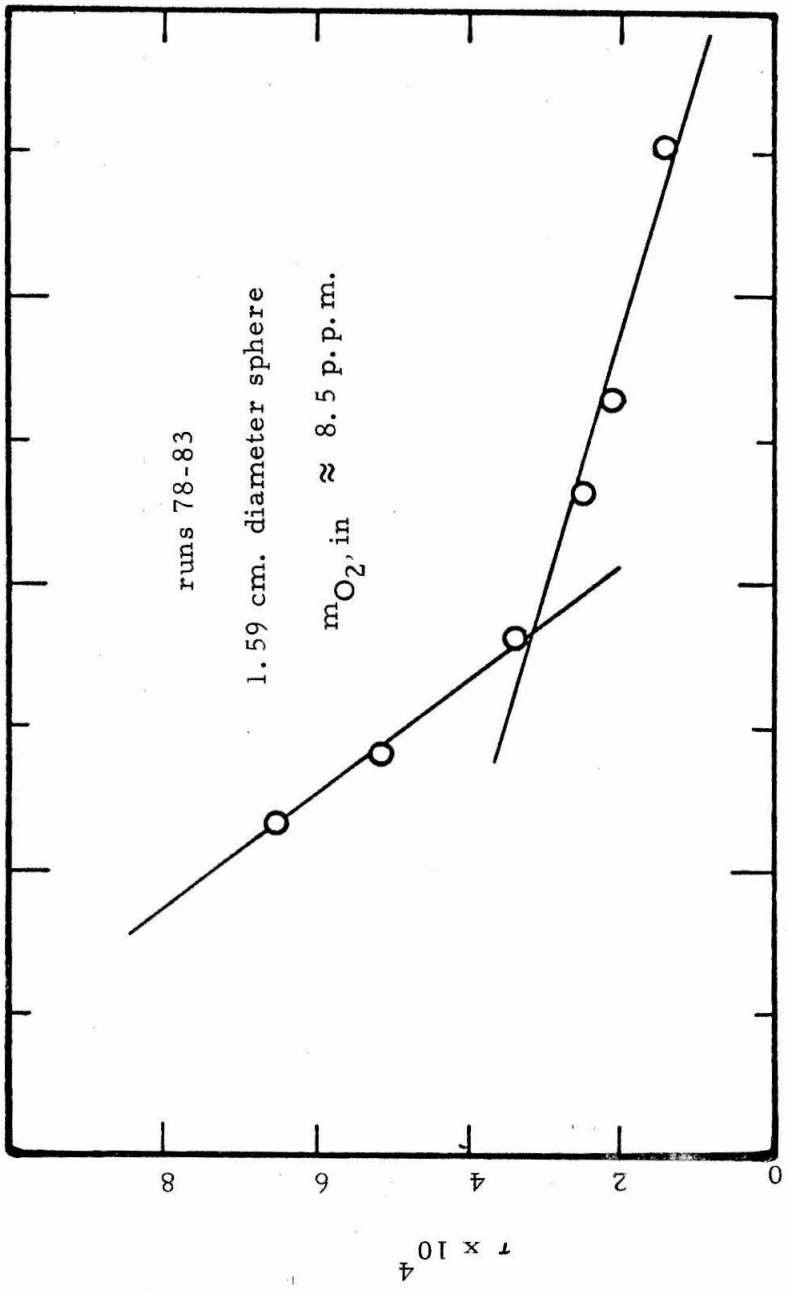

Figure 23.--Subcooling parameter versus Reynolds number.

approximately 750°C. It may be seen that for large Reynolds numbers r increases rapidly. This is a result of a breakdown in the model at low Reynolds numbers. There were bubbles leaving the film at these low Reynolds numbers because there was insufficient cool liquid to condense the bubbles.

Equation (3-21) was used to calculate the mass ratio vaporized;

$$\frac{w_2}{w_3} = \frac{c_{p,1} (T_o - T_{in})}{m_k \lambda''} \qquad (3\text{-}21)$$

Then, the mass ratio was converted to a molar ratio.

The Nusselt number for heat transfer from the vapor-liquid interface to the liquid was obtained from the following:

$$\overline{Nu_{D,1}} = \frac{2 (1 - r) q_c D}{k_1 \Delta T_1} \qquad (3\text{-}39)$$

where

$$\Delta T_1 = T_s - T_{in} \qquad (3\text{-}37)$$

The values of k_1 were obtained from the International Critical Tables (51).

The liquid Prandtl number and the Reynolds number - Prandtl number product were computed. These values plus the Nusselt number for the heat transfer into the liquid, the Reynolds number for the liquid, and the fraction of the liquid vaporized are tabulated in Table 16. The Reynolds number varied between approximately 60 and 700; the liquid Prandtl number varied between approximately 1.7 and 2.4.

The validity of the following relationship was checked by plotting $\overline{Nu_{D,1}}$ as a function of the product $Re_D Pr_1$:

$$\overline{Nu_{D,1}} = f(Re_D, Pr_1) \qquad (3\text{-}41)$$

As illustrated by Figures 24, 25, and 26, a good linear correlation exists between $Nu_{D,1}$ and the product, $Re_D Pr_1$. This correlation is discussed in greater detail later in this chapter.

All of the experimental data were not used in these figures, since many runs were made at duplicate values of the Reynolds number-Prandtl number product. The correlation is different for the various diameter spheres, but no attempt was made to find a geometrical factor to correlate the difference. The geometry is complex and spheres of only three diameters were used in the experiments. The dependence on the liquid Prandtl number could not be determined

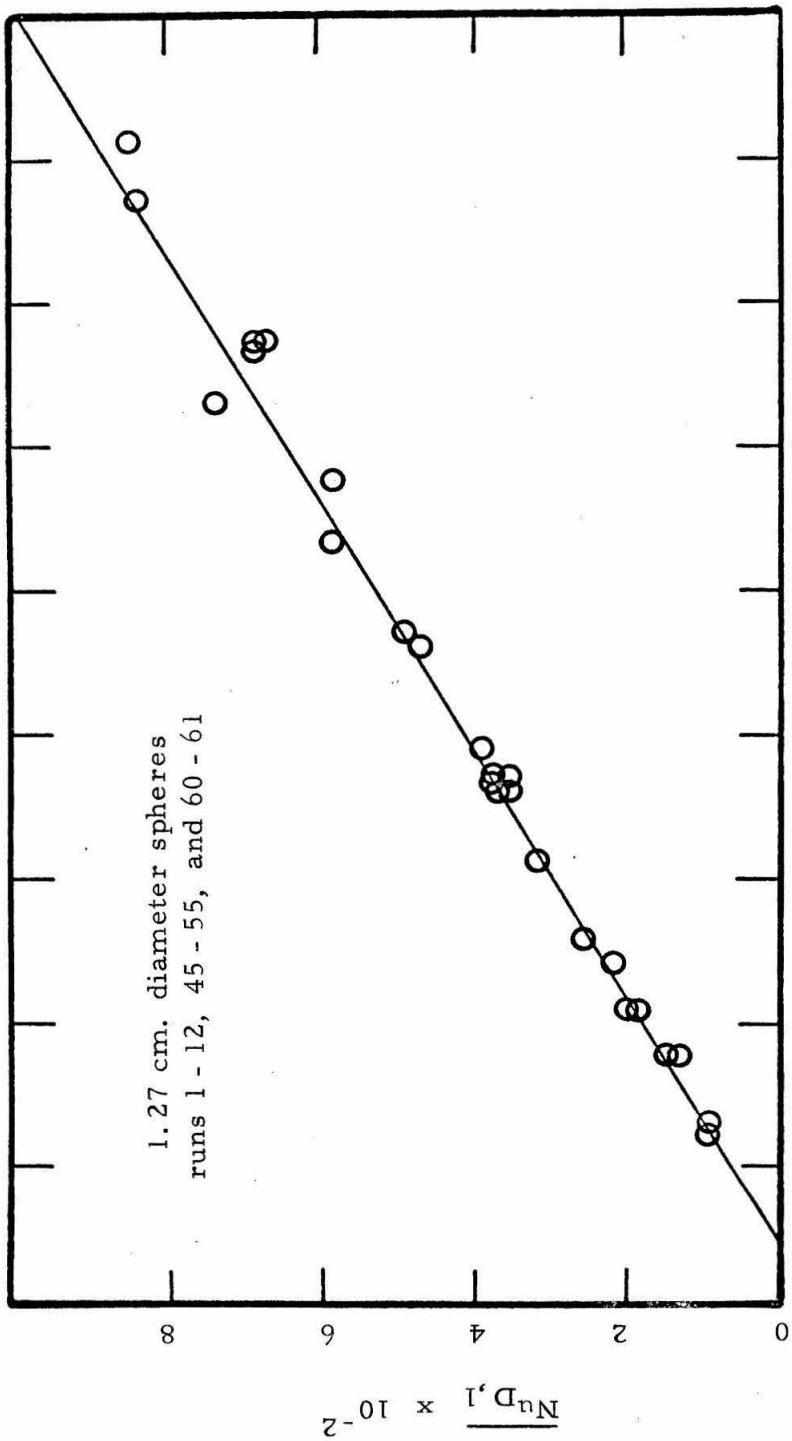

Figure 24. --Nusselt number for heat transfer to liquid on 1.27 cm. diameter sphere.

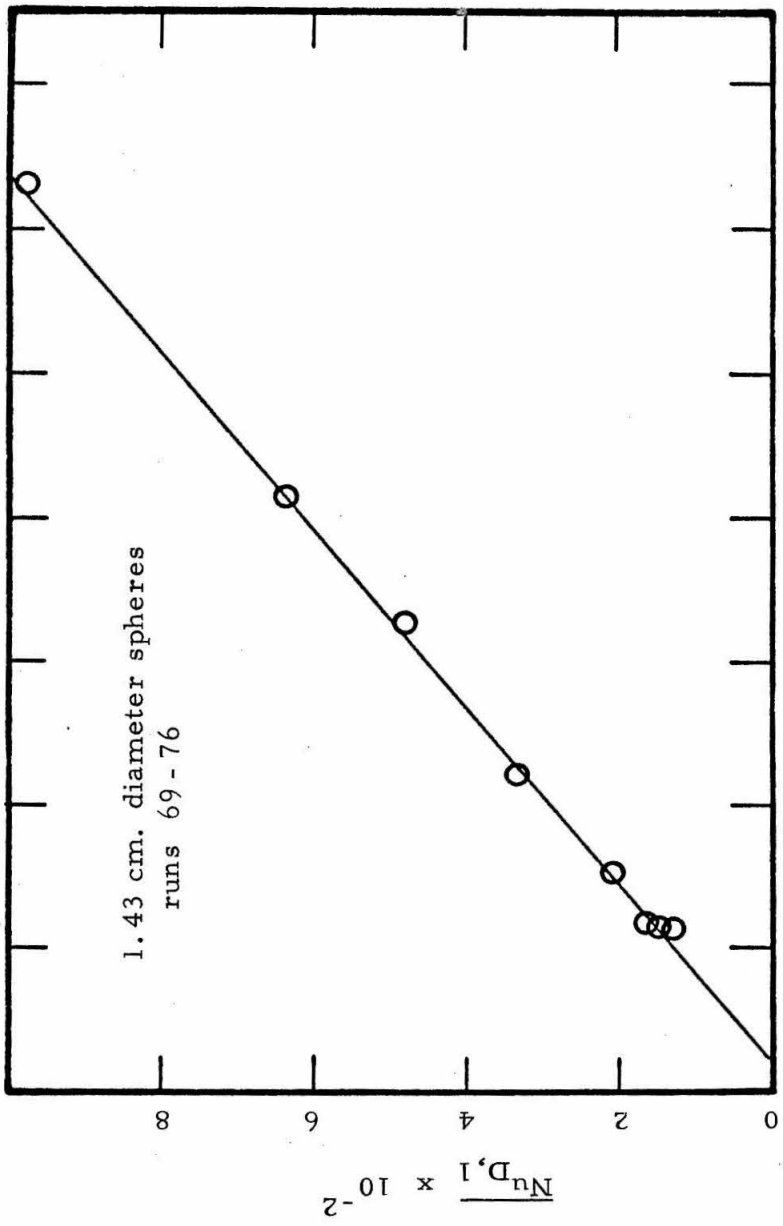

Figure 25.--Nusselt number for heat transfer to the liquid on 1.27cm. diameter sphere.

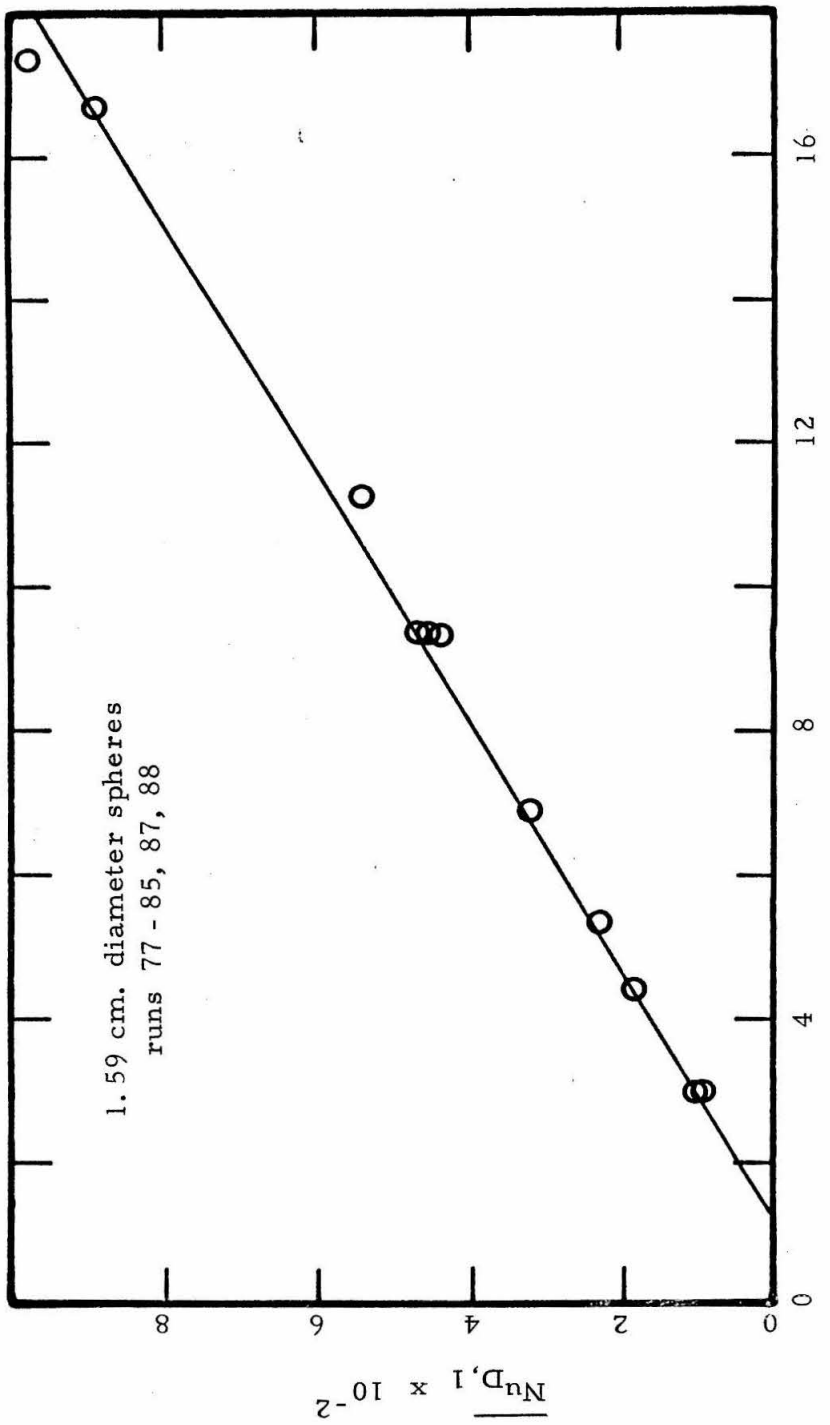

Figure 26.--Nusselt number for heat transfer to the liquid on 1.59 cm. diameter sphere.

accurately since the Prandtl number was approximately constant in all cases.

The applicability of the following equation was examined:

$$\frac{x_{j,o}}{x_{j,in}} = \frac{1}{1 + \frac{N_2 H_j}{N_3 P_{atm}}} \tag{3-62}$$

The above equation was rearranged to yield the percentage of oxygen removed,

$$\%O_2 \text{ removed} = \left\{ 1 - \frac{1}{1 + \frac{N_2 H_{O_2}}{N_3 P_{atm}}} \right\} x\,100\% \tag{4-11}$$

Equation (4-11) resulted in the solid lines in Figures 27 through 30. The data points in these figures were obtained by plotting the percentage of oxygen removed determined by the oxygen measurements using Equation (4-3) as a function of the mole ratio vaporized determined by the heat transfer measurements using Equation (3-21). Only the points in the region in which the model was valid were plotted. The points plotted are those on the constant r portions of Figures 20 through 23. For the points plotted, the percentage oxygen actually removed was within 20% of the theoretical percentage,

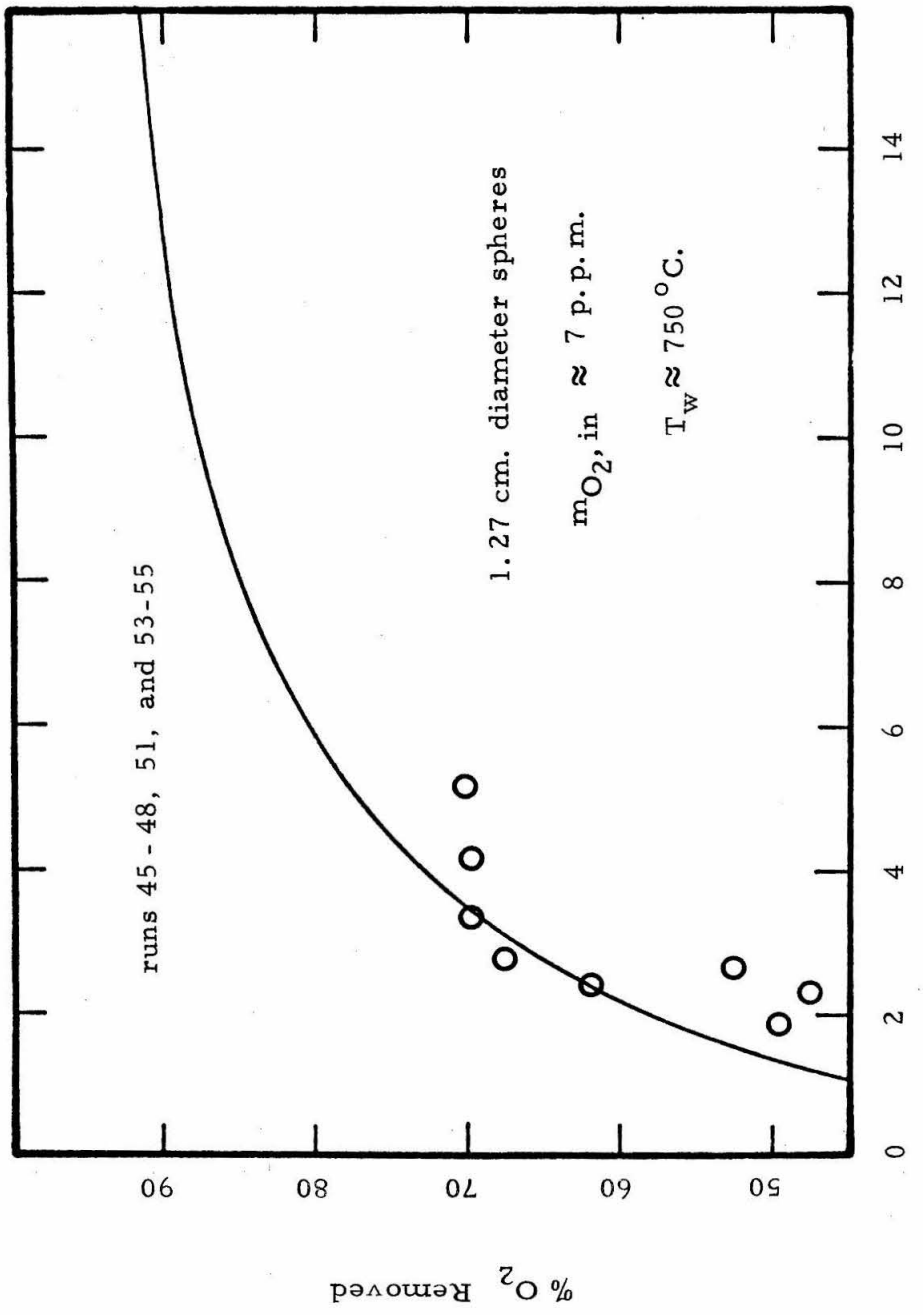

Figure 27.-- Percentage oxygen removed at various fractions vaporized.

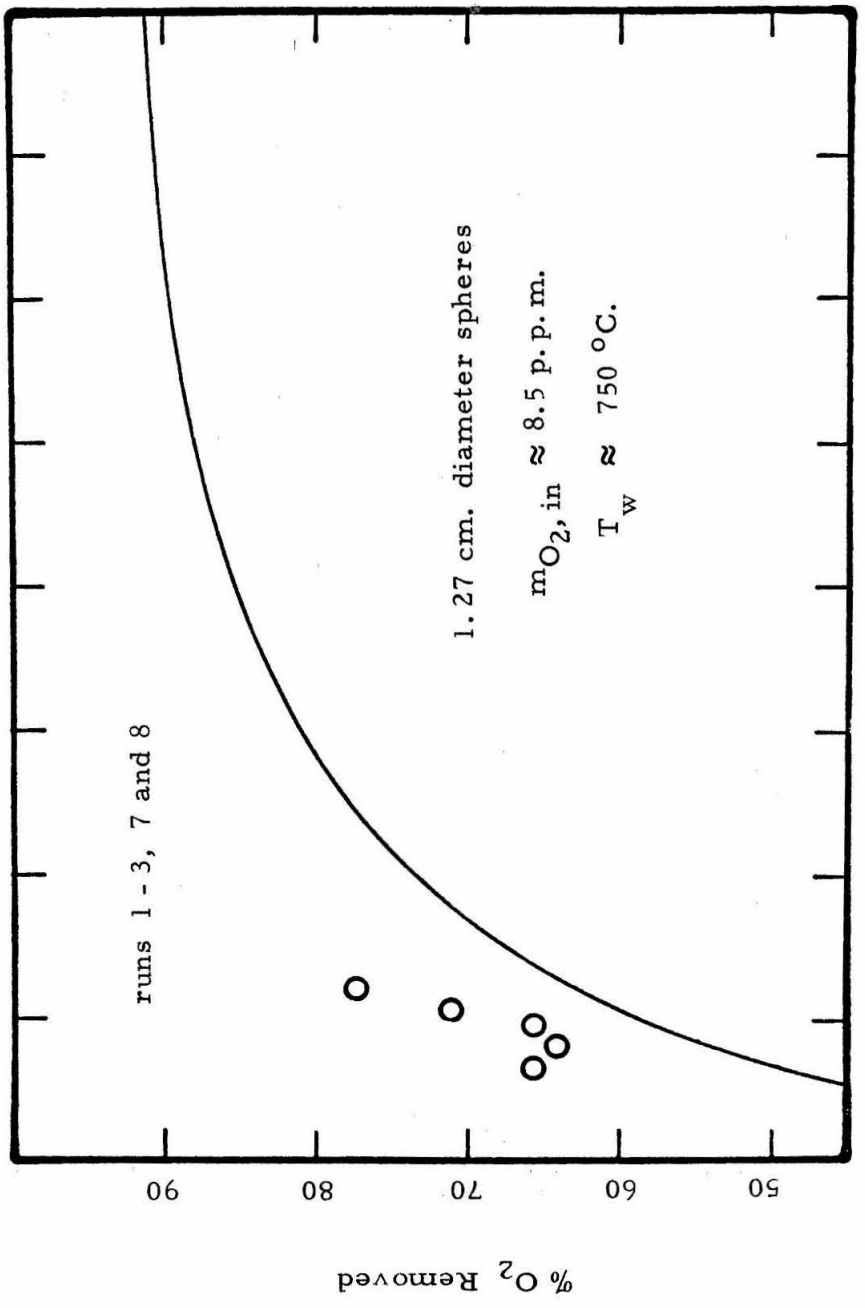

Figure 28. --Percentage oxygen removed at various fractions vaporized.

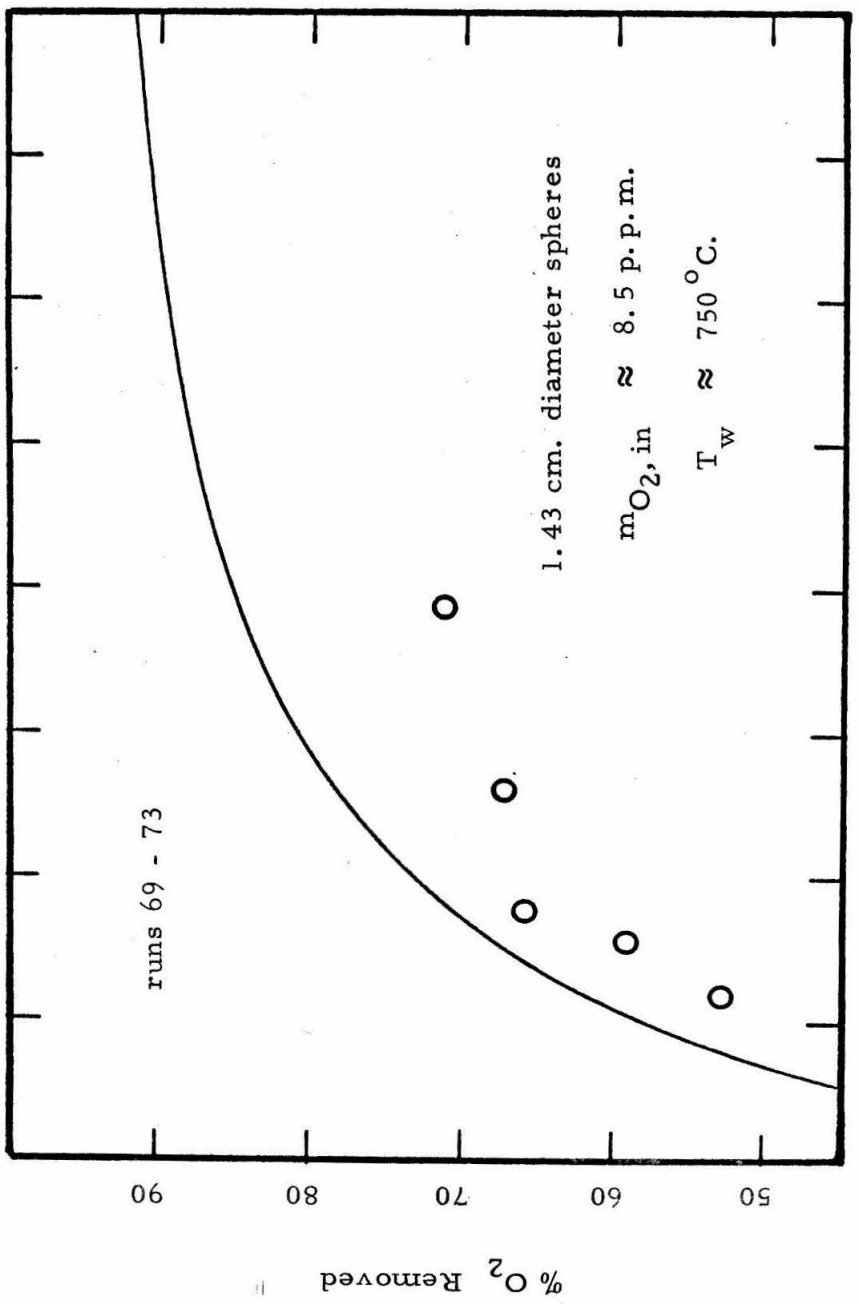

Figure 29.--Percentage oxygen removed at various fractions vaporized.

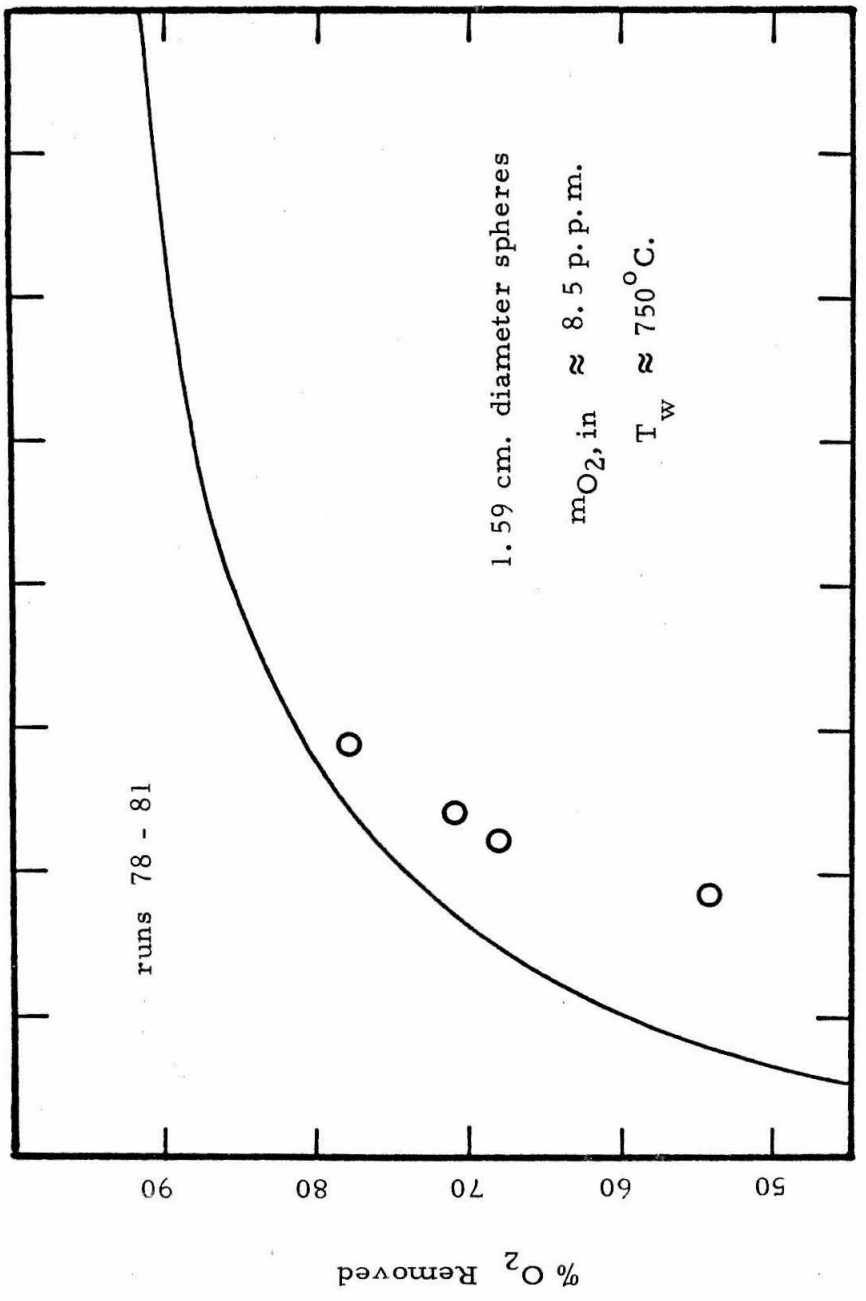

Figure 30. -- Percentage oxygen removed at various fractions vaporized.

and in most cases, the percentage actually removed was within 10% of the theoretical percentage. Therefore, it was concluded that the heat transfer results may be used to give an acceptable indication of the quantity of oxygen removed during highly subcooled film boiling. Although the model considered in Chapter III was quite simple, the model has been shown by Figures 27 through 30 to yield consistent results for runs in which the vapor condensed before leaving the film.

Discussion of Results

During the experimental runs non-condensables were removed from the boiling water. These non-condensables were analyzed with a gas chromatograph and found to contain oxygen, nitrogen, and hydrogen. By using the equations described in Chapter III, the composition of the film was obtained. The error analysis given in Appendix B indicated that the error in measuring the concentration of the oxygen was less than 9%; however, the error in measuring the concentration of the nitrogen and hydrogen in the film was as much as 15% and 21% respectively.

Since the error in the calculated rate of hydrogen production may reach a maximum of 47%, there could be scatter of the points in a plot of hydrogen generation rate versus reciprocal absolute

temperature. The rate of the surface reaction depended on the conditions of the surface. For example, during Run Number 77 a crack developed in the sphere and a local "hot spot" appeared near the crack. An unusually large hydrogen concentration was present during this run; as a result, the datum point was not used in any figure. The lack of accuracy in the calculation of the hydrogen generation rate and the dependence of this rate on surface conditions resulted in the scatter of the points in Figures 13 through 17. Runs 14 and 34 had hydrogen generation rates which were more rapid than the molar flow rate in the film. In these cases, it was assumed that the film was composed completely of hydrogen. An exact determination of the molar flow rate was difficult, since the rate of vaporization almost equaled the rate of reaction of the water vapor.

The results of the investigation of the hydrogen generation using type 440 stainless steel spheres were used to obtain values of the activation energy which was defined in Equation (3-68). The activation energy had an average value of 85 kilocalories per gram-mole. This average was weighted by the number of points in the figures used to obtain the individual activation energies. The activation energy obtained from the experiments of Potter et al. (56) using carbon steel, Figure 18, is 23.2 kilocalories per gram-mole. The

above difference in activation energy probably results from the differences in the steel type.

Run Number 91 as discussed in Appendix C was made with a gold plated sphere at a surface temperature of 869°C. No hydrogen was detected in the collected non-condensables. Since hydrogen was detected in all other runs made with surface temperatures in excess of 770°C using a stainless steel sphere, it was concluded that the gold prevented the formation of hydrogen. In addition, it was concluded that the hydrogen generation reaction occurred heterogeneously at the wall, rather than homogeneously in the film. Appendix D discusses in detail the effect of a varying concentration of gold on the sphere surface.

Table 14 indicates that there was no discernable trend in the rate of chemical reaction of oxygen with temperature. The error in measuring the amount of oxygen reacted appears to be greater than the amount of oxygen reacted. As a result, no plots of the rate of oxygen reaction as a function of reciprocal absolute temperature were made.

The following relationship has been derived in Chapter III:

$$\frac{\overline{Nu_D}}{\sqrt{Re_D}} \frac{\mu_v}{\mu_1} = 2.7 \left[\frac{(\rho\mu)_v \, Pr_v \, \lambda'' m_k}{(\rho\mu)_1 \, c_{p,v} \, \Delta T \, r} \right]^{1/2} \qquad (3-31)$$

The above equation was solved for r for each of the runs. The mass fraction of water in the film, m_k, was obtained as previously discussed. The obtained values of r were plotted as a function of the Reynolds number for several cases. At low Reynolds numbers, the flow rate was not rapid enough to supply cool liquid to the upper regions of the film. This occurred below a Reynolds number of 125 for spheres with a diameter of 1.27 centimeters, below a Reynolds number of 175 for spheres with a diameter of 1.43 centimeters, and below a Reynolds number of 400 for spheres with a diameter of 1.59 centimeters. As a result, the vapor dome became larger and larger as the Reynolds number decreased until the vapor dome reached the burette. The resulting region of instability was approximated by a straight line in Figures 20 through 23. The region in which no bubbles left the film was approximated by a second straight line in the same figures. It was concluded that in the region in which no vapor left the film an accurate measurement of heat transfer was made.

As illustrated by these figures, the error in r was not severe. The largest sources of error in the determination of r were the measurement of the mass flow rate and the measurement of the surface temperature. The maximum expected error in the measurement of the mass flow rate was 17%.

The parameter r is related to the subcooling by

$$r = \frac{q - q_l}{q} \tag{3-34}$$

where q_l is the heat transfer from the vapor-liquid interface into the liquid. Thus, for a liquid at T_s, q_l is zero and r is unity. Equation (3-31) then reduces to the equation derived by Witte (69) for a steam concentration in the film of unity.

Equation (3-43) relates r to the liquid parameters:

$$r = 1 - \left[\frac{\overline{Nu_{D,l}}}{\overline{Nu_D}}\right]\left[\frac{c_{p,l}\,\Delta T_l\,Pr_v}{c_{p,v}\,\Delta T\,Pr_l}\right]\left[\frac{\mu_v}{\mu_l}\right] \tag{3-43}$$

where

$$\overline{Nu_{D,l}} = f(Re_D, Pre) \tag{3-41}$$

Thus, if the functional relationship between the Reynolds number and the liquid Prandtl number is know, the subcooling parameter may be calculated. However, this calculation must be done simultaneously with Equation (3-31), because both equations contain the average overall Nusselt number.

The functional relationship between the Reynolds number-liquid Prandtl number product and the average Nusselt number for heat transfer into the liquid has been investigated with the result of Figures 24 through 26. The correlation is linear as shown in the figures. However, the error analysis suggests that large errors may be present.

The reason for the lack of scatter in the data is apparent by examining Equation (3-39),

$$\overline{Nu_{D,1}} = \frac{2(1 - r)\, q_c D}{k_1\, \Delta T_1} \tag{3-39}$$

This may be rewritten as

$$\overline{Nu_{D,1}} = \frac{(1 - r)\quad (D_t^{\,2} - D^2)}{2\, D^2} \left[\frac{T_o - T_{in}}{T_s - T_{in}}\right] Re_D Pr_1 \tag{4-12}$$

Since

$$r \sim 10^{-4}$$

then

$$\overline{Nu_{D,1}} = \left(\text{constant}\right)\left(Re_D Pr_1\right)\left(\frac{T_o - T_{in}}{T_s - T_{in}}\right) \tag{4-13}$$

Since the Reynolds number-liquid Prandtl number product is plotted on both the ordinate and the abscissa of Figures 24 through 26, these figures actually represent deviations of the following from unity:

$$\frac{T_o - T_{in}}{T_s - T_{in}}$$

The linear plots indicate that

$$(T_o - T_{in}) \alpha (T_s - T_{in}) \qquad (4\text{-}14)$$

The lack of scatter of the points in the linear plots is due to accuracy in temperature measurement rather than accuracy in flow rate measurement.

It was concluded that the functional relationship between the Reynolds number, liquid Prandtl number and the Nusselt number for heat transfer into the liquid is not the simple relationship obtained by Sideman, Equation (A-36). This conclusion was reached upon examining preliminary data; the conclusion is discussed fully in Appendix J. The geometry of the test section makes the actual Reynolds number - Nusselt number relationship difficult to obtain and of little value for other systems. A mathematical relationship

was not obtained; the results were left in the form of Figures 24, 25, and 26.

The subcooling parameter is a function of the fraction vaporized in a bounded system. Equation (3-21) may be used to obtain the fraction vaporized;

$$\frac{w_v}{w_l} = \frac{c_{p,l}\, r\, (T_7 - T_l)}{m_k\, \lambda''} \tag{3-21}$$

In a bounded system with an equilibrium existing between the gases in the vapor and the gases dissolved in the liquid, the composition of the film is given by Equation (3-49)

$$x_{j,v} = \frac{x_{j,l}\, P_{atm}}{H_j} \tag{3-49}$$

The outlet concentration is related to the inlet concentration by

$$\frac{x_{j,o}}{x_{j,in}} = \frac{1}{1 + \frac{N_v\, H_j}{N_l\, P_{atm}}} \tag{3-62}$$

Thus, r may be used to determine concentrations in the film. The

relationship between the fraction vaporized and the percentage oxygen removed has been obtained using the above equations and is plotted in Figures 27 through 30. The data points represent both the oxygen measurements and the heat transfer measurements. The oxygen measurements were used to determine the percentage of oxygen removed; the heat transfer measurements were used to determine the fraction vaporized. This relationship has been plotted only for the region in which no vapor leaves the film. The points lying outside of this region represent runs in which vapor left the film causing a breakdown of the model. Figures 27 through 30 were made for runs in which no vapor left the film. These figures demonstrate that the subcooling parameter may be used to obtain an estimate of the amount of oxygen removed during a run. This estimate will usually be within 10%. Therefore, the subcooling parameter also may be used to obtain an estimate of the concentration in the film.

CHAPTER V

CONCLUSIONS OF INVESTIGATION

Six conclusions were reached by analyzing the results of the experimental investigation:

1. An experimental apparatus was designed which permitted steady state film boiling on a sphere supported by the liquid flow. The sphere temperature was varied from 740°C to 1140°C and the Reynolds numbers were varied from approximately 60 to 700. It was concluded that because the sphere temperature remained constant throughout an experimental run, this design is an improvement over previously reported designs featuring transient systems.

2. During the forced convection film boiling of a subcooled liquid around a small sphere, the subcooled liquid may cause the vapor to condense before it leaves the film. Thus, the heat transfer effects counteract the effect of the Rayleigh-Taylor instability. This phenomena was used in the film boiling of water subcooled between 52 C° and 72 C° to facilitate the measurement of heat transfer rates.

3. If dissolved gases are present in a film boiling liquid, the gases will accumulate in the film. In this manner film boiling was used to remove up to 90% of the dissolved oxygen from water.

4. If during film boiling, the wall is composed of a material which may react chemically with the vapor, a hetrogeneous chemical

reaction may occur. When a steel wall is used in film boiling water, the steel may react with the water vapor and generate hydrogen. If the wall is composed of type 440 stainless steel, the activation energy of the above reaction is approximately 85 kilocalories per gram-mole. A chemical reaction at the wall may be eliminated by plating the wall with gold.

5. Equations were developed for determining the average overall Nusselt number as a function of the physical properties of the vapor, the Reynolds number, the mass fraction water vapor in the film, the temperature difference and a subcooling parameter. The subcooling parameter may be found from an equation as a function of the vapor and liquid properties, the temperature difference between the interface and the liquid, and the Nusselt number for the heat transfer from the interface into the liquid. This Nusselt number for heat transfer into the liquid is a function of the Reynolds number and the liquid Prandtl number.

6. If the forced convection film boiling around a sphere occurs in a bounded system in which the gases in the film are at equilibrium with the dissolved gases in the liquid, the subcooling parameter may be used to find the amount of dissolved gases remaining after the film boiling and to find the concentrations in the film.

NOTATION

English Symbols

A	surface area, cm.^{2}
A_i	chromatogram area for species "i", relative scale.
c_p	heat capacity, cal./g.-^oC.
D	diameter, cm.
f	frequency, Hz.
g	acceleration of gravity, cm./sec.^{2}
h	local heat transfer coefficient, cal./sec.-cm.^{2}-^oC.
$\bar{h}$	average heat transfer coefficient, cal./sec.-cm.^{2}-^oC.
H	Henry's law constant, atm.
k	thermal conductivity, cal./sec.-cm.-^oC.
L	length, cm.
m_i	mass fraction of species "i".
M_i	molecular weight of species "i".
N	molar flow rate, g.-moles/sec.
N_R	molar reaction rate, g.-moles/sec.-cm.^{2}
P_i	partial pressure, atm.
P	total pressure, atm.
q	heat transfer rate, cal./sec.-cm.^{2}
r	spacial coordinate, cm.
R	radius, cm.

t	time, sec.
u	velocity in x direction, cm./sec.
$\bar{u}$	average velocity, cm./sec.
v	velocity in y direction, cm./sec.
V	volume, ml.
V^*	volume corrected for determinate errors, ml.
w	mass flow rate, g./sec.
x	spacial coordinate, cm.
x_i	mole fraction of species "i".
y	spacial coordinate, cm.

Greek Symbols

α	absorptivity for radiation.
δ	film thickness, cm.
$\delta\gamma$	error in γ .
ΔE	activation energy, kcal./g.-mole.
ΔT	wall temperature minus saturation temperature, $^{o}C.$
ΔT_l	saturation temperature minus liquid temperature, $^{o}C.$
ϵ	emissivity for radiation.
θ	angle, radians.
κ	chromatograph calibration constant.
λ	latent heat of vaporization, cal./g.

$\overline{\lambda}$ wavelength, cm.

μ viscosity, dyne-sec./cm.^{2}

ξ manometer reading, cm. Hg.

ρ density, g./ml.

σ surface tension, dyne/cm.

σ_{SB} Stefan-Boltzman constant, cal./cm.^{2}-$^oK^4$

τ subcooling parameter.

Dimensionless Numbers

Gr_D Grashof number for two phase convection,

$$D^3 g \rho_v (\rho_l - \rho_v) / \mu_v^2$$

Nu_D local Nusselt number, hD/k.

$\overline{Nu_D}$ average Nusselt number, $\overline{h} D/k$.

Pr Prandtl number, $c_p \mu / k$

Re_D Reynolds number, $Du \rho / \mu$

Subscripts

air non-condensables

B bulk

BP normal boiling point

c convection and conduction

cool after ten minutes

D	indicates dimensionless number is based on characteristic diameter.
f	final.
h	immediate.
i	initial.
in	inlet.
j	solute.
k	solvent.
l	liquid.
L	indicates dimensionless number is based on characteristic length.
o	outlet.
r	radiation.
res	reservoir.
R	reacted.
s	saturation.
t	test section.
T	total.
v	vapor.
w	wall.
∞	free steam.

NOTE: Numerical subscripts refer to points in Figure 8.

LIST OF REFERENCES

1. Bankoff, S. G., "Taylor Instability of an Evaporating Plane Interface," A. I. Ch. E. J., 7, 485 (1961).

2. Beckman Instruments, Inc., "Fieldlab Oxygen Analyzer," Beckman Instruments, Inc., Fullerton, California, 1968.

3. Berenson, P. J., "Film-Boiling Heat Transfer from a Horizontal Surface," Trans. A. S. M. E., J. Heat Transfer, 81, 351 (1961).

4. Bradfield, W. S., "Liquid - Solid Contact in Stable Film Boiling," Ind. Eng. Chem. Fundamentals, 5, 2000 (1966).

5. Bradfield, W. S., "Wave Generation at a Stagnation Point in Stable Film Boiling," Paper read before the Internation Two Phase Flow Symposium , University of Exeter, Exeter, England, June, 1965.

6. Bradfield, W. S., Barkdoll, R. O., Byrne, J. T., "Some Effects of Boiling on Hydrodynamic Drag," Int. J. Heat and Mass Transfer, 5, 615 (1962).

7. Brauer, H., "Stromung und Warmeubergang bei Rieselfilmen," VDI - Forschungsheft 457, 22, Edition B, 1.

8. Bromley, L. A., "Effect of Heat Capacity of Condensate," Ind. Eng. Chem., 44, 2966 (1952).

9. Bromley, L. A., "Heat Transfer in Stable Film Boiling," Chem. Eng. Prog., 46, 221 (1950).

10. Bromley, L. A., LeRoy, N. R., Robbers, J. A., "Heat Transfer in Forced Convection Film Boiling," Ind. Eng. Chem., 45, 2639 (1953).

11. Campagne, N. V. L., "Mass Transfer from a Spinning Sphere in a Gas Jet," Paper read before the A. I. Ch. E. - I. Chem. E. Joint Meeting, London, June, 1965.

12. Cess, R. D., "Forced-Convection Film Boiling on a Flat Plate with Uniform Surface Heat Flux," Trans. A. S. M. E., J. Heat Transfer, 85, 395 (1963).

13. Cess, R. D., Sparrow, E. M., "Film Boiling in a Forced-Convection Boundary-Layer Flow," Trans. A. S. M. E., J. Heat Transfer, 83, 370 (1961).

14. Cess, R. D., Sparrow, E. M., "Subcooled Forced-Convection Film Boiling on a Flat Plate," Trans. A. S. M. E., J. Heat Transfer, 83, 377 (1961).

15. Chandrasekhar, S., Hydrodynamic and Hydromagnetic Stability, Oxford University Press, London, 1961.

16. Chang, Y. P., "Wave Theory of Heat Transfer in Film Boiling," Trans. A. S. M. E., J. Heat Transfer, 81, 1 (1959).

17. Chwolson, O. D., Traite de Physique, Vol. III, Part 2, Librairie Scientifique A. Hermann et Fils, Paris, 1909.

18. Drew, T. B., Mueller, A. C., "Boiling," Trans. A. I. Ch. E., 33, 449 (1937).

19. Ellion, M. E., "A Study of the Mechanism of Boiling Heat Transfer," Memorandum 20-88 Jet Propulsion Laboratory, California Institute of Technology, Pasadena, California, 1954.

20. Frederking, T. H. K., "Laminar Two-Phase Boundary Layers in Natural Convection Film Boiling," Zeitschrift fur angewandte Mathematik und Physik, 14, 207 (1963).

21. Frederking, T. H. K., Clark, J. A., "Natural Convection Film Boiling on a Sphere," Advan. Cryog. Eng., 8, 501 (1963).

22. Frederking, T. H. K., Daniels, D. J., "The Relationship between Bubble Diameter and Frequency of Removal from a Sphere during Film Boiling," Trans. A. S. M. E., J. Heat Transfer, 88, 87 (1966).

23. Frederking, T. H. K., Hopenfeld, J., "Laminar Two Phase Boundary Layers in Natural Convection Film Boiling of Subcooled Liquids," Zeitschrift fur Angewandte Mathmatik und Physik, 15, 388 (1964).

24. Frederking, T. H. K., Wu, Y. C., Clement, B. W., "Effects of Interfacial Instability on Film Boiling of Saturated Liquid Helium I above a Horizontal Surface," A. I. Ch. E. J., 12, 228 (1966).

25. Gaertner, R. F., "Photographic Study of Nucleate Pool Boiling on a Horizontal Surface," Report No. 63-RL-3357C, General Electric Research Laboratory, Research Information Section, Schenectady, New York, 1963.

26. Garner, F. H., Jenson, V. G., Keey, R. B., "Flow Pattern around Spheres and the Reynolds Analogy," Trans. Inst. Chem. Eng., 37, 14 (1959).

27. Gottfried, B. S., Bell, K. J., "Film Boiling of Spheroidal Droplets," Ind. Eng. Chem. Fundamentals, 5, 561 (1966).

28. Gottfried, B. S., Lee, C. J., Bell, K. J., "The Leidenfrost Phenomena: Film Boiling of Liquid Droplets on a Flat Plate," Int. J. Heat and Mass Transfer, 9, 1167 (1966).

29. Hantman, R. G., Ostrach, S., "The Kelvin - Helmholtz Instability with Arbitrarily Oriented Body Force," Engineering Division, Case Institute of Technology, Cleveland, 1966.

30. Hendricks, R. C., Baumeister, K. J., "Film Boiling from Submerged Spheres," NASA Technical Note No. D-5124, National Aeronautics and Space Administration, Washington, D. C., June, 1969.

31. Hesson, J. C., Witte, L. C., "Comment on 'Film Boiling Heat Transfer around a Sphere in Forced Convection' by K. Kobayasi," J. of Nuclear Science and Technology, 3, 448 (1966).

32. Hodgman, C. D. (ed.), Handbook of Chemistry and Physics, 42nd Edition, The Chemical Rubber Publishing Co., Cleveland, 1960.

33. Hougen, O. A., Watson, K. M., Ragatz, R. A., Chemical Process Principles, Part I, Material and Energy Balances, John Wiley & Sons, Inc., New York, 1954.

34. Ito, T., Nishikawa, K., "Two-Phase Boundary - Layer Treatment of Forced Convection Film Boiling," Int. J. Heat and Mass Transfer, 9, 117 (1966).

35. Jacobson, R. N., Shair, F. H., "Film Boiling from a Sphere during Forced Convection of Subcooled Water," Ind. Eng. Chem. Fundamentals, 9, 183 (1970).

36. Kapitza, P. L., "Wave Flow of Viscous Liquids, I, Free Flow," Zh. Eksp. Theoret. Fiz., 18, 3 (1948).

37. Kapitza, P. L., "Wave Flow of Viscous Liquids, II, Flow in Contact with Gas Streams and with Heat Transfer," Zh. Eksp. Theoret. Fiz., 18, 19 (1948).

38. Kent, R. T. (ed.), Mechanical Engineer's Handbook, 11th Edition, John Wiley & Son, Inc., New York, 1949.

39. Kobayasi, K., "Film Boiling Heat Transfer around a Sphere in Forced Convection," J. of Nuclear Science and Technology, 2, 62 (1965).

40. Kobayasi, K., "Counter-Comment to Hesson and Witte's Comment of 'Film Boiling Heat Transfer around a Sphere in Forced Convection'," J. of Nuclear Science and Technology, 3, 449 (1966).

41. Koh, J. C. Y., "Analysis of Film Boiling on Vertical Surfaces," Trans. A. S. M. E., J. Heat Transfer, 84, 55 (1962).

42. Kovalev, S. A., "an Investigation of Minimum Heat Fluxes in Pool Boiling of Water," Int. J. Heat and Mass Transfer, 9, 1219 (1966).

43. Lai, F. S., Hsu, Y. Y., "Temperature Distribution in a Fin Partially Cooled by Nucleate Boiling," A. I. Ch. E. J., 13, 817 (1967).

44. Leidenfrost, J. G., "On the Fixations of Water in Diverse Fire," trans. C. Wares, Int. J. Heat and Mass Transfer, 9, 1153 (1966).

45. Lewis, D. J., "The Instability of Liquid Surfaces when Accelerated in a Direction Perpendicular to their Planes, II," Proc. Roy. Soc., A, 202, 81 (1950).

46. Lienhard, J. H., Wong, P. T. Y., "The Dominant Unstable Wavelength and Minimum Heat Flux during Film Boiling on a Horizontal Cylinder," Trans. A. S. M. E., J. Heat Transfer, 86, 220 (1964).

47. McBeth, R. V., "The Burnout Phenomena in Forced-Convection Boiling," Advances in Chemical Engineering, 7, 208 (1968).

48. McFadden, P. W., Grosh, R. J., "High-Flux Heat Transfer Studies, an Analytical Investigation of Laminar Film Boiling," Argonne National Laboratory, Lemont, Illinois, 1959.

49. Merte, H. Jr., Clark, J. A., "Boiling Heat Transfer with Cryogenic Fluids at Standard, Fractional, and Near Zero Gravity," Trans. A. S. M. E., J. Heat Transfer, 86, 351 (1964).

50. Mickley, H. S., Sherwood, T. K., Reed, C. E., Applied Mathematics in Chemical Engineering, McGraw-Hill, New York, 1957.

51. National Research Council, International Critical Tables, Vol. V, McGraw-Hill, New York, 1929.

52. Nishikawa, K., Ito, T., "Two-Phase Boundary Layer Treatment of Free Convection Film Boiling," Int. J. Heat and Mass Transfer, 9, 103(1966).

53. Partridge, E. P., Hall, R. E., "Attack on Steel in High-Capacity Boilers as a Result of Overheating due to Steam Blanketing," Trans. A. S. M. E., 61, 597 (1939).

54. Perry, R. H., Chilton, C. H., Kirkpatrick, S. D. (eds.), Chemical Engineers' Handbook, 4th Edition, McGraw-Hill, New York, 1963.

55. Pitts, D. R., Yen, H. H., Jackson, T. W., "Transient Film Boiling of Water on a Horizontal Wire," Trans. A. S. M. E., J. Heat Transfer, 88, 476 (1968).

56. Potter, A. A., Solberg, H. L., Hawkins, G. A., "Investigation of the Oxidation of Metals by High-Temperature Steam," Trans. A. S. M. E., 59, 725 (1937).

57. Potter, A. A., Solberg, H. L., Hawkins, G. A., "Investigation of the Oxidation of Metals by High-Temperature Steam," Trans. A. S. M. E., 60, 610 (1938).

58. Rhea, L. G., Nevins, R. G., "Film Boiling Heat Transfer from an Oscillating Sphere," Trans. A. S. M. E., J. Heat Transfer, 91, 267 (1969).

59. Ruckenstein, E., "About Film Boiling Heat Transfer from a Horizontal Surface," Revue Physics Buc., 7, 293 (1962).

60. Ruckenstein, E., "Film Boiling on a Horizontal Surface," Int. J. Heat and Mass Transfer, 10, 911 (1967).

61. Sideman, S., "The Equivalence of the Penetration Theory and Potential - Flow Theories," Ind. Eng. Chem., 58, No. 2, 54 (1966).

62. Sparrow, E. M., "The Effect of Radiation on Film Boiling Heat Transfer," Int. J. Heat and Mass Transfer, 7, 229 (1964).

63. Sparrow, E. M., Cess, R. D., "The Effect of Subcooled Liquid on Laminar Film Boiling," Trans. A. S. M. E., J. Heat Transfer, 82, 149 (1962).

64. Taylor, G., "The Instability of Liquid Surfaces when Accelerated in a Direction Perpendicular to their Planes, I," Proc. Roy. Soc., A, 201, 192 (1950).

65. Tong, L. S., Boiling Heat Transfer and Two-Phase Flow, John Wiley and Sons, New York, 1965.

66. Weber, H. C., Meissner, H. P., Thermodynamics for Chemical Engineers, 2nd Edition, John Wiley and Sons, New York, 1957.

67. Westwater, J. W., "Boiling of Liquids," Advances in Chemical Engineering, 1, 1 (1956).

68. Westwater, J. W., "Boiling of Liquids," Advances in Chemical Engineering, 2, 1 (1958).

69. Witte, L. C., "Film Boiling from a Sphere," Ind. Eng. Chem. Fundamentals, 7, 517 (1968).

70. Witte, L. C., "Heat Transfer from a Sphere to Liquid Sodium during Forced Convection," Doctoral Thesis, Oklahoma State University, Stillwater, Oklahoma, 1965.

71. Witte, L. C., Baker, L., Haworth, D. R., "Heat Transfer from Spheres into Subcooled Liquid Sodium during Forced Convection," Trans. A. S. M. E., J. Heat Transfer, 88, 394 (1968).

72. Yeh, H. C., Yang, W. J., "Analysis of Laminar Film Boiling in Boundary Layer Flows with Appreciable Radiation," Applied Scientific Research, 20, 178 (1969).

73. Zuber, N., "On the Stability of Boiling Heat Transfer," Trans. A. S. M. E., 80, 711 (1958).

APPENDIX A

REVIEW OF LITERATURE PERTAINING TO FILM BOILING

Early Literature

The first published description of film boiling was by Leidenfrost in 1756 (44). Leidenfrost investigated the relatively slow vaporization of water droplets on an extremely hot metal surface and concluded,

> "Therefore, it has been sufficiently shown that water made more volatile is increased with degrees of heat until it comes to that point at which water boils and all swiftly is evaporated. Then truly if the heat excites more strongly I diminish the volatility of that same water and increase its fixation by the added heat."

Little more of importance was learned of film boiling until 1926 when Moscicki and Broder (68) observed film boiling on an electrically heated wire. Nukiyama (67) adapted the method described by Moscicki and Broder, and in 1934 published the curve shown in Figure 1 which is the first quantitative description of the regimes of boiling described by Leidenfrost in the above quotation.

The early literature concerning film boiling is described in detail in articles by Chwolson in 1909 (17), by Drew and Mueller in 1937 (18), by Westwater in 1958 (67) (68), by McFadden and Grosh in 1959 (48), and by Gottfried et al. in 1966 (28). The early research

was entirely experimental in nature. Because film boiling was regarded as a condition to be avoided in practical applications, it was not until 1950 that an analytical investigation of film boiling was published.

Free Convection Film Boiling

The first boiling situation investigated analytically was a cylinder in free convection. In 1950 Bromley (9) developed an equation for predicting heat transfer coefficients for horizontal and vertical cylinders by assuming the following:

1. The film is cylindrical and continuous.
2. There is laminar flow within the film.
3. The area from which the bubbles leave is small.
4. The vapor velocity is zero at the wall and the velocity at the interface lies between zero and the velocity, if the liquid were inviscid.
5. The liquid is at its saturation temperature.
6. The vapor-liquid interface is at the boiling point.
7. The vapor has no kinetic energy.
8. The film thickness is not time dependent at any point.
9. The surface temperature is constant.

10. The vapor properties are assumed to be constant at an average vapor temperature.

11. The radiation is negligible.

Bromley reduced the general equations for energy and momentum to:

$$dq = h\Delta T \, dA \tag{A-1}$$

$$\frac{d^2 v}{dx^2} = \frac{g}{\mu_v} (\rho_l - \rho_v) \tag{A-2}$$

He used the coordinate system shown in Figure 31 and the following boundary conditions:

1. at $x = 0$; $T = T_w$

2. at $x = 0$; $v = 0$

3. at $x = \delta$; $T = T_s$

4(a). at $x = \delta$; $v = 0$

4(b). at $x = \delta$; $(dv/dx)_v = (dv/dx)_l$

5. at $x = \delta$; $2 L q \, dy = \lambda' dw$

where

$$\lambda' = \lambda + 1/2 \, c_{p,v} \Delta T$$

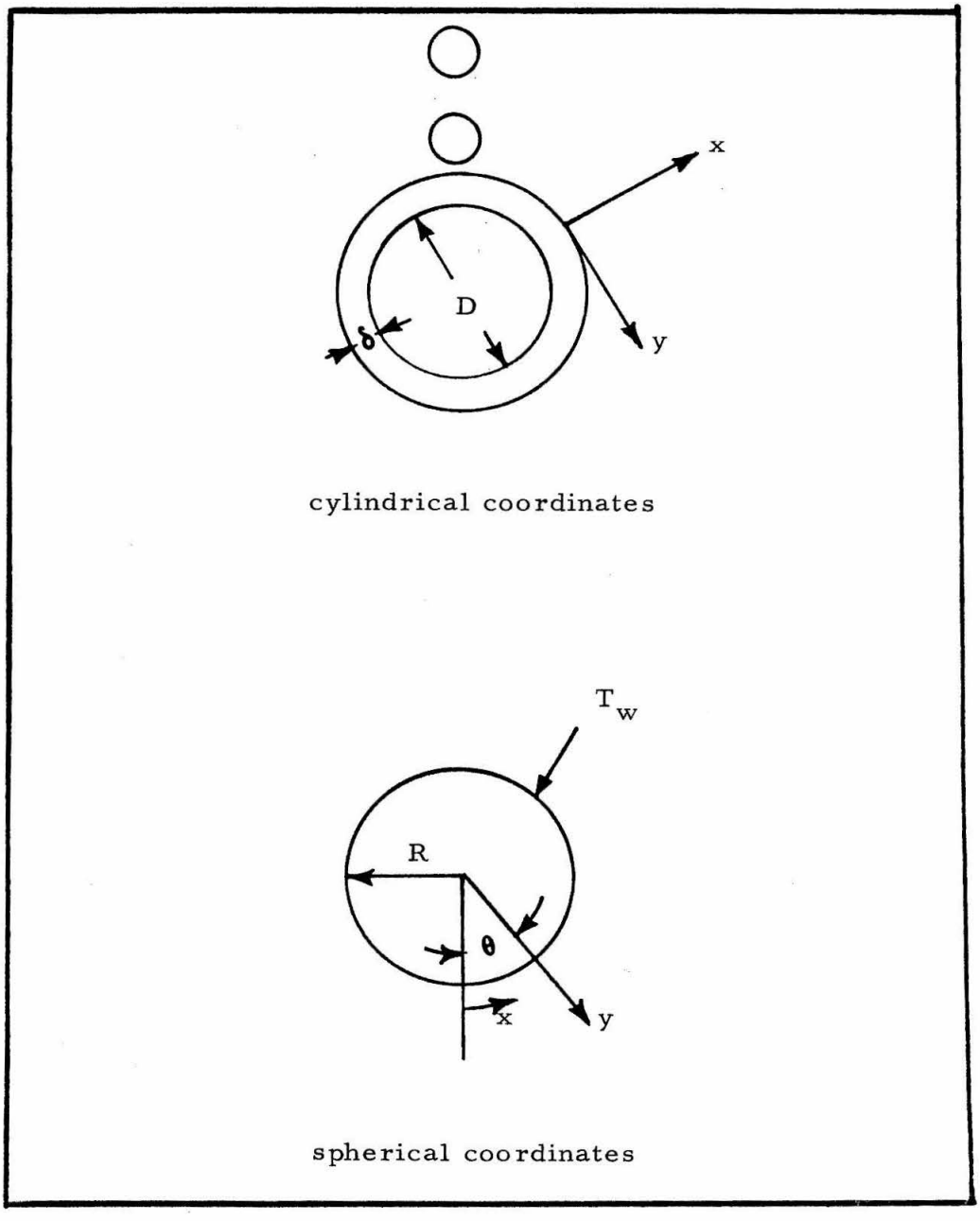

Figure 31. --Spherical and cylindrical coordinate systems.

The fifth boundary condition represents an energy balance at the liquid-vapor interface. The solution resulting from the above simplifications is

$$\frac{\overline{Nu_D}}{Gr_{D,v}^{1/4}} = (\text{constant}) \left(\frac{\lambda' Pr_v}{c_{p,v} \Delta T} \right)^{1/4} \qquad (A-3)$$

where

$$Gr_{D,v} = \frac{D^3 g_v (\rho_l - \rho_v)}{\mu_v^2} \qquad (A-4)$$

The value of the constant is 0.724 if boundary condition 4(b) is used and 0.512 if boundary condition 4(a) is used; Bromley suggested 0.62 as a compromise. Bromley obtained a similar result for a vertical cylinder.

Bromley (8) later suggest a modification of the above solution to account more accurately for vapor superheating with the following result:

$$\frac{\overline{Nu_D}}{Gr_{D,v}^{1/4}} = 0.62 \left[\frac{c_{p,v} \Delta T \, Pr_v}{\lambda} \right]^{1/4} \left[\frac{\lambda}{c_{p,v} \Delta T} + 0.4 \right]^{1/2} \qquad (A-5)$$

A more exact solution to the preceeding problem was made by McFadden and Grosh (48). They reduced the boundary layer

equations to ordinary differential equations which they solved numerically for the following cases:

1. compressible flow with variable specific heat,
2. variable specific heat with density variations in the film,
3. constant properties of the vapor.

McFadden and Grosh considered vapor inertia and assumed the liquid-vapor interface to be stationary. They also showed that their solution was applicable to vertical plates according to

$$\overline{Nu_D} = 0.77\ \overline{Nu_L} \tag{A-6}$$

also

$$\overline{Nu_D} = \frac{4}{3} Nu_D \tag{A-7}$$

Frederking (20) also solved the problem of free convection film boiling on a horizontal cylinder by using the integral method of von Karman to simplify the boundary layer equations. Frederking assumed that the properties of the vapor were constant at an average temperature and considered the vapor inertia term. He obtained the following solution for high vapor superheat:

$$\overline{Nu_D} = 0.802\left[\frac{99\ Gr_{D,v}\ Pr_v^{*2}}{560\ (Pr_v^{*} + 32/33)}\right]^{1/4} \qquad (A\text{-}8)$$

where

$$Pr_v^{*} = Pr_v\left(1 + \frac{35}{11}\ \frac{\lambda}{c_{p,v}\Delta T}\right) \qquad (A\text{-}9)$$

Transient film boiling on a thin horizontal cylinder was investigated analytically and experimentally by Pitts et al. (55). They assumed a uniform vapor film thickness which increased with time, and thereby, obtained a transcendental expression for determining the film thickness as a function of time. Their discussion includes a review of transient boiling studies.

The solutions of Bromley, McFadden and Grosh (constant properties), and Frederking (high superheat) are compared in Figure 32.

In 1954 Ellion (19) applied Bromley's simple solution to a vertical flat plate with free convection. The boundary conditions were the same as those used by Bromley with the exception that the vapor velocity was zero at the liquid-vapor interface. The solution obtained by Ellion is

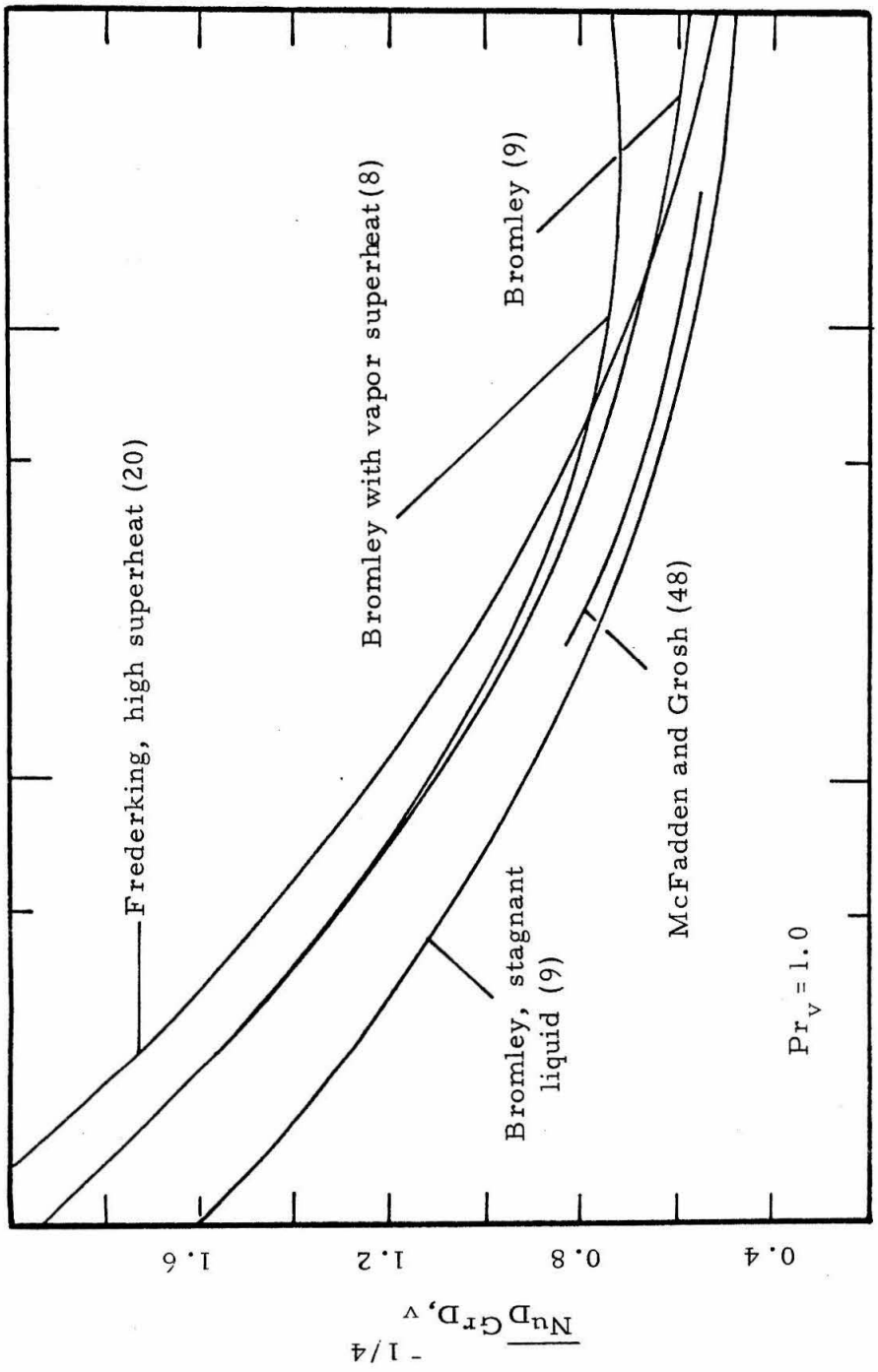

Figure 32. --Comparison of theoretical results for free convection film boiling on a horizontal cylinder.

$$\frac{\overline{Nu_L}}{Gr_{L,v}^{1/4}} = 0.717\left(\frac{\lambda Pr_v}{c_{p,v}\Delta T}\right)^{1/4} \qquad (A-10)$$

In 1959 McFadden and Grosh (48) presented their solution for a vertical flat plate with free convection as previously mentioned, and in 1962 Koh (41) extended their solution taking into account vapor velocity and shear stress at the liquid-vapor interface. He began with the boundary layer equations and by using a similarity transformation reduced them to ordinary differential equations which he solved numerically. The additional parameter which is required in this solution is the ratio

$$\frac{(\rho\mu)_v}{(\rho\mu)_l}$$

By using the same techniques he used for the horizontal cylinder solution, Frederking (20) also solved the vertical flat plate problem. In this case, his solution for high vapor superheat is

$$\frac{\overline{Nu_L}}{Gr_{L,v}^{1/4}} = \left[\frac{\frac{22}{105}\,Pr_v^{*\,2}}{Pr_v^{*} + 80/99}\right]^{1/4} \qquad (A-11)$$

where

$$Pr_v^* = Pr_v \left[1 + \frac{35}{11} \left(\frac{\lambda}{c_{p,v} \Delta T} \right) \right] \qquad (A-12)$$

Figure 33 is a comparison of the results of Ellion, Frederking (high superheat), Koh, and McFadden and Grosh (constant properties).

Free convection film boiling from a horizontal plate was investigated in 1958 by Zuber (73) who used an analysis based on the Rayleigh-Taylor instability, which is an instability due to gravity forces acting on a more dense layer above a less dense layer. A detailed discussion of this instability was given by Chandrasekhar (15). Zuber's work was extended by Chang (16) who obtained the following heat transfer result for a horizontal plate:

$$\overline{Nu_L} = 0.234 \left(Pr_v \, Gr_{L,v} \right)^{1/3} \qquad (A-13)$$

Berenson (3) and Ruckenstein (59) (60) extended Chang's solution to include surface tension effects. Their solution is

$$\frac{\overline{Nu_L}}{Gr_{L,v}^{1/4}} = 0.425 \left\{ \frac{\lambda' Pr_v \, L}{c_{p,v} \Delta T} \left[\frac{g (\rho_l - \rho_v)}{g_o \sigma} \right]^{1/2} \right\}^{1/4} \qquad (A-14)$$

Frederking et al. (24) suggested the following relationship for the case of small viscosity and surface tension effects

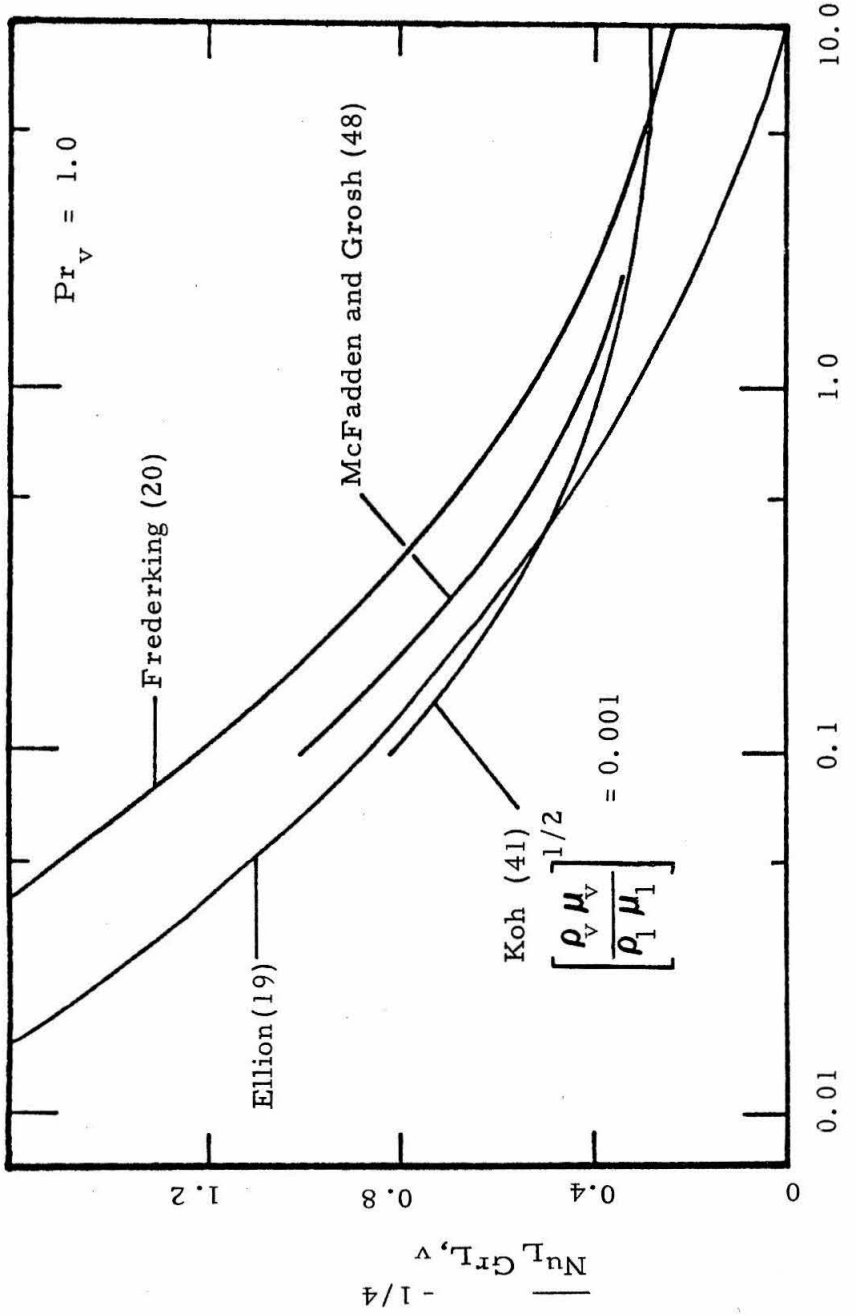

Figure 33. --Comparison of theoretical results obtained by various investigators for free convection film boiling on a vertical plate.

$$\overline{Nu}_L = (\text{constant})\,(Gr_{L,v})^{1/3}\left(Pr_v \frac{\lambda'}{c_{p,v}\Delta T}\right)^{2/3} \qquad \text{(A-15)}$$

Bankoff (1) investigated the special case of a porous horizontal plate with all vapor being removed through the plate.

A comparison of the Chang, Berenson-Ruckenstein, and Frederking et al. solutions is presented in Figure 34 for a vapor Prandtl number of unity. Hosler and Westwater have obtained data which indicates that the relationship derived by Berenson and Ruckenstein more accurately predicts the average Nusselt number. Frederking et al. (24) performed an experimental investigation which indicated that for cryogenic systems their equation best describes the heat transfer.

The case of natural convection film boiling on a sphere was solved by Frederking and Clark (21) using the boundary layer theory. The general equations were first reduced to those below. The equations for the vapor were

$$\frac{\partial ur}{\partial x} + \frac{\partial vr}{\partial y} = 0 \qquad \text{(A-16)}$$

$$u\frac{\partial u}{\partial x} + v\frac{\partial v}{\partial y} = g\frac{(\rho_l - \rho_v)}{\rho_v}\sin\frac{x}{R} + \frac{\mu_v}{\rho_v}\frac{\partial^2 u}{\partial y^2} \qquad \text{(A-17)}$$

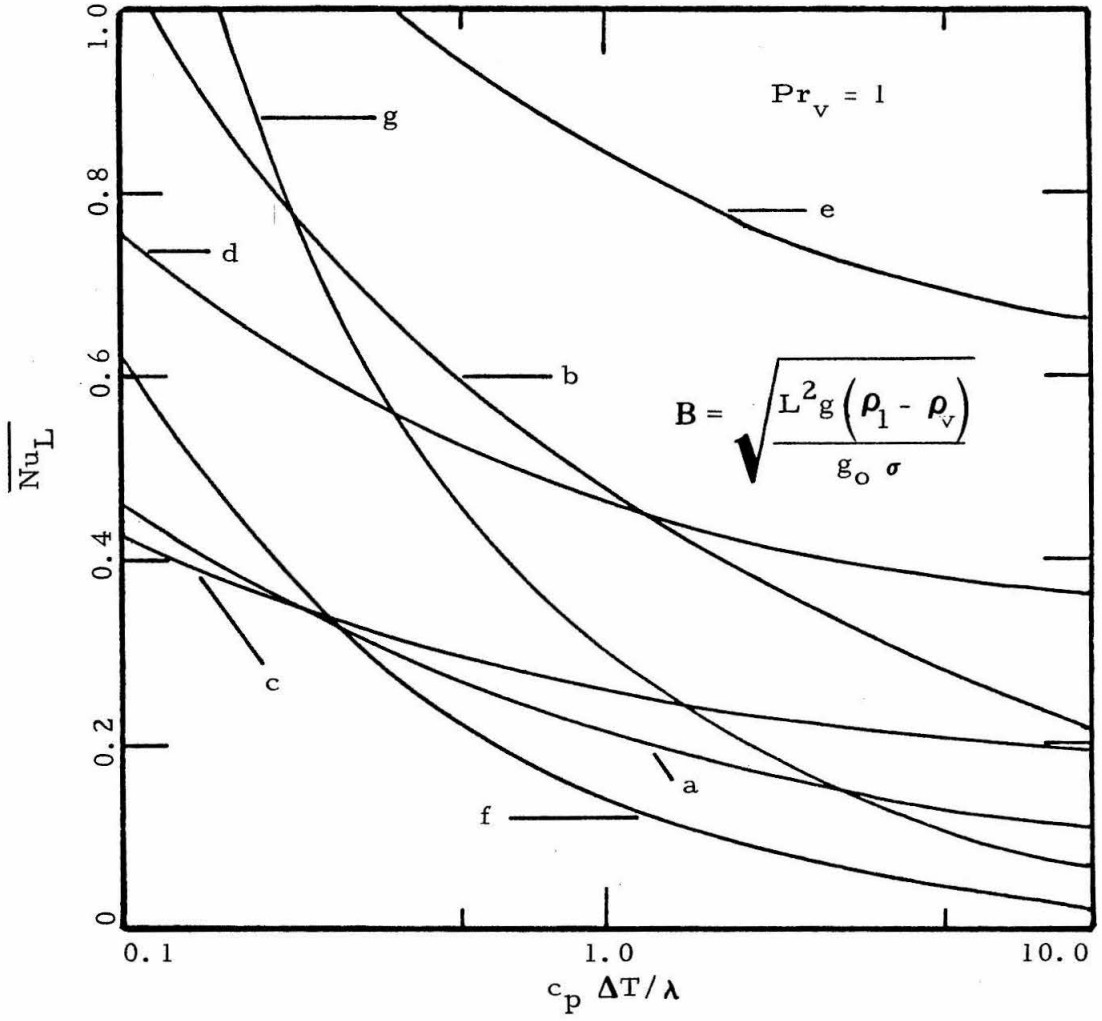

Chang (16) { a. $Gr_L = 0.1$; b. $Gr_L = 1.0$

Berenson (3) { c. $Gr_L = 0.1$; $B = 1.0$; d. $Gr_L = 1.0$; $B = 1.0$; e. $Gr_L = 1.0$; $B = 10.0$

Frederking et al. (24) { f. $Gr_L = 0.1$; g. $Gr_L = 1.0$

Figure 34. --Correlations for heat transfer on a horizontal plate.

$$u \frac{\partial T}{\partial x} + v \frac{\partial T}{\partial y} = \frac{k_v}{\rho_v c_{p,v}} \frac{\partial^2 T}{\partial y^2} \qquad \text{(A-18)}$$

The R term is the radius of the sphere as shown in Figure 32. The equations for the liquid are the same with the "v" subscript replaced by an "l" subscript. The boundary conditions were

$$u = v = 0 \quad \text{at} \quad y = 0$$

$$u \longrightarrow 0 \quad \text{as} \quad y \longrightarrow \infty$$

and at the interface

$$v_v = v_l$$

$$\tau_v = \tau_l$$

$$dw_v = dw_l$$

$$k_v \, dA \left[-\left(\partial T / \partial y \right)_v \right] = dw_v$$

The solution to the above equations is

$$\frac{\overline{Nu_D}}{Gr_{D,v}^{1/4}} = 0.586 \, Pr_v \left(\frac{\lambda}{c_{p,v} \Delta T} \right)^{1/4} \qquad \text{(A-19)}$$

The above result was recently extended by Rhea and Nevins (58) to cover the case of an oscillating sphere. An experimental investigation

of free convection film boiling on a sphere was conducted by Merte and Clark (49). They found an unusual gravity dependence which they attributed to turbulence in the film.

Frederking and Daniels (22) noted a relationship between the frequency of bubble removal and the bubble diameter during film boiling on a cylinder. They found that the product of the frequency and the square root of the diameter equaled a constant.

Recently, Hendricks and Baumeister (30) considered a model consisting of a vapor dome on top of a sphere into which vapor flows from a thin vapor region existing on the lower portion of the sphere. Their analysis was based on a model similar in concept to that of Frederking and Clark for the lower portion of the sphere and on a model similar in concept to the Berenson-Ruckstein horizontal plate model for the vapor dome on top of the sphere. Their solution is

$$\overline{Nu_D} = \left[Gr_{D,v} Pr_v \frac{4\lambda'}{c_{p,v}\Delta T} \sqrt{\frac{(\rho_l - \rho_v) g D^2}{\sigma g_o}} \right]^{1/4} \left\{ \frac{1}{4} \left[\frac{-2G/3}{\sqrt{\frac{(\rho_l - \rho_v) g D^2}{\sigma g_o}}} \right]^{1/4} + 1.77 (1 + \cos\theta^*) \right\} + \csc\theta^* (1 + \cos\theta^*) \qquad \text{(A-20)}$$

where G and θ^* are functions of the parameter

$$Gr_{D,v} Pr_v \frac{\lambda}{c_{p,v}\,\Delta T}$$

and have been evaluated numerically, and

$$\lambda' = \lambda \left[1 + 0.4 \left(\frac{c_{p,v}\,\Delta T}{\lambda} \right) \right]$$

Forced Convection Film Boiling

In 1953 Bromley et al. (10) investigated forced convection film boiling. They considered a horizontal cylinder and assumed that for high flow rates conduction through the film occurs only on the lower half of the cylinder. Their result is

$$\frac{\overline{Nu_D}}{\sqrt{Re_D}} \frac{\mu_v}{\mu_l} = 2.7 \left[Pr_v \frac{(\rho\mu)_v}{(\rho\mu)_l} \left(\frac{\lambda^*}{c_{p,v}\,\Delta T} \right) \right]^{1/2} \qquad \text{(A-21)}$$

where

$$\lambda^* = \lambda \left(1 + 0.4\, c_{p,v}\,\Delta T/\lambda\right)^2$$

The constant 2.7 was adjusted experimentally to fit their data.

Forced convection film boiling over a flat plate was examined by Cess and Sparrow (13) using the boundary layer theory. Their model and coordinate system are shown in Figure 35. They began with the

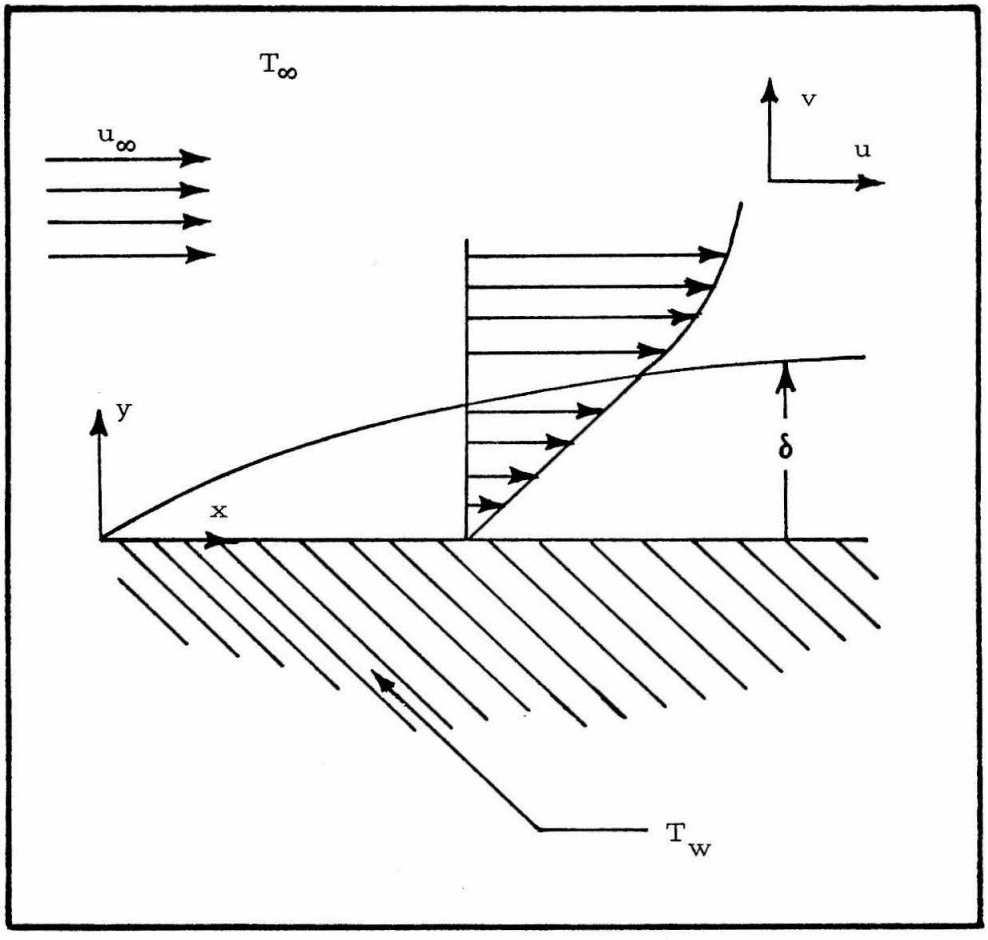

Figure 35. --Coordinate system used for forced convection film boiling on a flat plate.

continuity equation,

$$\frac{\partial u}{\partial x} + \frac{\partial v}{\partial y} = 0 \qquad \text{(A-22)}$$

In this case, buoyancy effects were assumed to be negligible in comparison to forced convection effects. Thus,

$$\rho \left[\frac{u\partial u}{\partial x} + \frac{v\partial u}{\partial y} \right] = \mu \frac{\partial^2 u}{\partial y^2} \qquad \text{(A-23)}$$

Again radiation, viscous dissipation, and kinetic energy were neglected. The energy equation is then

$$\rho c_p \left[\frac{u\partial T}{\partial x} + \frac{v\partial T}{\partial y} \right] = k \frac{\partial^2 T}{\partial y^2} \qquad \text{(A-24)}$$

The equations for the two phases are identical and must be solved simultaneously. The boundary conditions used for the solution of the above equations were

at $y = \delta$

1. $\tau_l = \tau_v$
2. $u_l = u_v$
3. $T = T_s$

$$4.\quad \rho_l\left[u\frac{d\delta}{dx} - v\right]_l = \rho_v\left[u\frac{d\delta}{dx} - v\right]_v$$

at $y = 0$

1. $u = v = 0$

2. $T = T_w$

at $y = \infty$

1. $u = u_\infty$

The resulting solution is

$$\frac{\overline{Nu_L}}{\sqrt{Re_L}}\left(\frac{\mu_v}{\mu_l}\right)\left[1 + \sqrt{\pi}\,\frac{\overline{Nu_L}}{\sqrt{Re_L}}\left(\frac{\mu_v}{\mu_l}\right)\right]^{1/2} = \left[\frac{(\rho\mu)_l}{(\rho\mu)_v}\,\frac{c_{p,v}\Delta T}{Pr_v\,\lambda}\right]^{-1/2} \qquad (A\text{-}25)$$

This is an asymptotic solution for large values of the term on the right.

The preceeding problem also was solved for a uniform heat flux rather than a uniform surface temperature by Cess (12). The result is

$$\overline{Nu_L} = 1.414\left[\frac{(\rho\mu)_l}{(\rho\mu)_v}\,\frac{c_{p,v}\Delta T}{\lambda Pr_v}\right]^{-1/2} \qquad (A\text{-}26)$$

Cess and Sparrow's solution for forced convection was solved numerically and in more detail by Ito and Nishikawa (34). Their solution required the $\rho\mu$ ratio as an additional parameter. The importance of this additional parameter can be seen in Figure 36 where the solution of Cess and Sparrow, Cess, and Ito and Nishikawa are plotted for a vapor Prandtl number of unity and representative values of the $\rho\mu$ ratio.

Bromley's solution for forced convection on a cylinder was extended by Kobayasi (39), (31), (40) to cover the case of forced convection on a sphere. Kobayasi applied Bernoulli's theorem to obtain a set of equations which describe both forced and free convection effects. These equations are

$$\Lambda = \frac{\sqrt{8}}{9}\left\{\int_0^{\theta_s}\left[\left(\Psi \sin\theta - \sin 2\theta\right)\sin^4\theta\right]^{1/3} d\theta\right\}^{3/2} \qquad \text{(A-27)}$$

where

$$\Lambda = \frac{4}{3}\left(\frac{1}{Pr_v}\,\frac{\mu_v^2}{\mu_l^2}\,\frac{\rho_l}{\rho_v}\,\frac{c_{p,v}\Delta T}{\lambda}\right)^{1/2}\frac{\overline{Nu_D}^2}{Re_D} \qquad \text{(A-28)}$$

$$\Psi = 16\,\frac{\overline{Nu_D}^2}{Re_D}\,\frac{\mu_v}{\mu_l}\,\frac{1}{(1-\cos\theta_s)^2} + \frac{32}{9}\,\frac{gR^3\rho_l^2}{\mu_l^2 Re_D^2} \qquad \text{(A-29)}$$

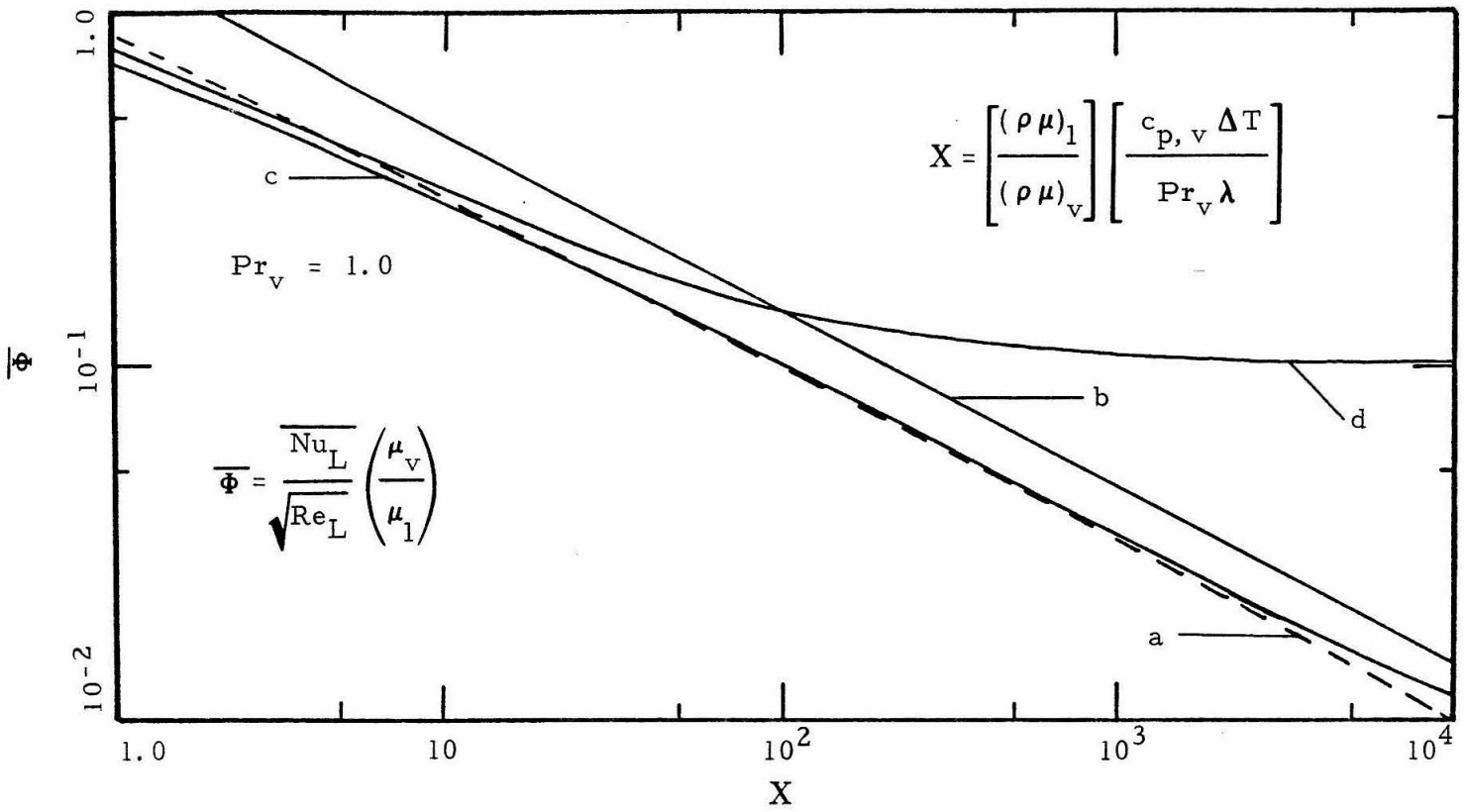

Cess and Sparrow (13)

a. $\overline{\Phi}/2\,(1 + \overline{\Phi}/2)^{1/2} = X^{-1/2}/2$

b. $\overline{\Phi} = 1.414\, X^{-1/2}$

Ito and Nishikawa (34)

c. $\left[(\rho\mu)_v / (\rho\mu)_l\right]^{1/2} = 0.1$

d. $\left[(\rho\mu)_v / (\rho\mu)_l\right]^{1/2} = 0.16$

Figure 36. --Comparison of solutions for forced convection film boiling on a flat plate.

and

$$\Psi = -2 \cos \theta_s \qquad \text{(A-30)}$$

where θ is the angle (coordinates in Figure 31) beyond which the film is sufficiently thick that heat transfer by conduction does not occur. For very high velocities $\theta = 90^{\circ}$, and also

$$16 \frac{\overline{Nu_D}^2}{Re_D} \frac{\mu_v}{\mu_1} \frac{1}{(1 - \cos \theta_s)^2} >> \frac{32}{9} \frac{1}{Re_D^2} gR^3 \frac{\rho_1^2}{\rho_1^2} \qquad \text{(A-31)}$$

The above equations then reduce to

$$\frac{\overline{Nu_D}}{\sqrt{Re_D}} \frac{\mu_v}{\mu_1} = (\text{constant}) \left[Pr_v \frac{\mu_v}{\mu_1} \frac{\rho_v}{\rho_1} \left(\frac{\lambda}{c_{p,v} \Delta T} + 0.68 \right) \right]^{1/2} \qquad \text{(A-32)}$$

which is similar to the solutions obtained by Bromley for a cylinder and by Cess and Sparrow for a flat plate. The above equation also was derived in a simple manner by Witte (69). The value of the constant in Kobayasi's result may be evaluated analytically; however, Witte suggested that an experimentally determined value better describes the heat transfer relationships. At low velocities Equation (A-27) reduces to an equation similar to that obtained by Frederking and Clark (21), Equation (A-19), for film boiling on a sphere.

Liquid Drops

As previously mentioned, in 1756 Leidenfrost investigated the slow evaporation of liquid drops on a hot surface. In 1966 Gottfried et al. (27) (28) published an analytical description of this evaporation. They assumed that mass was removed from the droplet by evaporation on the lower surface and by diffusion from the upper surface, and that the droplet was supported by the excess pressure of the vapor in the film. The evaporation rate was determined by satisfying momentum, heat and mass balances. Their result for negligible radiation is

$$\frac{\rho_l D_o^2}{t \mu_v} = (\text{constant}) \quad Gr_{D_o, v}\left[\frac{c_{p,v} \Delta T}{\lambda' Pr_v}\right]^{1/2} \qquad (A-33)$$

where

$$\lambda' = \lambda (1 + c_{p,v} \Delta T)$$

and D_o is the initial diameter of the liquid droplet. By a comparison to experimental data, the constant was found to be 0.0166.

Liquid Subcooling

The analyses thus far discussed have made the important assumption that the liquid considered was at its saturation temperature.

The effect of subcooling the liquid below its saturation temperature is to decrease the film thickness and to increase the rate of heat transfer through the film. Much of the preceeding work on free and forced convection film boiling has been extended by considering the effect of a subcooled liquid.

Chang (16) applied Neuman's solution for melting ice and found that the effect of a subcooled liquid can be introduced by using a "generalized" Prandtl number.

$$Pr_v^* = Pr\left[\frac{2\lambda}{c_{p,v}\Delta T} + \frac{2\Delta T_1 c_{p,1}\rho_1}{c_{p,v}\Delta T\,\rho_v}\right] \qquad (A-34)$$

This result is accurate for small degrees of subcooling and may be used in Chang's solution of a horizontal plate and also in Ellion's (19) solution for a vertical plate.

Frederking and Hopenfeld (23) extended the vertical plate solution of Frederking to include a highly subcooled region, a moderately subcooled region, and a slightly subcooled region. Their solution for a moderately subcooled region is

$$\overline{Nu_L} = \frac{2}{3}\left\{Pr_v Gr_{L,v}\left[\frac{\lambda}{c_{p,v}\Delta T}\right]+\left[\frac{k_1\Delta T_1}{k_v\Delta T}\right]^4 \frac{Gr_{L,1}Pr_1^2}{(1+Pr_1)}\right\}^{1/4} \qquad (A-35)$$

The free convection solution of McFadden and Grosh (48) was extended to apply to a subcooled liquid by Sparrow and Cess in 1962 (63). They reduced the boundary layer equations to ordinary differential equations which they solved numerically. The additional parameters required to describe the subcooling are

$$Pr_l, \qquad \frac{c_{p,l}\Delta T_l}{\lambda}, \qquad \Xi$$

where

$$\Xi = \left[\frac{(\rho\mu)_v}{(\rho\mu)_l}\right]^{1/2}\left[\frac{\rho_l - \rho_v}{\rho_v}\right]^{1/4}\left[\frac{c_{p,l}}{\beta_L \lambda}\right]^{1/4}$$

In 1965 Nishikawa and Ito (52) extended the solution of Koh (41) to apply to a subcooled liquid. Their solution involved the additional parameter

$$\sqrt{\frac{(\rho\mu)_v}{(\rho\mu)_l}}$$

The solutions of Chang, Sparrow and Cess, Nishikawa and Ito, and Frederking and Hopenfeld (moderate subcooling) for free convection film boiling on a flat plate in a subcooled liquid are compared in Figure 37. This comparison is made with vapor and liquid

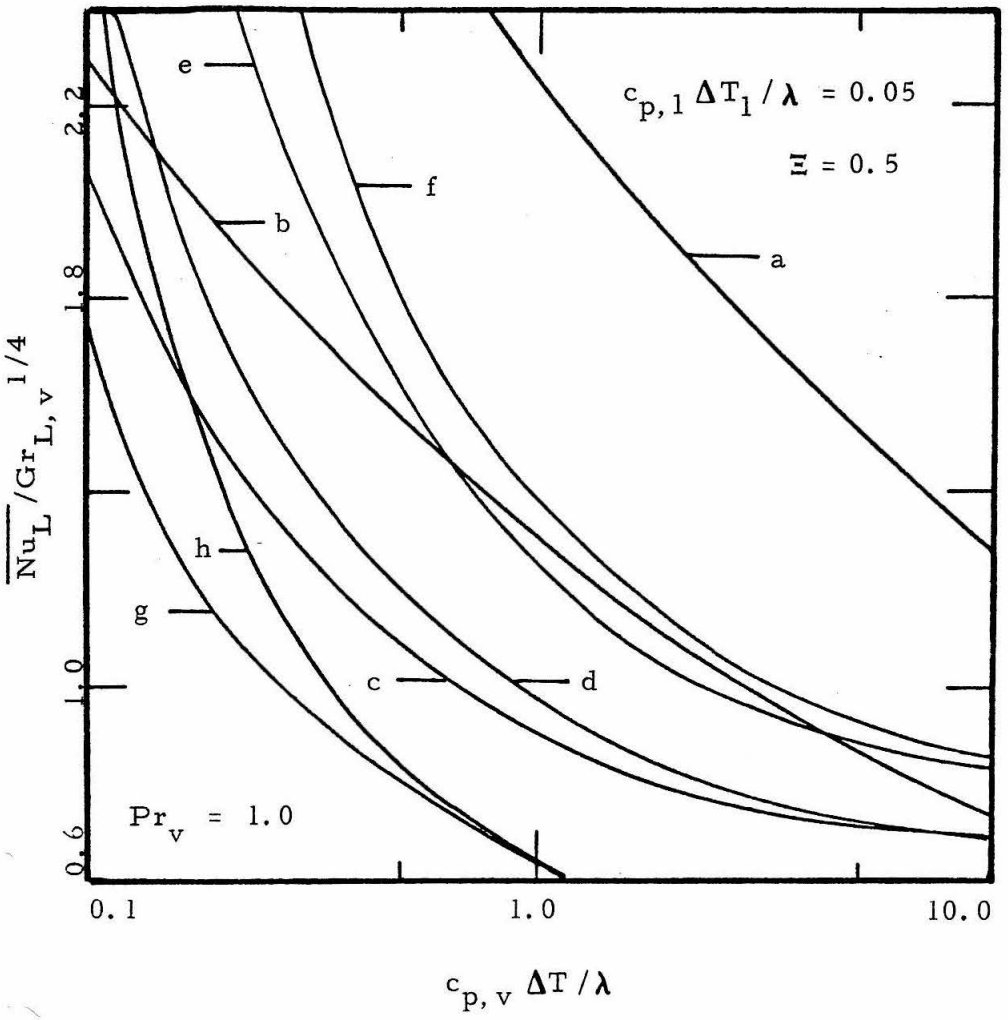

Chang (16)

a. $\rho_l / \rho_v = 2000$

b. $\rho_l / \rho_v = 200$

Sparrow and Cess (63)

c. $Pr_l = 2$

d. $Pr_l = 1$

Nishikawa and Ito (52)

e. $Pr_l = 2;\ \sqrt{(\rho\mu)_v/(\rho\mu)_l} = 0.1$

f. $Pr_l = 1;\ \sqrt{(\rho\mu)_v/(\rho\mu)_l} = 0.1$

Frederking and Hopenfeld (23)

g. $Pr_l = 2$

h. $Pr_l = 1$

Figure 37. --Comparison for free convection film boiling on a flat plate with subcooling.

Prandtl numbers of unity.

Cess and Sparrow (14) extended their analysis of forced convection on a flat plate (13) to include subcooling of the liquid. Their numerical solution used the additional parameter

$$\frac{Pr_v}{Pr_l} \frac{c_{p,l}\Delta T_l}{c_{p,v}\Delta T}$$

Ito and Nishikawa (34) included subcooling of the liquid in their analysis of forced convection on a flat plate. Their numerical result required the following parameter to describe the effects of the subcooled liquid

$$\frac{c_{p,v}\,\Delta T_l}{\sqrt{Pr_l}\,\frac{(\rho\mu)_v}{(\rho\mu)_l}}$$

A comparison of the results of Cess and Sparrow with those of Ito and Nishikawa is included in the paper by Ito and Nishikawa (34). The results correspond for a small $\rho\mu$ ratio, a small degree of superheating of the vapor, and a small degree of subcooling of the liquid.

An experimental investigation of subcooled film boiling of liquid sodium on a sphere has been made by Witte et al. (70) (71). They concluded that the following equation derived by Sideman (61) for

forced convection heat transfer with no film boiling and for slip at the wall described the phenomena:

$$q = 1.13 \left[\frac{u_\infty (\rho k c_p)_l}{D}\right]^{1/2} (T_w - T_B) \qquad (A-36)$$

Jacobson and Shair (35) noted that subcooling of the liquid can result in instantaneous condensation of the vapor bubbles. A detailed description of the phenomena is presented in Chapter I, "Description of Apparatus" and in Appendix J.

Radiation Effects

The preceeding discussion of film boiling literature used the important assumption that radiation is negligible. During film boiling of cryogenic liquids, this may be the case; however, during film boiling of a liquid such as water, radiation will probably account for at least several per cent of the total heat transferred, and during the film boiling of liquid metals, radiation may account for the bulk of the heat transferred.

The simplest correction which can be made for radiation is to consider the heating surface and the liquid-vapor interface as flat parallel plates with a non-absorbing vapor between them. This method was used by Bromley (9) to describe radiation from a cylinder

in free convection film boiling. He found that

$$h_r = \frac{\sigma_{SB}}{\frac{1}{\epsilon} + \frac{1}{\alpha} - 1} \left(\frac{T_w^4 - T_l^4}{\Delta T} \right) \qquad (A-37)$$

Because the liquid considered was saturated, and because radiation will increase the film thickness and decrease h_c, the coefficient for total heat transfer is

$$h = h_c \left(\frac{h_c}{h_r} \right)^{1/3} + h_r \qquad (A-38)$$

For forced convection film boiling around a horizontal cylinder, Bromley (10) recommended that

$$h = h_c + \frac{7}{8} h_r \qquad (A-39)$$

Ellion (19) also applied the above simplification to describe radiation during free convection film boiling on a vertical flat plate. He suggested

$$h = h_c \left(\frac{q_c}{q_c + q_r} \right)^{1/4} + h_r \qquad (A-40)$$

Kobayasi (39) recommended the same approach for free and forced convection film boiling on a sphere. He suggested

$$h = h_c + h_r \qquad \text{(A-41)}$$

A more extensive analysis of the effect of radiation was made by Sparrow (62). He considered the additional problem of emission and absorption by the vapor in the film. He concluded that the effects of a radiatively-participating vapor on heat transfer are negligible

Yeh and Yang (72) recently have presented a theoretical study of heat transfer during free convection film boiling on a plate and a sphere. They began with an energy equation containing a radiation term, and by a similarity transformation reduced the energy and momentum equations to a set of ordinary differential equations. These can be solved numerically for either a saturated or subcooled liquid.

Interfacial Waves

In the previous analysis the interface was assumed to be smooth and without waves. However, as Westwater (68) first pointed out, the vapor-liquid interface may have waves. The physical situation of film boiling on a vertical flat plate is similar to that of a liquid film falling down a solid surface. Kapitza (36) (37) investigated a

falling liquid film. He assumed the wavelength to be much greater than the film thickness and the amplitude of the waves to be much smaller than the film thickness. As a first approximation, he found that the phase velocity equals three times the interfacial velocity and

$$\overline{\lambda} = \frac{3.32}{v_o} \left[\frac{\delta\ \sigma}{\rho_1}\right]^{1/2} \qquad \text{(A-42)}$$

where $\overline{\lambda}$ is the wavelength and v_o is the interface velocity.

Bradfield (5) performed an analytical and experimental analysis of wave generation at a stagnation point during free convection film boiling on a vertical cylinder with a hemispherical lower end. He assumed a liquid mass moving against a gas layer spring and damper at the stagnation point with the wave generation and the heat pulse acting as a forcing function. He found the wave frequency to be related to the radius of the hemisphere, the vapor and liquid properties, and the temperature difference.

A photographic investigation of waves on a vertical cylinder during film boiling was made by Brauer (7). He also used an electrical contact device to measure the frequency of the waves in the vapor film.

The presence of film boiling may result in large reductions in friction drag as pointed out by Bradfield et al. (6). The presence of

the film results in a condition comparable to slip at the solid surface. Drag reduction is included in several of the preceeding discussions such as Cess and Sparrow (13) and Ito and Nishikawa (52).

Simultaneous Nucleate and Film Boiling

In the preceeding discussion only film boiling was considered. Often, nucleate boiling and film boiling may be present simultaneously or film boiling may change to nucleate boiling and vice versa. The transition from nucleate boiling to film boiling is discussed in detail by McBeth (47). It also is possible for film boiling to exist along with nucleate boiling and non-boiling convection on the same surface. An investigation of simultaneous nucleate and film boiling on a horizontal cylinder was made by Kovalev (42). A similar investigation was made by Lai and Hsu (43). They investigated a fin which was cooled simultaneously by nucleate boiling and non-boiling convection.

It has been noted by Bradfield (4) that the vapor film present during film boiling may collapse for brief periods. This liquid solid contact depends on the roughness of the surface, subcooling of the liquid, and thermal conductivity of the solid. Bradfield's photographic study indicated that controlled liquid-solid contact may be possible.

APPENDIX B

ERROR ANALYSIS

The nineteen measurements made during an experimental run may contain random error. An estimation of the maximum possible magnitude of this error was made and is listed in Table 2 in Chapter II.

These errors in measurement will effect the calculated results. The relationship between the maximum error in measurement and the maximum error in a calculated parameter is given by the following equation (50):

$$\delta Q = \left(\frac{\partial \gamma}{\partial q_1}\right) \delta q_1 + \left(\frac{\partial \gamma}{\partial q_2}\right) \delta q_2 + \cdots + \left(\frac{\partial \gamma}{\partial q_n}\right) \delta q_n \qquad \text{(B-1)}$$

where

$$Q = \gamma(q_1, q_2, \ldots, q_n) \qquad \text{(B-2)}$$

δq_n = the maximum expected error in measurement, q_n

δQ = the maximum possible error expected in the calculated parameter, Q.

The above equation results in an addition of maximum possible errors, and therefore, it results in an upper bound on the error in the calculated parameter. Because the possibility of a simultaneous occurance

of several extreme errors is highly unlikely, the above equation yields an exaggeration of the maximum error. However, the equation is valuable in determining the relative magnitude of error in the various parameters. Equation (B-1) was applied to the various equations used in the reduction of data.

The equation for determining the oxygen concentration in the film is

$$x_{O_2,2} = \frac{x_{O_2,o} P_{atm}}{H_{O_2}} \tag{B-3}$$

The maximum possible error in the calculated oxygen concentration then is given by

$$\delta x_{O_2,2} = \frac{x_{O_2,o} P_{atm}}{H_{O_2}} \left[\frac{\delta x_{O_2,o}}{x_{O_2,o}} \right] \tag{B-4}$$

The equation for computing the molar ratio vaporized from the oxygen measurements, Equation (3-62), becomes

$$\delta\left(\frac{N_2}{N_3}\right) = \frac{x_{O_2,in} P_{atm}}{x_{O_2,o} H_{O_2}} \left(\frac{\delta x_{O_2,in}}{x_{O_2,in}} + \frac{\delta x_{O_2,o}}{x_{O_2,o}} \right) \tag{B-5}$$

The above error in the molar ratio vaporized enters into the calculation of the nitrogen concentration in the film. By applying Equation (B-1) to Equation (3-62),

$$\delta x_{N_2} = x_{N_2} \left\{ \frac{\delta x_{N_2, in}}{x_{N_2, in}} + \frac{\frac{H_{N_2}}{P_{atm}} \left(\delta \frac{N_2}{N_3} \right)}{1 + \frac{H_{N_2}}{P_{atm}} \frac{N_2}{N_3}} \right\} \qquad (B-6)$$

A simplification was made to give an approximation of the size of the error expected in the inlet nitrogen concentration:

$$\frac{\delta x_{N_2, in}}{x_{N_2, in}} \simeq \frac{\delta x_{O_2, in}}{x_{O_2, in}} \qquad (B-7)$$

The assumption was made during the reduction of data that the molar ratio of hydrogen to nitrogen in the film was equal to the ratio of hydrogen to nitrogen in the collected non-condensables. The maximum error expected in the concentration of hydrogen in the film is then

$$\delta x_{H_2, 2} = x_{H_2, 2} \left[\frac{\delta x_{N_2, 2}}{x_{N_2, 2}} + \frac{\delta A_{H_2}}{A_{H_2}} + \frac{\delta A_{N_2}}{A_{N_2}} \right] \qquad (B-8)$$

The maximum error expected in λ'' may be expressed as

$$\delta\lambda'' = \sum_{i=j}^{k-1} c_{p,i} \frac{m_i}{m_{H_2O}} (T_2 - T_s) \left[\frac{\delta m_i}{m_i} + \frac{\delta m_{H_2O}}{m_{H_2O}} + \frac{\delta(T_2 - T_s)}{(T_2 - T_s)} \right]$$

$$+ c_{p,H_2O}\, \delta(T_2 - T_s) + c_{p,1}\, \delta(T_s - T_7) \qquad \text{(B-9)}$$

The maximum error in T_s was estimated to be $16^{\circ}C$. This estimation is based on the difference between T_s and T_o in Table 15. The value of T_s should be very close to T_o, and as seen in the table, a discrepancy of up to $16^{\circ}C$ exists on runs in which accurate data were obtained. Several of the runs had rapid hydrogen generation, and consequently, these runs did not have accurate oxygen concentration data. These runs were Numbers 14, 33, 34, 76, and 87. Equation (B-9) requires the error in the water vapor concentration in the film found by

$$-\delta x_{H_2O} = \delta x_{H_2} + \delta x_{N_2} + \delta x_{O_2} \qquad \text{(B-10)}$$

The minus sign is necessary in the above equations because the steam concentration was obtained by subtracting the other concentrations from unity. Therefore, a positive error in the other concentrations results in a negative error in the steam concentration.

The error in the thermal conductivity of the gases in the film is related to the error in the concentrations in the film by

$$\delta k_v = \sum_{i=j}^{k} k_i x_i \left(\frac{\delta x_i}{x_i} \right) \qquad \text{(B-11)}$$

The above equation assumes that a negligible error is introduced in the determination of the thermal conductivity by error in the measurement of the film temperature. The equation also assumes that error introduced by error in the method of computing the thermal conductivity is negligible.

The error in the density of the film is given by

$$\delta \rho_v = \sum_{i=j}^{k} x_i \rho_i \frac{\delta x_i}{x_i} + \rho_v \frac{\delta T_2}{T_2} \qquad \text{(B-12)}$$

The maximum error in r depends on the other computed maximum parameters according to

$$\delta r = r \left[\frac{\delta k_v}{k_v} + \frac{\delta \rho_v}{\rho_v} + \frac{\delta \lambda''}{\lambda''} + \frac{\delta \Delta T}{\Delta T} + \frac{\delta w}{w} + \frac{2\delta(T_o - T_{in})}{(T_o - T_{in})} \right] \qquad \text{(B-13)}$$

The error in the quantity of heat transferred by radiation is not included in the above.

The error in the measured value of the surface temperature is related to the error in the reciprocal of the absolute temperature by

$$\delta\left(\frac{1}{T_w}\right) = \frac{1}{T_w}\left(\frac{\delta T_w}{T_w}\right) \tag{B-14}$$

The error in the rate of hydrogen generation is given by

$$\delta\left(N_{R,H_2}\right) = \left(\frac{N_3 x_{H_2,2}}{A}\right)\left[\frac{N_2}{N_3}\left(\frac{\delta w}{w} + \frac{\delta x_{H_2,2}}{x_{H_2,2}} + \frac{\delta N_2/N_3}{N_2/N_3}\right) + \frac{1}{H_{H_2}}\left(\frac{\delta w}{w} + \frac{\delta x_{H_2,2}}{x_{H_2,2}}\right)\right] \tag{B-15}$$

The percentage of error in the molar flow rate is assumed to equal the percentage of error in the mass flow rate. The mass fraction vaporized as determined from the heat transfer measurements has a maximum expected error which is given by the following equation:

$$\delta\left(\frac{w_2}{w_3}\right) = \frac{w_2}{w_3}\left[\frac{\delta r}{r} + \frac{\delta(T_o - T_{in})}{(T_o - T_{in})} + \frac{\delta x_{H_2O}}{x_{H_2O}} + \frac{\delta \lambda''}{\lambda''}\right] \tag{B-16}$$

The percentage of oxygen removed during the film boiling has an estimated maximum error which is given by the following equation:

$$\delta(\%\ O_2 \text{ removed}) = \frac{x_{O_2,o}}{x_{O_2,in}}\left(\frac{\delta x_{O_2,o}}{x_{O_2,o}} + \frac{\delta x_{O_2,in}}{x_{O_2,in}}\right) \tag{B-17}$$

The error in the Reynolds number depends largely on the error in the flow rate measurement; therefore,

$$\delta \mathrm{Re}_D = \mathrm{Re}_D\left(\frac{\delta w}{w}\right) \tag{B-18}$$

The maximum expected error in the Nusselt number for heat transfer to the liquid depends on the following relationship:

$$\delta \mathrm{Nu}_{D,1} = \mathrm{Nu}_{D,1}\left[\frac{\delta(1-r)}{1-r} + \frac{\delta w}{w} + \frac{\delta \Delta T_1}{\Delta T_1} + \frac{\delta(T_o - T_{in})}{(T_o - T_{in})}\right] \tag{B-19}$$

The preceeding equations may be used to obtain an approximation of the maximum random error. They have been evaluated for two cases. The first was Run Number 1 which had a high liquid flow rate and a low surface temperature. The second was Run Number 13 which had a low liquid flow rate and a high surface temperature. These two runs are near the two extremes over which the data were taken.

The results of these calculations are presented in Table 5 which lists the value of the quantity, the expected maximum error in the value, and the percentage of maximum error. The maximum expected error ranges from zero for the thermal conductivity to 47% for the rate of hydrogen generation.

TABLE 5

MAXIMUM POSSIBLE ERROR

Quantity	Run	γ	$\delta\gamma$	$\frac{\delta\gamma}{\gamma}$ (%)
$x_{O_2,2}$	1	0.1161	0.0079	6.8
	13	0.0968	0.0079	8.2
$N_2/N_3 \times 10^5$ (O_2 measurement)	1	2.547	0.367	14.4
	13	3.613	0.527	14.6
$x_{N_2,2}$	1	0.2484	0.0333	13.4
	13	0.2159	0.0308	14.3
$x_{H_2,2}$	1	0.0005	0.0001	19.4
	13	0.01967	0.0040	20.3
$x_{H_2O,2}$	1	0.6350	-0.0413	-6.5
	13	0.6677	-0.0427	-6.4
λ'' (cal./g.)	1	776.9	26.7	3.4
	13	821.8	27.3	3.3
$k_v \times 10^4$ (cal./sec.-cm.)	1	1.24	0.0003	nil
	13	1.55	0.0172	1.1
$\rho_v \times 10^4$ (g./cc.)	1	3.92	0.102	2.6
	13	3.33	0.083	2.5
$\tau \times 10^5$	1	8.58	1.43	16.7
	13	88.09	25.90	29.4
w (g./cc.)	1	2.32	0.1	4.3
	13	0.61	0.1	16.4
$A \times N_{R,H_2} \times 10^8$ (g.-moles/sec.)	1	0.252	0.095	4.3
	13	3.30	0.155	47.0

TABLE 5 (Continued)

Quantity	Run	γ	$\delta\gamma$	$\delta\gamma/\gamma$ (%)
$N_2/N_3 \times 10^5$ (Heat trans.)	1	1.666	0.278	16.7
	13	1.470	0.432	29.4
$\%O_2$ removed	1	64.1	1.7	2.7
	13	71.7	1.5	2.1
Re_D	1	318.5	13.7	4.3
	13	85.4	14.0	16.4
$Nu_{D,1}$	1	671.1	210.	31.3
	13	133.9	58.0	43.3

APPENDIX C

ELIMINATION OF CHEMICAL REACTIONS BY GOLD PLATING OF THE SPHERE

Hydrogen and oxygen chemically react with steel at high temperatures. Hydrogen was found in the collected non-condensables in all runs made with a steel sphere with a surface temperature above 770°C. By coating the steel spheres used in the experimental runs with a non-reacting substance these reactions should be eliminated.

To investigate this possibility, a gold plated sphere was used in the previously described apparatus. Since no reaction could be expected to occur using the gold plated sphere, no hydrogen should have been found in the collected non-condensables.

There are two problems involved in the use of gold plated spheres. The first is that the gold readily diffuses into the steel at high temperatures. To retard this diffusion the spheres were plated with a layer of nickel before they were plated with gold. The problem of the gold diffusing is discussed in detail in Appendix D.

The second problem encountered in using gold plated spheres results from the low emissivity of the gold. According to the Handbook of Chemistry and Physics (32), oxidized steels have an emissivity of about 0.9 and gold has an emissivity of about 0.03. Therefore, when using a gold plated sphere the optical pyrometer

reads a temperature which is considerably lower than the correct temperature; the necessary correction is difficult to make.

Run Number 91 was made using a gold plated sphere. The sphere remained shiny during the run indicating that little diffusion of gold into the steel occurred. The procedure used for this run was identical with that described in Chapter III. In Run Number 91 no hydrogen was found in the non-condensables.

The results obtained for Runs 1 through 90 of the final series of runs were used to calculate the surface temperature for Run Number 91. The Reynolds number for this run was 250.6. Since Run 91 was made under conditions identical to those of Runs 1 through 8, Figure 20 was used to determine r for Run Number 91. The value of r was 1.05×10^{-5}.

The procedure used to obtain r for Runs 1 through 90 was repeated for Run 91 by using various values of T_w. The value of T_w which resulted in the correct value of r was 869°C. In using the above procedure the radiative heat transfer was assumed to be negligible because of the low emissivity of the gold.

The various other heat transfer parameters also were computed for Run Number 91 and they are listed in Table 6. Since a relatively high surface temperature was found to exist during Run Number 91 and since no hydrogen was found in the non-condensables, it may be

TABLE 6

CALCULATED HEAT TRANSFER PARAMETERS
FOR RUN NO. 91

Quantity	Value
T_w	869°C
T_s	84.0°C
$T_s - T_o$	-4.8°C
N_v/N_l	2.27×10^{-5}
τ	1.05×10^{-4}
Re_D	250.6
Pr_l	2.227
$Re_D Pr_l$	558.1
$\bar{h}$	0.0312 cal./cm.^{2}-sec.°C
q	24.5 cal./cm.^{2}-sec.
$\overline{Nu_{D,l}}$	621.2

concluded that the gold prevented any steam-iron reaction from occurring at the wall. It also may be concluded that the hydrogen occurs from a reaction at the wall and not from a homogeneous reaction; since if a homogeneous reaction were present, the gold would not have eliminated the reaction.

APPENDIX D

DIFFUSION OF GOLD INTO A STAINLESS STEEL SPHERE

Several spheres were plated with gold to retard the iron-steam reaction and the iron-oxygen reaction. Appendix C indicates that the gold may eliminate the iron-steam reaction. However, the gold will diffuse into the stainless steel spheres at high temperatures. Since a thin layer of gold, 0.00010 inches, was used, iron might appear on the surface if the sphere was held at a high temperature for a long period. In an attempt to eliminate this diffusion, a layer of nickel was plated on the stainless steel spheres before the gold plating.

Since the gold retards the steam-iron reaction, the rate of hydrogen production from this reaction should give an approximation of the concentration of iron on the surface. This is turn may be used to determine the rate of diffusion of the gold into the iron and of the iron into the gold.

To test the above hypothesis, Runs 35 through 43 were made at temperatures exceeding 750°C with two gold plated spheres of one-half inch diameter. Table 7 lists the total time that the spheres were kept at a specific temperature in the apparatus at the mid-point of each run. Since the runs were at slightly different temperatures, the temperatures listed in Table 7 are average temperatures. Run 43

TABLE 7

TIME-TEMPERATURE DATA FOR GOLD PLATED SPHERES

SPHERE A	
Run 35	2041 sec. at 852°C
Run 36	4611 sec. at 852°C
Run 37	7104 sec. at 852°C
SPHERE B	
Run 38	1306 sec. at 788°C
Run 39	3811 sec. at 788°C
Run 40	6187 sec. at 788°C
Run 41	8706 sec. at 788°C
Run 42	11219 sec. at 788°C
Run 43	12480 sec. at 788°C and 827 sec. at 951°C

was made at a considerably higher temperature than the earlier runs made with Sphere B and is listed accordingly in the table.

The rates of hydrogen generation were calculated and plotted in Figure 38 as a function of the reciprocal of the absolute temperature. The runs were all made in numerical order and are numbered in the figure. The line in the figure represents the results obtained with a stainless steel sphere under similar circumstances.

Sphere A previously had been used for Run Number 91, which is discussed in Appendix C. At the conclusion of Run Number 91 the sphere was a shiny gold color indicating that a high concentration of gold remained on the surface. However, at the conclusion of Run Number 35, the sphere was black indicating a large concentration of oxidized metals on the surface. The runs made with Sphere A do not show any correlation between the hydrogen generation rate and the time that the spheres were maintained at a high temperature in the apparatus. The runs made with Sphere B show a reduction of hydrogen generation rate after a long period in the apparatus. This trend possibly may result from a thick coating of oxides on the surface causing the reaction rate to become diffusion limited.

There are several problems present in the above experiments. First, the nickel and iron oxides effect the rates of diffusion; therefore, the diffusivities are concentration dependent. Secondly, the

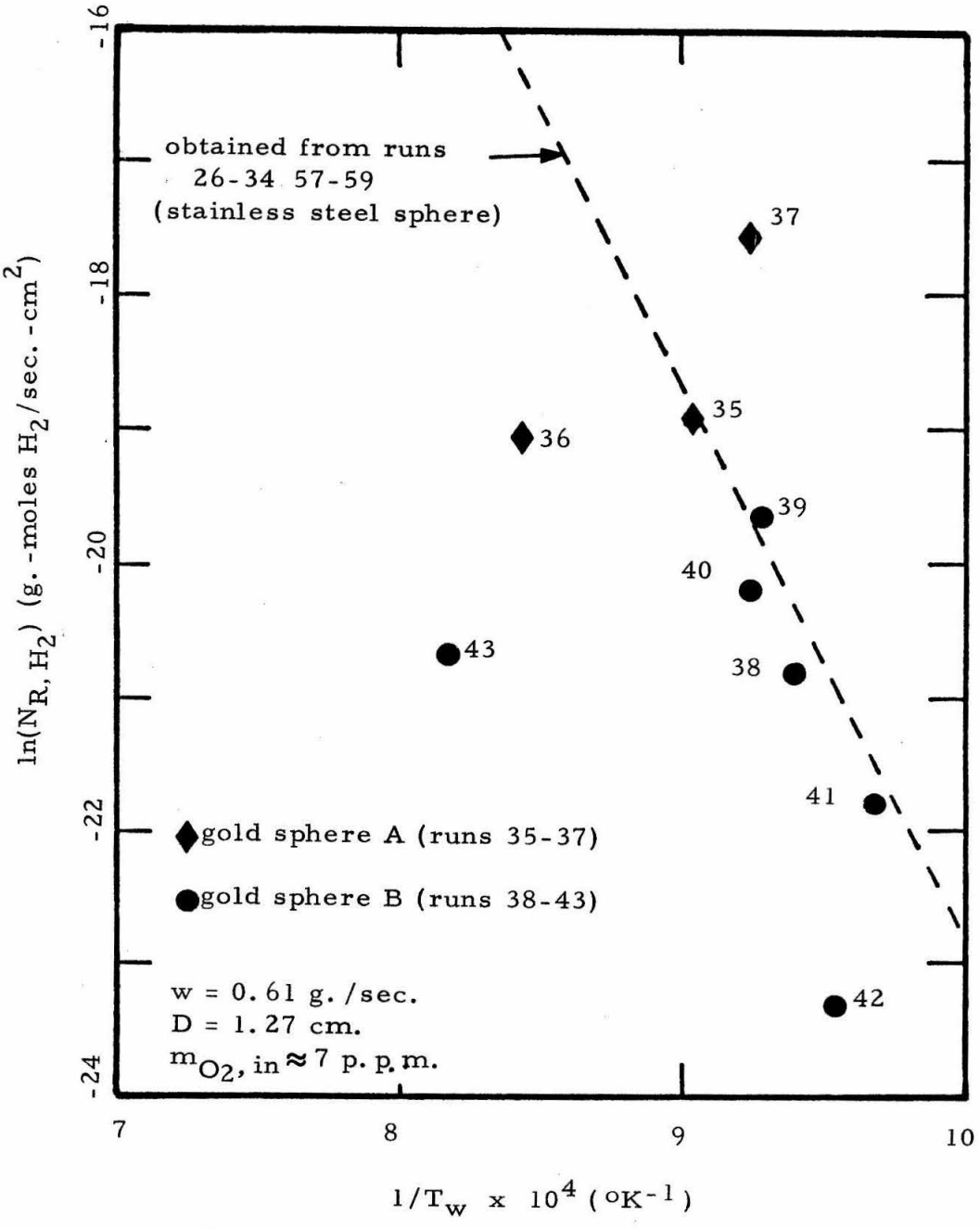

Figure 38.--Experimental runs made with spheres partially covered with gold.

steam may diffuse through the gold layer and react with iron within the sphere. For these reasons an analytical investigation of the above experiments was not attempted. A further and more extensive experimental investigation is needed before any concrete conclusions may be drawn regarding the diffusion of gold into the spheres.

APPENDIX E

CALIBRATION OF CHROMATOGRAPH

The output of the chromatograph was a voltage versus time trace on a strip chart recorder. The area under the curve was proportional to the quantity of each component injected into the carrier gas. The maximum voltage for each component also was proportional to the quantity of each component injected, but only at a constant carrier flow rate.

Nine mixtures of hydrogen, nitrogen, oxygen and argon were prepared for use in the calibration. The first three mixtures were very rich in hydrogen; consequently, the tail of the hydrogen peak overshadowed the oxygen peak. Therefore, the first three mixtures were not used for the calibration. Table 9 lists the exact composition of these mixtures.

The mixtures were prepared as follows. A pressure vessel was evacuated at room temperature for twelve hours to remove contaminates. The atmospheric pressure was read with a mercury manometer. A quantity of hydrogen was bled into the pressure vessel and the partial pressure was read with the manometer. Next, a quantity of dry air was bled into the pressure vessel and its partial pressure was recorded. The composition of this air was taken as 78.03% nitrogen, 20.99% oxygen, and 0.98% inerts. Then the

TABLE 8

PARTIAL PRESSURES OF CALIBRATION MIXTURES

No.	Partial Pressure (cm. Hg.)					Total Pressure (cm. Hg.)
	Hydrogen	Oxygen	Nitrogen	Inerts	Argon (added)	
1.	11.26	9.18	34.11	0.44	71.0	136.0
2.	11.26	9.18	34.11	0.44	96.8	151.8
3.	11.26	9.18	34.11	0.44	148.5	204.1
4.	1.91	13.12	48.77	0.61	61.6	126.0
5.	1.91	13.12	48.77	0.61	87.4	151.8
6.	1.91	13.12	48.77	0.61	113.2	177.6
7.	1.91	13.12	48.77	0.61	139.0	203.4
8.	1.91	13.12	48.77	0.61	164.8	229.2
9.	1.27	8.69	32.30	0.40	186.5	229.2

TABLE 9

COMPOSITION OF CALIBRATION MIXTURES

No.	Moles Injected x 10^5			Mole Fraction		
	H_2	O_2	N_2	H_2	O_2	N_2
1.	0.4023	0.3280	1.219	0.08279	0.06750	0.2508
2.	0.3605	0.2939	1.092	0.07418	0.06047	0.2247
3.	0.2689	0.2192	0.8145	0.05533	0.04511	0.1676
4.	0.07367	0.5059	1.881	0.01516	0.1041	0.3870
5.	0.06113	0.4200	1.561	0.01258	0.08643	0.3213
6.	0.05224	0.3590	1.334	0.01075	0.07387	0.2746
7.	0.04560	0.3134	1.165	0.00939	0.06450	0.2398
8.	0.04050	0.2782	1.034	0.00833	0.05724	0.2128
9.	0.02682	0.1842	0.6857	0.00552	0.03791	0.1409

Sample Size = 1.2 c.c.

pressure vessel was pressurized to various pressures using argon. Each pressure was measured with the meter on the pressure regulator. This procedure was used first to prepare samples one, two and three and then repeated for mixtures four through eight. Mixture nine was prepared by reducing the total pressure on mixture number eight and repressurizing it with argon.

Since the mole fractions of nitrogen and oxygen encountered during a film boiling experiment could be expected to be greater than those of Table 9, two injection volumes were selected. First, a large injection volume of 1.2 milliliters was used to check the linearity of the voltage-time area to quantity injected proportionality over a wide range. A smaller injection volume used in the film boiling experiments. The quantity of each component injected into the chromatograph using the 1.2 milliliters injection volume was calculated by the ideal gas law. The results are presented in Table 9.

The mixtures were passed through the chromatograph using the larger injection volume and a carrier gas flow rate of 26.1 milliliters per minute and a chromatograph attenuation of 100. At all times the flow through the second column and detector was maintained at 13.3 milliliters per minute. The relative areas under the curves were recorded and the results are plotted in Figures 39, 40, and 41.

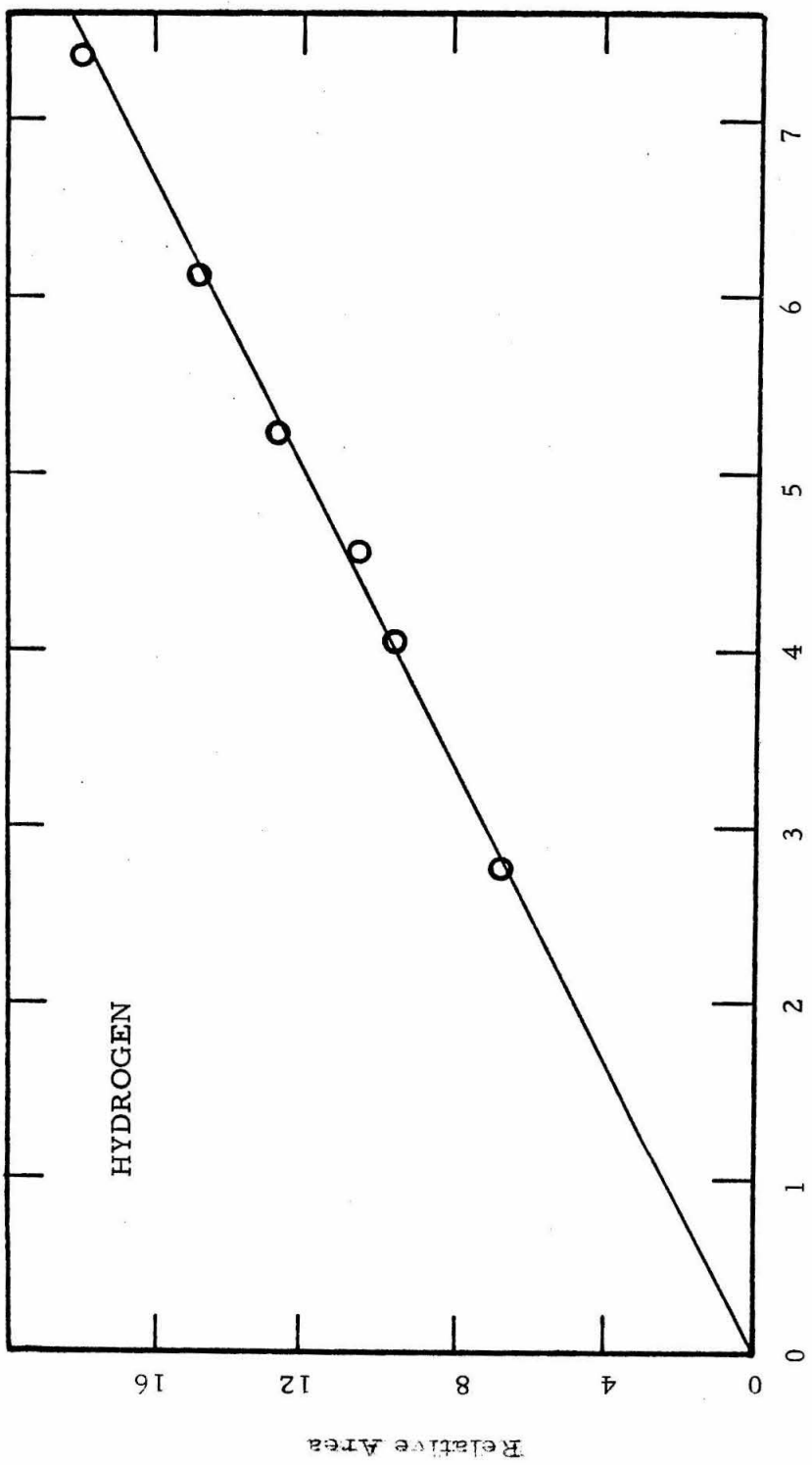

Figure 39.--Gas chromatograph calibration for hydrogen.

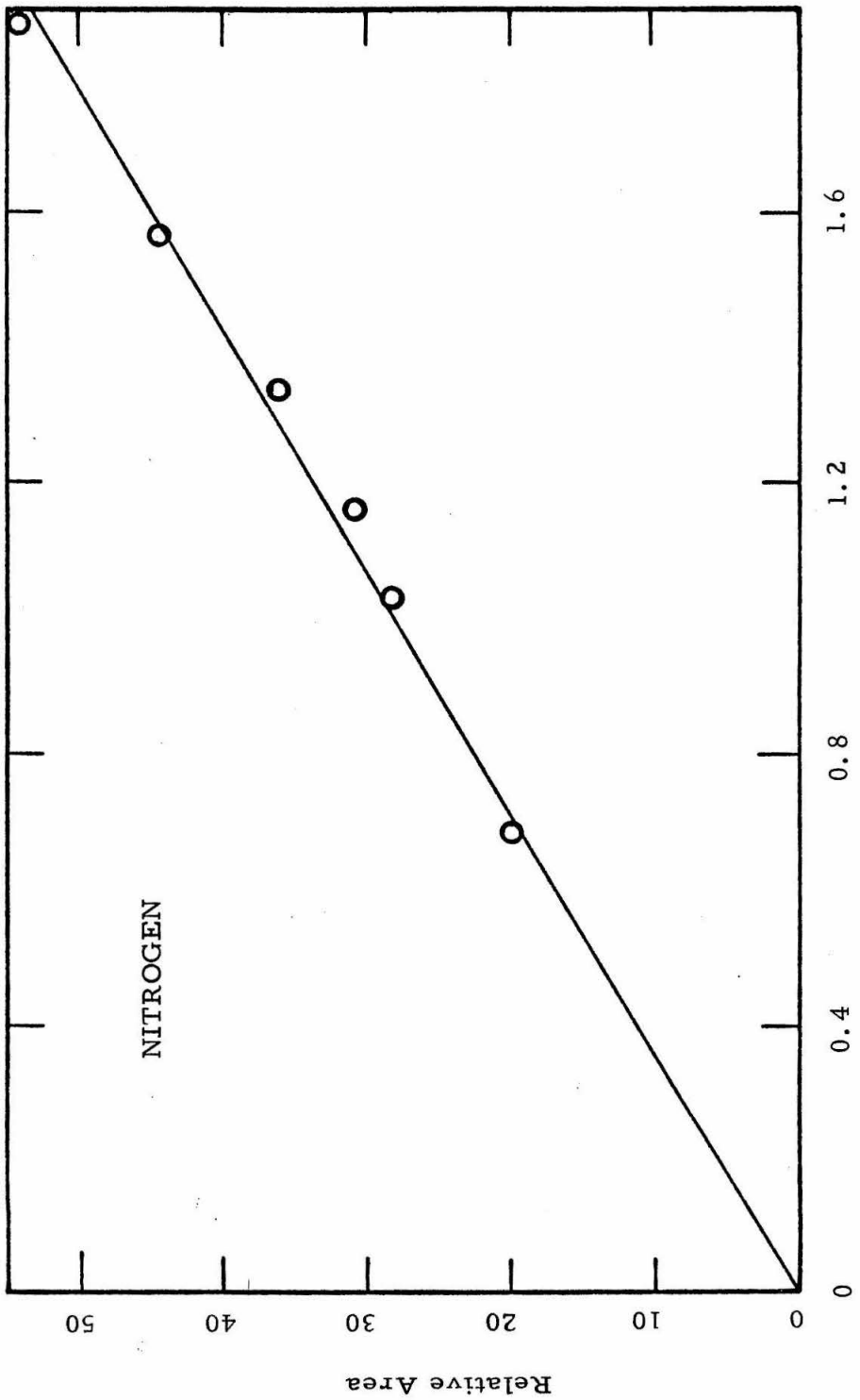

Figure 40.--Gas chromatograph calibration for nitrogen.

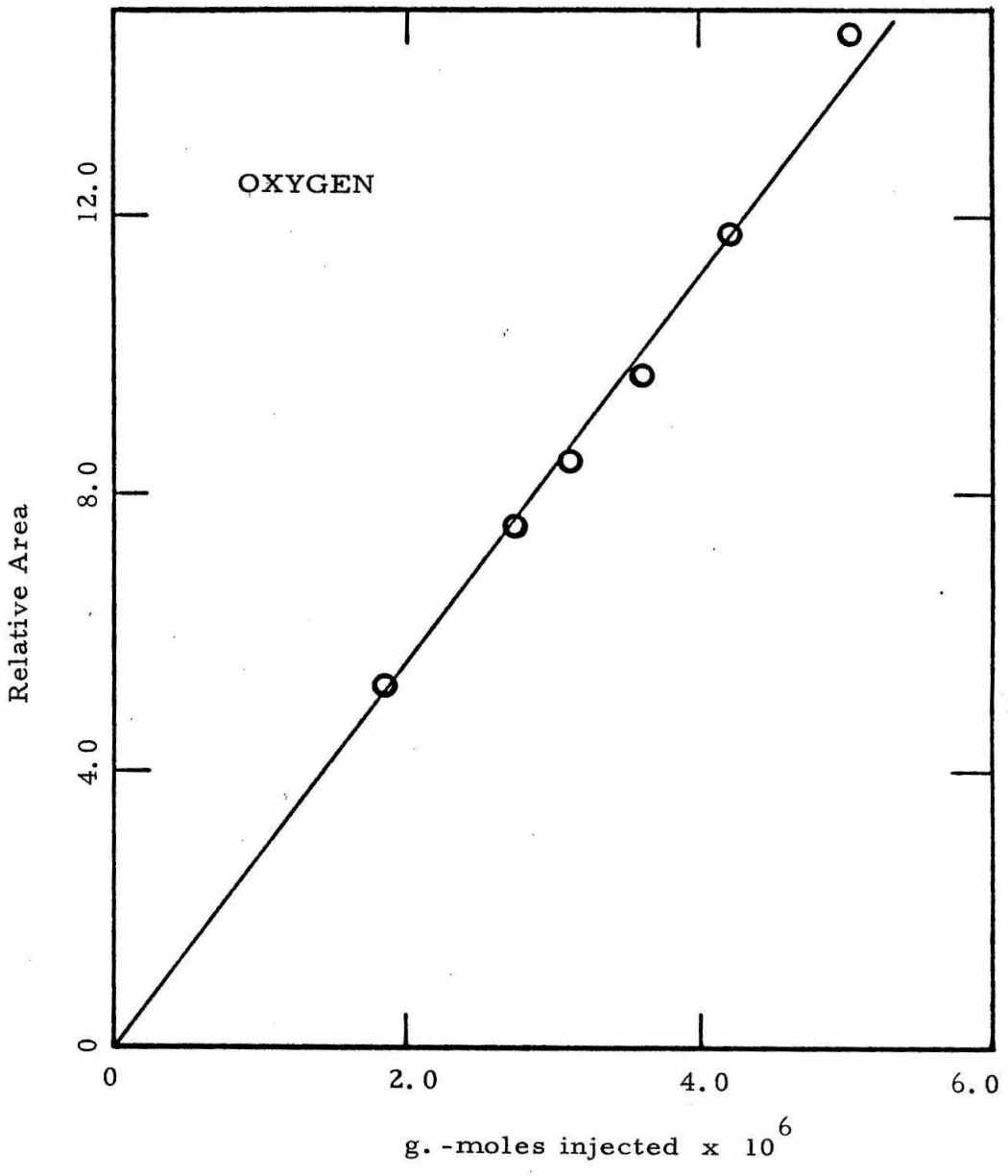

Figure 41.--Gas chromatograph calibration for oxygen.

These figures indicate that the chromatograph response was linear for the injection quantities expected in the experimental runs.

The volume of the small injection volume was determined as follows. Sample number four was passed through the chromatograph using the small injection volume and a carrier gas flow rate of 26.1 milliliters per minute. The area under the nitrogen curve was found to be 23.20 on the previous relative scale. This corresponded to 8.23×10^{-6} per gram-mole of nitrogen. From the ideal gas law this corresponded to an injection volume of 0.525 milliliters.

Since the ratio of the chromatogram area to quantity injected was constant, the following proportionality factors were used:

$$\kappa \frac{\text{Area } O_2}{\text{Area } N_2} = \frac{\text{g.-moles } O_2 \text{ injected}}{\text{g.-moles } N_2 \text{ injected}}$$

$$\kappa' \frac{\text{Area } H_2}{\text{Area } N_2} = \frac{\text{g.-moles } H_2 \text{ injected}}{\text{g.-moles } N_2 \text{ injected}}$$

The values for κ and κ' were determined from Figures 39, 40, and 41 and are:

$$\kappa = 0.9983$$

$$\kappa' = 0.1151$$

APPENDIX F

TABULATED DATA

TABLE 10

TEMPERATURE DATA (FINAL SERIES OF RUNS)

No.	T_{in} (°F)	T_o (°F)	T_{res} (°F)	T_{air} (°F)	T_w (°C)	w (scale)	time (min:sec)	$m_{O_2, in}$ (ppm)	$m_{O_2, o}$ (ppm)
1.	75.5	189.5	74.5	75.0	744	15.0	12:20.4	8.19	2.94
2.	76.0	194.5	78.0	76.0	752	13.4	14:41.8	7.93	2.72
3.	75.0	200.5	75.0	75.5	760	11.6	16:35.6	8.35	2.30
4.	74.5	194.5	78.0	73.0	803	8.1	30:15.9	8.00	2.66
5.	74.5	190.0	74.0	75.2	796	7.1	30:15.7	8.40	2.86
6.	76.5	198.0	78.0	76.0	770	6.1	36:00	7.90	1.74
7.	74.0	194.0	74.5	75.0	746	17.15	10:39.4	8.30	2.84
8.	74.9	204.5	76.5	75.5	750	10.1	19:01.7	8.11	1.85
9.	76.5	205.5	80.0	77.0	755	10.1	18:40.0	7.70	1.73
10.	74.5	197.5	78.5	75.5	760	10.1	21:14.3	8.13	2.71
11.	75.5	194.0	77.0	77.0	769	10.1	23:04.1	8.11	2.90
12.	76.0	200.0	80.0	77.0	743	10.1	19:36.8	8.01	2.07
13.	74.9	200.5	75.0	75.5	919	7.0	27:17.1	8.62	2.44
14.	72.0	---	72.0	73.0	1143	7.0	46.9	8.38	---
15.	75.5	209.0	78.0	79.5	873	7.0	25:05.6	8.04	1.40
16.	73.0	198.0	72.0	75.0	945	7.0	17:17.3	9.04	2.08
17.	77.5	193.5	80.0	78.5	809	7.0	31:10.6	8.12	2.61
18.	74.8	208.5	77.5	75.5	844	7.0	30:24.3	7.99	1.45
19.	73.0	193.0	73.0	73.0	820	7.0	32:07.7	8.38	2.91
20.	76.5	193.0	78.5	77.3	812	7.0	33:40.1	8.32	2.88

TABLE 10 (Continued)

No.	T_{in} (°F)	T_o (°F)	T_{res} (°F)	T_{air} (°F)	T_w (°C)	w (scale)	time (min:sec)	$m_{O_2, in}$ (ppm)	$m_{O_2, o}$ (ppm)
21.	73.0	188.0	72.0	74.0	787	7.0	30:27.9	8.28	3.00
22.	75.5	199.2	79.0	77.0	872	7.0	28:00.5	8.03	2.20
23.	72.5	188.0	72.0	73.0	757	7.0	29:46.6	8.36	2.81
24.	76.5	198.0	79.5	78.0	751	7.0	28:33.6	8.18	2.19
25.	78.0	205.0	79.5	79.5	825	7.0	26:30.2	8.12	2.14
26.	76.0	194.0	94.0	77.3	752	7.0	37:01.8	7.09	2.40
27.	76.0	202.0	95.0	76.5	761	7.0	31:27.8	7.23	2.03
28.	78.5	205.0	94.5	78.5	782	7.0	32:30.2	7.24	1.95
29.	76.5	208.0	94.8	78.0	799	7.0	30:16.6	7.01	1.60
30.	75.0	209.5	98.5	76.0	811	7.0	16:19.1	7.00	1.78
31.	75.5	212.0	98.5	76.5	900	7.0	15:34.8	6.98	1.58
32.	75.0	210.0	94.0	75.5	845	7.0	24:45.7	7.27	1.37
33.	74.5	188.5	94.5	75.5	969	7.0	3:42.7	7.27	---
34.	74.0	186.0	94.0	75.5	1083	7.0	2:25.4	7.38	---
35.	74.0	192.0	94.8	75.5	833	7.0	31:10.0	7.10	2.09
36.	75.5	191.5	97.0	77.5	912	6.7	35:16.3	7.02	3.38
37.	75.8	200.0	98.5	76.0	810	7.0	30:08.9	7.09	1.94
38.	74.5	190.5	94.5	75.0	791	7.0	31:51.8	7.13	3.42
39.	76.8	190.5	95.0	77.5	804	7.0	30:43.1	7.17	3.04
40.	78.0	194.5	95.0	77.5	808	7.0	30:21.9	7.10	2.90

TABLE 10 (Continued)

No.	T_{in} (°F)	T_o (°F)	T_{res} (°F)	T_{air} (°F)	T_w (°C)	w (scale)	time (min:sec)	$m_{O_2, in}$ (ppm)	$m_{O_2, o}$ (ppm)
41.	75.5	189.5	88.5	76.0	761	7.0	32:18.3	7.48	3.47
42.	74.8	190.0	95.5	75.5	774	7.0	30:00.0	6.98	2.94
43.	74.5	209.8	94.5	75.5	951	7.0	22:02.4	7.28	1.53
44.	72.0	188.5	72.5	73.5	761	15.3	13:01.8	8.12	3.51
45.	82.0	189.5	94.5	75.5	760	16.4	12:34.1	6.87	3.47
46.	81.5	193.5	94.5	76.0	753	12.6	11:37.6	7.12	3.39
47.	77.5	200.8	94.5	75.3	754	10.4	17:51.4	7.41	2.38
48.	75.0	203.0	95.5	74.5	759	8.3	21:47.2	7.06	2.10
49.	74.0	187.5	94.3	74.0	757	7.0	31:41.1	7.20	2.92
50.	75.0	191.0	94.8	75.5	760	6.2	31:50.9	7.21	2.51
51.	76.0	203.0	94.5	75.0	756	9.2	12:42.0	7.08	2.19
52.	75.5	193.5	95.0	75.0	755	7.5	24:20.8	7.03	2.70
53.	79.5	200.0	95.5	74.5	758	11.7	12:08.0	7.01	2.66
54.	74.8	207.0	94.5	75.0	758	5.5	40:07.8	7.42	2.12
55.	79.5	194.0	95.0	75.0	761	14.0	11:18.1	7.10	3.71
56.	75.0	202.0	94.5	75.0	786	7.0	30:05.2	7.28	2.38
57.	75.5	204.0	98.0	75.5	811	7.0	25:28.8	7.08	2.02
58.	74.5	200.0	94.8	75.0	893	7.0	21:51.2	7.08	2.37
59.	75.0	203.5	98.0	76.0	938	7.0	17:00.0	7.38	1.60
60.	62.0	190.0	46.5	74.5	749	14.3	9:33.3	9.30	3.68

TABLE 10 (Continued)

No.	T_{in} (°F)	T_o (°F)	T_{res} (°F)	T_{air} (°F)	T_w (°C)	w (scale)	time (min:sec)	$m_{O_2, in}$ (ppm)	$m_{O_2, o}$ (ppm)
61.	60.0	190.5	41.0	74.5	744	14.3	12:39.6	11.48	3.70
62.	61.0	190.0	45.0	74.0	755	14.3	10:13.6	10.90	3.80
63.	60.5	192.0	41.0	74.8	754	14.3	11:41.8	11.10	3.65
64.	70.5	189.0	41.5	74.0	760	7.3	23:11.1	11.20	3.45
65.	71.0	189.0	40.5	74.0	772	7.0	29:50.9	11.30	3.80
66.	71.5	211.0	42.5	74.8	874	7.0	20:20.9	11.35	2.10
67.	71.5	192.5	41.0	74.8	845	7.0	22:34.4	11.60	3.60
68.	74.0	212.0	57.0	74.8	925	7.0	11:36.2	10.10	2.40
69.	74.5	198.0	78.5	74.5	750	14.3	13:03.1	7.90	3.22
70.	75.5	202.5	80.0	75.0	751	12.2	15:00.0	8.14	2.80
71.	74.5	188.5	76.5	75.0	754	19.4	7:01.9	8.12	3.83
72.	75.0	210.0	79.5	75.0	770	9.7	12:59.6	7.90	2.68
73.	73.0	208.0	73.0	74.3	748	7.9	22:01.3	8.32	2.30
74.	75.0	189.5	79.5	75.0	759	7.0	23:22.5	7.73	3.80
75.	74.0	210.5	77.5	74.8	810	7.0	31:00.0	8.44	2.96
76.	75.0	212.0	79.5	75.5	934	7.0	15:14.2	8.20	2.57
77.	73.0	189.5	74.3	74.0	751	19.9	8:16.6	8.19	4.00
78.	77.5	194.0	79.5	78.0	749	19.4	9:08.8	8.09	3.70
79.	71.5	197.0	72.0	74.0	749	14.65	10:38.3	9.10	2.89
80.	74.0	204.5	77.5	75.0	750	12.85	12:07.8	8.10	2.32

TABLE 10 (Continued)

No.	T_{in} (°F)	T_o (°F)	T_{res} (°F)	T_{air} (°F)	T_w (°C)	w (scale)	time (min:sec)	$m_{O_2,in}$ (ppm)	$m_{O_2,o}$ (ppm)
81.	74.0	210.0	77.5	74.8	743	10.7	15:02.1	7.83	1.70
82.	73.5	210.3	71.5	74.5	764	9.2	18:02.0	8.62	1.54
83.	76.0	211.0	75.0	77.0	743	8.3	15:00.0	8.48	1.48
84.	76.5	208.5	78.0	77.5	760	12.9	12:10.0	7.88	2.29
85.	76.3	208.0	79.0	76.5	783	12.9	11:41.6	7.72	1.90
86.	75.0	208.5	74.5	75.5	815	12.9	11:35.9	8.04	1.81
87.	74.8	209.0	75.5	77.0	813	12.9	9:34.2	8.11	1.84
88.	77.0	212.5	79.0	78.0	813	7.0	20:02.4	7.72	1.00
89.	75.3	213.0	79.5	78.0	868	7.0	15:00.0	7.68	0.90
90.	75.5	213.0	79.8	78.5	831	7.0	21:57.1	7.68	0.81
91.	74.5	192.0	73.0	74.5	---	13.0	14:29.0	8.64	3.25

TABLE 11

PRESSURE AND VOLUME DATA (FINAL SERIES OF DATA)

No.	V_i (ml.)	V_f (ml.)	ξ_i (in. Hg)	ξ_f (in. Hg)	P_{atm} (mm. Hg)	V_h (ml.)	V_c (ml.)	A_{H_2}	A_{O_2}	A_{N_2}
1.	3.7	26.3	-0.13	-0.13	740.8	27.0	26.8	2.3	58.8	130.4
2.	2.1	25.1	-0.15	-0.15	740.8	25.3	25.1	---	63.2	126.5
3.	4.0	28.0	-0.05	0.0	745.1	28.6	28.4	---	65.6	133.0
4.	2.0	23.5	0.0	0.0	745.1	24.0	23.8	---	68.0	131.7
5.	2.8	20.2	0.0	0.0	744.2	20.6	20.5	4.8	60.1	129.8
6.	2.6	20.5	0.0	0.0	744.2	20.7	20.6	0.6	62.1	129.5
7.	2.4	26.6	-0.15	-0.15	743.2	27.2	27.1	---	58.6	123.2
8.	2.5	25.7	0.0	0.0	743.2	26.3	26.0	---	65.7	126.7
9.	3.0	24.7	0.0	0.0	743.2	25.6	25.5	---	67.3	127.5
10.	2.0	23.8	0.0	0.0	743.2	24.4	24.4	---	64.0	125.5
11.	2.0	24.1	0.0	0.0	745.5	24.9	24.9	---	58.6	125.4
12.	3.0	24.1	0.0	0.0	745.5	25.5	25.2	---	60.0	121.5
13.	2.3	20.0	0.0	0.0	744.5	20.2	20.2	96.2	58.3	121.5
14.	4.0	44.0	0.0	0.0	748.2	50.2	50.2	8600.0	1.3	2.6
15.	2.0	22.7	0.0	0.0	748.2	23.1	19.5	4.8	60.2	122.6
16.	3.5	27.5	0.0	0.0	753.1	28.0	28.0	970.0	33.2	81.7
17.	2.0	19.5	0.0	0.0	753.1	19.7	19.7	42.5	54.7	129.0
18.	2.0	23.1	0.0	0.0	753.1	23.4	23.4	173.2	49.0	110.5
19.	2.0	20.0	0.0	0.0	748.5	20.4	20.4	15.7	61.7	119.5
20.	2.0	20.1	0.0	0.0	748.5	21.5	21.3	44.3	50.3	130.0

TABLE 11 (Continued)

No.	V_i (ml.)	V_f (ml.)	ξ_i (in. Hg)	ξ_f (in. Hg)	P_{atm} (mm. Hg)	V_h (ml.)	V_c (ml.)	A_{H_2}	A_{O_2}	A_{N_2}
21.	2.2	20.0	0.0	0.0	747.5	20.3	20.3	8.5	63.8	133.2
22.	2.6	20.0	0.0	0.0	747.5	20.4	20.4	70.3	60.4	130.2
23.	2.0	18.6	0.0	0.0	744.0	19.0	19.0	22.5	64.1	127.7
24.	2.4	21.1	0.0	0.0	744.0	21.5	21.5	1.3	64.7	125.5
25.	2.0	18.7	0.0	0.0	745.1	18.9	18.9	20.2	57.2	113.5
26.	2.0	21.0	0.0	0.0	742.9	22.4	22.3	19.2	56.0	120.0
27.	3.6	21.1	0.0	0.0	745.8	21.6	21.6	4.2	62.3	124.9
28.	2.0	19.0	0.0	0.0	745.8	19.3	19.3	9.9	59.3	122.8
29.	2.0	19.3	0.0	0.0	745.8	19.6	19.6	54.7	58.6	118.9
30.	2.0	12.9	0.0	0.0	742.2	13.2	13.2	151.2	50.5	109.0
31.	2.3	21.1	0.0	0.0	742.2	21.5	21.3	767.0	17.7	61.6
32.	4.0	27.3	0.0	0.0	742.2	28.0	27.8	650.0	24.5	64.2
33.	5.0	25.2	0.0	0.0	742.2	26.6	26.6	1232.0	----	34.3
34.	3.0	30.5	0.0	0.0	742.2	33.6	33.4	1335.0	---	14.8
35.	2.1	18.2	0.0	0.0	742.2	18.4	18.4	102.8	52.0	115.9
36.	2.8	18.0	0.0	0.0	747.0	18.2	18.2	92.3	58.8	112.7
37.	2.0	21.6	0.0	0.0	744.4	21.9	21.8	319.8	56.2	102.3
38.	2.5	15.1	0.0	0.0	744.4	15.2	15.2	16.8	57.5	136.4
39.	2.0	15.6	0.0	0.0	744.4	15.4	15.8	52.0	58.5	130.1
40.	2.0	16.1	0.0	0.0	744.4	16.2	16.1	29.5	59.1	125.7

TABLE 11 (Continued)

No.	V_i (ml.)	V_f (ml.)	ξ_i (in. Hg)	ξ_f (in. Hg)	P_{atm} (mm. Hg)	V_h (ml.)	V_c (ml.)	A_{H_2}	A_{O_2}	A_{N_2}
41.	3.3	17.9	0.0	0.0	745.9	18.0	17.4	5.5	58.6	124.6
42.	2.0	15.6	0.0	0.0	745.9	15.7	15.6	1.3	62.8	123.0
43.	2.0	15.0	0.0	0.0	745.9	15.4	15.3	18.8	63.0	120.0
44.	3.1	27.3	-0.13	-0.13	747.1	28.2	28.2	1.3	64.1	124.3
45.	3.0	23.0	-0.13	-0.13	747.1	23.1	23.0	0.2	61.2	122.8
46.	3.0	18.3	-0.03	-0.03	747.1	19.0	19.0	0.2	60.6	124.3
47.	2.0	22.3	0.00	-0.00	746.3	23.0	23.0	0.1	58.3	118.0
48.	2.5	19.8	0.0	0.0	746.3	19.9	20.0	0.1	60.8	110.6
49.	2.6	17.6	0.0	0.0	746.3	17.7	17.7	0.1	61.7	118.5
50.	3.5	15.9	0.0	0.0	746.3	16.0	16.0	0.1	63.9	121.7
51.	2.3	14.4	0.0	0.0	746.3	15.0	15.0	0.1	62.4	119.3
52.	2.3	16.9	0.0	0.0	746.3	17.2	17.2	0.1	64.1	122.7
53.	2.9	17.9	0.0	0.0	746.3	18.2	18.2	0.1	60.8	113.1
54.	2.0	16.0	0.0	0.0	746.3	16.0	16.0	0.1	62.7	119.2
55.	2.1	18.0	0.0	0.0	746.3	18.2	18.4	0.2	67.1	132.9
56.	2.3	19.2	0.0	0.0	746.1	19.3	19.3	0.1	60.5	120.1
57.	5.0	19.4	0.0	0.0	746.1	19.6	19.6	14.2	57.1	118.6
58.	2.3	23.6	0.0	0.0	746.1	23.7	23.7	695.0	32.0	76.4
59.	4.1	31.0	0.0	0.0	746.1	31.0	30.7	961.0	16.0	52.5
60.	2.5	24.1	-0.05	-0.15	746.1	24.6	24.5	1.6	62.3	125.1

TABLE 11 (continued)

No.	V_i (ml.)	V_f (ml.)	ξ_i (in. Hg)	ξ_f (in. Hg)	P_{atm} (mm. Hg)	V_h (ml.)	V_c (ml.)	A_{H_2}	A_{O_2}	A_{N_2}
61.	2.0	33.1	-0.13	-0.13	746.1	33.9	33.8	0.1	61.7	121.8
62.	2.0	26.3	-0.13	0.16	746.1	27.8	27.8	0.1	61.2	120.0
63.	3.2	31.0	0.0	0.0	746.1	32.0	32.0	0.5	60.6	115.6
64.	2.1	21.3	0.0	0.0	747.1	21.6	21.6	3.4	64.4	122.1
65.	2.0	20.6	0.0	0.0	747.1	21.0	21.0	0.8	63.6	119.6
66.	2.1	19.5	0.0	0.0	747.1	19.7	19.7	33.9	56.1	109.5
67.	2.4	19.1	0.0	0.0	748.0	19.3	19.3	51.7	55.8	117.9
68.	3.3	18.0	0.0	0.0	748.0	18.1	18.0	461.0	41.2	84.9
69.	2.1	26.4	-0.15	-0.15	748.0	26.8	26.6	22.0	58.9	118.5
70.	3.2	26.2	-0.1	-0.1	748.0	26.8	26.6	0.1	59.4	114.4
71.	2.8	20.5	-0.23	-0.23	748.0	21.8	21.6	0.1	57.7	125.9
72.	2.2	18.3	0.0	0.0	748.0	18.8	18.6	0.1	60.2	117.3
73.	2.4	22.2	0.0	0.0	748.0	22.6	22.4	0.1	60.3	116.2
74.	2.4	14.2	0.0	0.0	748.0	14.4	14.4	0.1	63.7	125.9
75.	2.0	18.1	0.0	0.0	745.4	18.4	18.2	28.0	53.9	100.2
76.	2.6	24.1	0.0	0.0	745.4	24.2	24.0	714.0	---	56.5
77.	2.1	25.1	-0.22	-0.22	745.4	25.7	25.5	96.8	55.4	105.8
78.	2.3	26.1	-0.22	-0.22	745.4	26.3	26.0	0.6	60.1	112.8
79.	3.3	24.8	-0.19	-0.19	745.4	25.1	24.8	0.1	59.9	111.8
80.	2.8	24.6	-0.12	-0.12	745.4	24.9	24.7	0.1	64.1	123.8

TABLE 11 (Continued)

No.	V_i (ml.)	V_f (ml.)	ξ_i (in. Hg)	ξ_f (in. Hg)	P_{atm} (mm. Hg)	V_h (ml.)	V_c (ml.)	A_{H_2}	A_{O_2}	A_{N_2}
81.	3.3	24.8	0.0	0.0	745.4	25.6	25.5	0.1	63.1	117.6
82.	2.0	24.7	0.0	0.0	745.4	25.0	25.0	0.1	67.4	120.0
83.	2.1	18.0	0.0	0.0	745.4	18.5	18.4	0.1	59.9	114.6
84.	3.3	25.2	-0.8	-0.8	745.1	26.4	25.8	0.1	53.9	113.2
85.	3.8	25.1	-0.8	-0.8	745.1	25.5	25.3	0.2	60.1	117.0
86.	3.1	24.2	-0.8	-0.8	745.1	24.8	24.5	0.2	62.0	114.9
87.	3.3	21.0	-0.8	-0.8	745.1	21.7	21.6	0.3	59.6	117.0
88.	3.1	19.1	0.0	0.0	745.1	19.6	19.5	0.3	61.3	116.4
89.	2.4	20.1	0.0	0.0	745.1	20.6	20.5	519.0	29.3	85.4
90.	2.0	18.2	0.0	0.0	745.1	18.7	18.6	34.0	51.4	110.1
91.	2.5	25.0	-0.13	-0.13	744.0	26.9	26.5	---	60.9	130.8

APPENDIX G

TABULATED RESULTS

TABLE 12

VOLUME OF COLLECTED NON-CONDENSABLES

No.	P_i (atm.)	P_f (atm.)	V_i^* (ml.)	V_f^* (ml.)	water (v. p.) (mm. Hg)	w (g/sec)	w·t (kg.)	ΔV(dry) (S. T. P.) (ml/kg)
1.	.926	.948	5.8	28.2	22.4	2.32	1.718	11.08
2.	.924	.946	4.2	27.0	23.2	1.98	1.746	11.02
3.	.932	.956	6.1	29.9	22.6	1.60	1.593	12.81
4.	.930	.951	4.1	25.4	20.8	.83	1.507	12.10
5.	.930	.947	4.9	22.2	22.4	.61	1.108	13.24
6.	.930	.947	4.7	22.5	23.2	.43	.929	16.20
7.	.927	.951	4.5	28.6	22.4	2.78	1.778	11.54
8.	.928	.951	4.6	27.5	22.6	1.27	1.450	13.43
9.	.928	.950	5.1	26.7	23.8	1.27	1.422	12.85
10.	.928	.949	4.1	25.9	22.6	1.27	1.618	11.42
11.	.931	.952	4.1	26.2	23.8	1.27	1.758	10.65
12.	.932	.952	5.1	25.9	23.8	1.27	1.495	11.80
13.	.930	.947	4.4	22.1	22.6	.61	.999	15.00
14.	.936	.975	6.1	46.1	20.8	.61	.029	1230.48
15.	.934	.955	4.1	21.2	25.8	.61	1.056	13.68
16.	.942	.966	5.6	29.6	22.4	.61	.633	32.86
17.	.941	.958	4.1	21.6	20.8	.61	1.141	13.09
18.	.941	.961	4.1	25.2	22.6	.61	1.113	16.29
19.	.935	.952	4.1	22.1	20.8	.61	1.176	13.12
20.	.935	.952	4.1	22.0	24.0	.61	1.232	12.29

TABLE 12 (Continued)

No.	P_i (atm.)	P_f (atm.)	V_i^* (ml.)	V_f^* (ml.)	water (v. p.) (mm. Hg.)	w (g/sec)	w·t (kg.)	ΔV(dry) (S. T. P.) (ml/kg)
21.	.934	.951	4.3	22.1	21.6	.61	1.115	13.63
22.	.934	.951	4.7	22.1	24.0	.61	1.025	14.37
23.	.929	.947	4.1	20.7	20.6	.61	1.090	12.99
24.	.929	.947	4.5	23.2	24.6	.61	1.045	15.03
25.	.930	.947	4.1	20.8	25.8	.61	.970	14.40
26.	.927	.946	4.4	23.0	24.0	.61	1.355	11.55
27.	.933	.950	5.7	23.2	23.5	.61	1.152	12.88
28.	.931	.948	4.1	37.7	25.2	.61	1.190	23.66
29.	.931	.948	4.1	21.4	24.5	.61	1.108	13.13
30.	.927	.937	4.1	15.0	23.2	.61	.597	15.25
31.	.927	.945	4.4	23.0	23.5	.61	.570	27.47
32.	.929	.951	6.1	29.2	22.7	.61	.906	21.70
33.	.930	.949	7.1	27.3	22.7	.61	.136	126.45
34.	.928	.954	5.1	32.3	22.7	.61	.089	261.71
35.	.927	.942	4.1	20.3	22.7	.61	1.141	11.95
36.	.934	.948	4.9	20.1	24.0	.55	1.164	11.01
37.	.929	.948	4.1	23.6	23.2	.61	1.103	14.95
38.	.930	.942	4.6	17.2	22.4	.61	1.166	9.11
39.	.929	.943	4.1	17.7	24.3	.61	1.124	10.13
40.	.929	.943	4.1	18.1	24.3	.61	1.111	10.55

TABLE 12 (Continued)

No.	P_i (atm.)	P_f (atm.)	V_i* (ml.)	V_f* (ml.)	water (v. p.) (mm. Hg)	w (g/sec)	w·t (kg.)	ΔV(dry) (S. T. P.) (ml/kg)
41.	.933	.947	5.4	19.4	23.2	.61	1.182	10.02
42.	.931	.945	4.1	17.7	22.6	.61	1.098	10.46
43.	.931	.944	4.1	17.0	22.6	.61	.807	13.49
44.	.928	.949	5.2	29.4	21.3	2.39	1.869	11.05
45.	.926	.945	5.1	25.0	22.6	2.62	1.976	8.51
46.	.932	.947	5.1	20.4	23.2	1.81	1.263	10.25
47.	.932	.952	4.1	24.4	22.6	1.34	1.436	12.04
48.	.932	.949	4.6	21.8	21.8	.89	1.163	12.58
49.	.933	.947	4.7	19.7	21.6	.61	1.160	11.00
50.	.933	.948	5.6	21.0	22.6	.45	.860	15.20
51.	.932	.944	4.4	16.5	22.4	1.08	.823	12.42
52.	.932	.946	4.4	19.0	22.4	.72	1.052	11.75
53.	.933	.947	5.0	20.0	21.8	1.62	1.179	10.80
54.	.932	.946	4.1	18.1	22.4	.72	1.734	6.84
55.	.932	.948	4.2	20.0	22.4	2.12	1.438	9.33
56.	.933	.949	4.4	21.3	22.4	.61	1.101	13.03
57.	.935	.949	7.1	21.5	22.6	.61	.933	13.14
58.	.932	.953	4.4	25.7	22.4	.61	.800	22.72
59.	.934	.960	6.2	32.8	23.2	.61	.622	36.70
60.	.929	.944	4.6	26.1	21.8	2.18	1.250	14.54

TABLE 12 (Continued)

No.	P_i (atm.)	P_f (atm.)	V_i* (ml.)	V_f* (ml.)	water (v. p.) (mm. Hg)	w (g/sec)	w·t (kg.)	ΔV(dry) (S. T. P.) (ml/kg)
61.	.923	.954	4.1	35.1	21.8	2.18	1.656	16.01
62.	.923	.966	4.1	28.4	21.6	2.18	1.338	15.81
63.	.932	.960	5.3	33.1	22.1	2.18	1.530	15.65
64.	.933	.952	4.2	23.4	21.6	.68	.946	17.35
65.	.933	.951	4.1	22.7	21.6	.61	1.092	14.53
66.	.933	.950	4.2	21.6	22.1	.61	.745	19.88
67.	.935	.951	4.5	22.2	22.1	.61	.826	18.25
68.	.935	.950	5.4	20.0	22.1	.61	.425	29.30
69.	.925	.948	4.2	28.3	21.8	2.18	1.707	12.00
70.	.929	.951	5.3	28.1	22.4	1.73	1.557	12.48
71.	.920	.937	4.9	22.4	22.4	3.28	1.384	10.61
72.	.929	.945	4.3	20.2	22.4	1.19	.928	14.50
73.	.935	.954	4.5	24.1	21.8	.81	1.070	15.68
74.	.934	.946	4.5	16.3	22.4	.61	.856	11.68
75.	.931	.946	4.1	20.0	22.1	.61	1.135	11.87
76.	.931	.952	4.7	26.0	22.6	.61	.558	32.52
77.	.917	.939	4.2	27.0	21.6	3.37	1.674	11.48
78.	.917	.940	4.4	27.9	24.6	3.28	1.800	10.89
79.	.920	.941	5.4	26.6	21.6	2.25	1.436	12.48
80.	.924	.945	4.9	26.5	22.4	1.88	1.368	13.36

TABLE 12 (Continued)

No.	P_i (atm.)	P_f (atm.)	V_i^* (ml.)	V_f^* (ml.)	water (v. p.) (mm. Hg)	w (g/sec)	w·t (kg.)	ΔV(dry) (S. T. P.) (ml/kg)
81.	.932	.953	5.4	26.8	22.1	1.40	1.263	14.48
82.	.931	.953	4.1	26.8	21.8	1.08	1.169	16.60
83.	.930	.946	4.2	20.0	23.8	.89	.801	16.60
84.	.926	.948	5.4	26.7	24.3	1.88	1.372	13.09
85.	.927	.948	5.9	27.0	23.5	1.88	1.319	13.54
86.	.926	.947	5.2	26.0	22.6	1.88	1.308	13.47
87.	.926	.944	5.4	23.0	23.8	1.88	1.079	13.71
88.	.931	.947	5.2	21.1	24.6	.61	.733	18.23
89.	.931	.948	4.5	22.1	24.6	.61	.549	26.97
90.	.930	.946	4.1	20.2	24.9	.61	.803	16.79
91.	.929	.950	4.6	26.7	21.9	1.90	1.651	11.43

TABLE 13

CONCENTRATIONS IN LIQUID AND COMPOSITION OF FILM

	Dissolved Gases at P_{atm}			Composition of Film		
No.	air_{in} (cc/kg)	$O_{2,in}$ (ppm)	$O_{2,o}$ (ppm)	x_{H_2}	x_{O_2}	x_{N_2}
1.	16.07	8.20	2.94	.0005	.1161	.2484
2.	16.57	7.94	2.72	.0000	.1074	.2509
3.	17.32	8.41	2.32	.0000	.0913	.2021
4.	16.76	8.06	2.68	.0000	.1056	.2443
5.	16.44	8.45	2.88	.0010	.1134	.2378
6.	16.59	7.94	1.75	.0001	.0690	.1516
7.	17.22	8.34	2.85	.0000	.1125	.2587
8.	16.77	8.15	1.86	.0000	.0733	.1582
9.	16.12	7.73	1.74	.0000	.0685	.1505
10.	16.82	8.17	2.72	.0000	.1073	.2447
11.	16.82	8.17	2.92	.0000	.1152	.2657
12.	16.77	8.07	2.09	.0000	.0822	.1828
13.	17.91	8.67	2.45	.0197	.0968	.2159
14.	17.44	8.47	.00	.0291	.0000	.0001
15.	16.83	8.13	1.42	.0065	.0558	.1184
16.	18.78	9.20	2.12	.2434	.0835	.1781
17.	17.15	8.26	2.66	.0091	.1047	.2400
18.	16.91	8.13	1.48	.0225	.0582	.1247
19.	16.39	8.48	2.94	.0037	.1161	.2418
20.	17.40	8.42	2.91	.0104	.1149	.2651
21.	16.31	8.36	3.03	.0019	.1195	.2542
22.	16.92	8.11	2.22	.0123	.0876	.1975
23.	17.34	8.41	2.83	.0052	.1114	.2549
24.	16.14	8.22	2.20	.0002	.0868	.1777
25.	16.97	8.18	2.15	.0039	.0850	.1890
26.	14.61	7.12	2.41	.0040	.0950	.2160
27.	14.82	7.29	2.05	.0007	.0807	.1756
28.	14.82	7.30	1.97	.0016	.0775	.1673
29.	14.51	7.06	1.61	.0072	.0636	.1368
30.	14.34	7.02	1.79	.0243	.0704	.1522

TABLE 13 (Continued)

	Dissolved Gases at P_{atm}			Composition of Film		
No.	air_{in} (cc/kg)	$O_{2,in}$ (ppm)	$O_{2,o}$ (ppm)	x_{H_2}	x_{O_2}	x_{N_2}
31.	14.29	7.00	1.58	.1907	.0625	.1331
32.	14.84	7.29	1.32	.1262	.0522	.1083
33.	14.84	7.29	4.31	*****	.1701	.4397
34.	14.19	7.40	4.91	*****	.1938	.4775
35.	14.54	7.12	2.10	.0186	.0827	.1822
36.	14.54	7.09	3.41	.0311	.1345	.3303
37.	14.64	7.13	1.95	.0609	.0770	.1692
38.	14.79	7.17	3.44	.0048	.1357	.3353
39.	14.91	7.21	3.06	.0133	.1206	.2900
40.	14.74	7.14	2.92	.0074	.1150	.2737
41.	15.57	7.54	3.50	.0017	.1379	.3386
42.	14.36	7.04	2.96	.0003	.1169	.2753
43.	15.12	7.34	1.54	.0024	.0608	.1303
44.	16.81	8.20	3.54	.0004	.1397	.3335
45.	14.18	6.94	3.50	.0001	.1381	.3419
46.	14.79	7.19	3.42	.0001	.1350	.3318
47.	15.48	7.47	2.40	.0000	.0946	.2162
48.	14.77	7.12	2.12	.0000	.0835	.1889
49.	14.98	7.26	2.94	.0000	.1161	.2757
50.	15.03	7.27	2.59	.0000	.1022	.2370
51.	14.77	7.14	2.21	.0000	.0871	.1973
52.	14.51	7.09	2.72	.0000	.1074	.2489
53.	14.47	7.07	2.68	.0000	.1058	.2447
54.	14.57	7.48	2.14	.0000	.0843	.1720
55.	14.72	7.16	3.74	.0001	.1475	.3719
56.	15.17	7.34	2.40	.0000	.0946	.2161
57.	14.77	7.14	2.04	.0025	.0803	.1798
58.	14.77	7.14	2.39	.2266	.0942	.2164
59.	15.38	7.44	1.61	.2895	.0636	.1374
60.	19.31	9.78	3.71	.0000	.1463	.3202

TABLE 13 (Continued)

	Dissolved Gases at P_{atm}			Composition of Film		
No.	air_{in} (cc/kg)	$O_{2,in}$ (ppm)	$O_{2,o}$ (ppm)	x_{H_2}	x_{O_2}	x_{N_2}
61.	22.58	11.57	3.73	.0000	.1471	.3067
62.	21.83	10.99	3.83	.0000	.1511	.3284
63.	22.16	11.19	3.68	.0002	.1451	.3106
64.	22.21	11.31	3.48	.0009	.1373	.2873
65.	22.51	11.41	3.84	.0002	.1513	.3233
66.	22.61	11.46	2.12	.0059	.0836	.1656
67.	23.10	11.73	3.64	.0152	.1435	.3019
68.	20.42	10.21	2.43	.1241	.0957	.1986
69.	16.68	7.99	3.25	.0066	.1283	.3108
70.	16.80	8.23	2.83	.0000	.1116	.2524
71.	16.97	8.21	3.87	.0000	.1527	.3771
72.	16.68	7.99	2.61	.0000	.1028	.2386
73.	17.39	8.32	2.32	.0000	.0917	.2078
74.	16.35	7.81	2.99	.0000	.1180	.2827
75.	17.98	8.50	2.98	.0084	.1176	.2814
76.	17.12	8.26	2.53	.3290	.0997	.2262
77.	17.10	8.25	4.03	.0419	.1589	.3977
78.	16.92	8.15	3.73	.0002	.1470	.3624
79.	18.74	9.17	2.91	.0000	.1146	.2560
80.	16.92	8.16	2.34	.0000	.0921	.2071
81.	16.52	7.89	1.71	.0000	.0675	.1488
82.	17.88	8.68	1.55	.0000	.0612	.1290
83.	17.62	8.54	1.49	.0000	.0588	.1241
84.	16.61	7.93	2.31	.0000	.0909	.2077
85.	16.29	7.87	1.91	.0000	.0754	.1655
86.	16.82	8.10	1.82	.0000	.0719	.1571
87.	16.97	8.17	1.85	.0000	.0731	.1599
88.	16.29	7.77	1.01	.0000	.0397	.0840
89.	16.19	7.73	.91	.0525	.0357	.0750
90.	16.19	7.73	.82	.0036	.0322	.0672
91.	17.81	8.69	3.27	*****	.1288	.2983

TABLE 14

RATIO VAPORIZED, RATIO OXYGEN TO NITROGEN IN FILM, PERCENTAGE OXYGEN REMOVED, AND KINETIC RESULTS

No.	$\frac{N_2}{N_3} \times 10^5$	$\frac{x_{O_2}}{x_{N_2}}$ (exp)	$\frac{x_{O_2}}{x_{N_2}}$ (th)	% O_2 removed	O_2 reacted (molar ratio)	$\ln N_R$ (H_2)
1.	2.547	.4376	.4671	64.1	.0852	-21.42
2.	2.732	.4848	.4279	65.7	.0150	******
3.	3.752	.4786	.4519	72.5	.0283	******
4.	2.864	.5010	.4323	66.7	-.0724	******
5.	2.763	.4493	.4770	66.0	-.0488	-22.01
6.	5.050	.4653	.4551	78.0	-.1849	-24.44
7.	2.743	.4616	.4348	65.8	.0509	******
8.	4.827	.5032	.4631	77.2	-.0211	******
9.	4.923	.5122	.4553	77.5	-.0365	******
10.	2.853	.4949	.4387	66.7	.0082	******
11.	2.563	.4535	.4335	64.2	.0963	******
12.	4.094	.4792	.4498	74.2	.0880	******
13.	3.613	.4656	.4484	71.7	-.0304	-18.85
14.	******	.4852	.5154	****	.7368	-10.66
15.	6.766	.4765	.4714	82.6	.0642	-21.96
16.	4.773	.3943	.4687	77.0	.0542	-16.12
17.	3.012	.4115	.4365	67.9	.0536	-19.75
18.	6.434	.4303	.4666	81.9	.0667	-18.26
19.	2.681	.5010	.4801	65.3	-.1185	-20.74
20.	2.695	.3755	.4333	65.4	.1535	-19.69
21.	2.511	.4648	.4700	63.8	-.1517	-21.46
22.	3.780	.4502	.4437	72.6	-.0367	-19.29
23.	2.818	.4871	.4371	66.4	-.0743	-20.36
24.	3.902	.5003	.4887	73.2	-.1873	-23.32
25.	3.986	.4890	.4494	73.6	-.1059	-20.40
26.	2.788	.4529	.4399	66.1	-.0775	-20.63
27.	3.654	.4840	.4595	71.9	-.1416	-22.21
28.	3.870	.4686	.4631	73.1	-1.0087	-21.34
29.	4.823	.4783	.4648	77.2	-.0738	-19.63
30.	4.183	.4496	.4627	74.6	-.1614	-18.53

TABLE 14 (Continued)

No.	$\frac{N_2}{N_3} \times 10^5$	$\frac{x_{O_2}}{x_{N_2}}$ (exp)	$\frac{x_{O_2}}{x_{N_2}}$ (th)	% O_2 removed	O_2 reacted (molar ratio)	$\ln N_R$ (H_2)
31.	4.875	.2788	.4696	77.4	.2557	-16.35
32.	6.430	.3703	.4821	81.8	.2418	-16.54
33.	.985	.4244	.3868	40.9	-3.6267	-15.08
34.	.722	.6557	.4058	33.6	-7.1813	-14.20
35.	3.420	.4354	.4536	70.6	.0386	-18.95
36.	1.536	.5063	.4073	51.9	-.3531	-19.04
37.	3.787	.5331	.4547	72.6	-.1602	-17.69
38.	1.547	.4091	.4046	52.0	-.0016	-20.81
39.	1.938	.4363	.4158	57.6	-.0246	-19.65
40.	2.066	.4563	.4203	59.2	-.0965	-20.20
41.	1.649	.4564	.4073	53.6	-.1051	-21.79
42.	1.960	.4955	.4245	57.9	-.2139	-23.33
43.	5.361	.5095	.4666	79.0	-.1082	-20.67
44.	1.874	.5004	.4190	56.8	-.1295	-21.81
45.	1.398	.4836	.4041	49.5	-.1535	-23.71
46.	1.570	.4731	.4068	52.4	-.2478	-24.06
47.	3.015	.4794	.4378	67.9	-.0980	******
48.	3.369	.5335	.4422	70.3	-.2489	******
49.	2.091	.5053	.4212	59.4	-.2211	******
50.	2.576	.5255	.4312	64.4	-.5972	******
51.	3.185	.5076	.4414	69.1	-.2104	******
52.	2.288	.5069	.4313	61.6	-.2921	******
53.	2.333	.5217	.4323	62.1	-.2048	******
54.	3.566	.5104	.4903	71.4	.3827	******
55.	1.303	.4899	.3967	47.7	-.2809	-23.96
56.	2.937	.4888	.4379	67.3	-.2371	******
57.	3.573	.4672	.4466	71.5	-.1599	-20.93
58.	2.835	.4065	.4354	66.5	-.1315	-16.58
59.	5.153	.2957	.4629	78.3	.2184	-15.89
60.	2.334	.4833	.4569	62.1	-.1141	-23.91

TABLE 14 (Continued)

No.	$\frac{N_2}{N_3}$ x 10^5	$\frac{x_{O_2}}{x_{N_2}}$ (exp)	$\frac{x_{O_2}}{x_{N_2}}$ (th)	% O_2 removed	O_2 reacted (molar ratio)	$\ln N_R$ (H_2)
61.	3.000	.4916	.4797	67.8	.0398	******
62.	2.665	.4949	.4601	65.1	-.0437	******
63.	2.912	.5087	.4671	67.1	-.0026	-22.58
64.	3.205	.5118	.4781	69.2	-.0694	-21.89
65.	2.816	.5160	.4679	66.4	.0680	-23.40
66.	6.284	.4972	.5048	81.5	.0143	-19.62
67.	3.170	.4593	.4753	69.0	.0199	-19.20
68.	4.577	.4709	.4817	76.2	-.2075	-16.83
69.	2.073	.4823	.4130	59.2	-.1616	-19.27
70.	2.721	.5039	.4421	65.6	-.1058	******
71.	1.598	.4447	.4048	52.8	-.0752	******
72.	2.942	.4980	.4311	67.3	-.2796	******
73.	3.678	.5036	.4411	72.1	-.2506	******
74.	2.299	.4910	.4174	61.7	-.1387	******
75.	2.641	.4834	.4178	64.9	.0193	-20.16
76.	3.234	.4294	.4408	69.4	-.3172	-16.35
77.	1.494	.5081	.3995	51.2	-.2229	-17.39
78.	1.693	.5170	.4055	54.3	-.1977	-22.59
79.	3.074	.5199	.4475	68.3	.0266	******
80.	3.554	.5024	.4449	71.4	-.0954	******
81.	5.144	.5207	.4537	78.3	-.1462	******
82.	6.558	.5450	.4743	82.1	-.1721	******
83.	6.747	.5072	.4737	82.5	-.1321	******
84.	3.482	.4621	.4377	70.9	-.0492	******
85.	4.440	.4985	.4557	75.7	-.0799	******
86.	4.910	.5236	.4574	77.5	-.0534	******
87.	4.861	.4943	.4569	77.3	-.0253	-23.98
88.	9.586	.5110	.4728	87.0	-.3006	-25.18
89.	10.747	.3329	.4762	88.3	.0761	-17.42
90.	12.099	.4530	.4789	89.5	-.0418	-19.99
91.	2.366	.4518	.4319	62.4	.0654	******

TABLE 15

HEAT TRANSFER RESULTS

No.	$\frac{q_r}{q_c+q_r}$ (%)	$\bar{h}\times10^2$ $\left(\frac{cal}{cm^2\text{-}^oC}\right)$	q_c $\left(\frac{cal}{cm^2}\right)$	T_s (^oC)	T_s-T_o (^oC)	$\tau\times10^4$
1.	5.0	4.193	27.6	86.8	-.7	8.58
2.	5.8	3.646	24.2	87.1	-3.2	9.62
3.	7.0	3.056	20.5	89.6	-4.0	11.74
4.	16.5	1.274	9.1	87.4	-2.9	31.74
5.	22.8	.842	6.0	87.3	-.5	54.12
6.	27.8	.610	4.1	92.3	.1	84.57
7.	4.0	5.326	35.1	86.5	-3.5	6.27
8.	8.2	2.518	16.6	91.9	-3.9	14.74
9.	8.4	2.484	16.5	92.4	-4.0	15.25
10.	8.9	2.318	15.6	87.3	-4.6	15.21
11.	9.6	2.184	14.9	86.1	-3.9	16.47
12.	8.3	2.427	15.8	90.7	-2.6	15.49
13.	32.4	.683	5.7	88.1	-5.5	83.09
14.	****	-.520	-5.4	98.4	76.1	185.56
15.	21.8	.958	7.0	93.9	-4.5	48.12
16.	35.5	.623	5.4	80.3	****	170.30
17.	23.8	.819	5.9	87.2	-2.5	58.78
18.	23.5	.911	6.8	92.8	-5.2	57.00
19.	24.0	.833	6.1	86.9	-2.5	54.28
20.	23.9	.816	5.9	85.7	-3.8	57.10
21.	22.1	.855	6.0	86.3	-.3	51.82
22.	28.0	.761	6.0	89.5	-3.4	69.45
23.	19.2	.938	6.2	86.5	-.2	45.61
24.	18.2	1.007	6.6	90.7	-1.5	43.03
25.	18.4	1.027	6.9	90.2	-5.9	40.80
26.	18.8	.966	6.4	88.8	-1.2	45.26
27.	18.2	1.028	6.9	91.0	-3.4	41.14
28.	19.7	.984	6.8	91.4	-4.7	44.63
29.	20.2	.994	7.0	92.7	-5.0	46.05
30.	20.7	.992	7.1	91.4	-7.2	48.01

TABLE 15 (Continued)

No.	$\frac{q_r}{q_c+q_r}$ (%)	$\bar{h}\times10^2$ $\left(\frac{cal}{cm^2\text{-}^oC}\right)$	q_c $\left(\frac{cal}{cm^2}\right)$	T_s (^oC)	T_s-T_o (^oC)	$\tau\times10^4$
31.	28.0	.808	6.6	85.9	****	104.97
32.	23.3	.917	6.9	89.9	-9.0	78.64
33.	42.1	.442	4.4	****	****	402.87
34.	61.0	.262	2.9	****	****	******
35.	25.5	.791	5.9	90.0	1.1	70.10
36.	38.0	.521	4.3	80.7	-7.9	113.58
37.	22.2	.903	6.5	89.1	-4.2	64.83
38.	22.3	.846	6.0	81.8	-6.3	47.29
39.	23.5	.817	5.9	84.2	-5.9	56.05
40.	23.2	.842	6.1	85.4	-4.8	52.46
41.	20.2	.893	6.1	81.6	-5.9	42.77
42.	21.3	.868	6.0	85.6	-2.2	49.40
43.	34.9	.659	5.7	93.2	-5.5	90.84
44.	5.0	4.269	29.0	81.9	-5.1	7.33
45.	5.0	4.326	29.3	81.5	-6.0	7.74
46.	6.7	3.091	20.7	82.2	-7.5	10.70
47.	8.3	2.499	16.6	89.0	-4.8	14.51
48.	12.2	1.640	11.0	90.4	-4.6	23.16
49.	19.9	.905	6.1	85.6	-.8	46.20
50.	26.7	.624	4.2	87.8	-.5	75.89
51.	10.0	2.032	13.5	90.0	-5.0	18.14
52.	16.1	1.170	7.8	87.1	-2.6	33.95
53.	7.1	2.965	19.9	87.4	-6.0	11.88
54.	14.6	1.337	8.9	91.0	-6.2	28.63
55.	5.8	3.680	25.1	79.5	****	8.18
56.	19.9	.976	6.8	89.0	-5.5	41.96
57.	21.6	.935	6.7	90.8	-4.8	47.53
58.	29.7	.730	5.9	84.6	-8.7	138.46
59.	33.8	.664	5.7	81.0	****	169.54
60.	4.8	4.368	29.1	82.2	-5.6	6.50

TABLE 15 (Continued)

No.	$\frac{q_r}{q_c+q_r}$ (%)	$\bar{h}\times10^2$ $\left(\frac{cal}{cm^2\text{-}^oC}\right)$	q_c $\left(\frac{cal}{cm^2}\right)$	T_s (^oC)	T_s-T_o (^oC)	$\tau\times10^4$
61.	4.6	4.500	29.8	82.8	-5.2	6.26
62.	4.9	4.355	29.3	81.6	-6.2	6.39
63.	4.8	4.459	29.9	82.7	-6.2	6.29
64.	17.3	1.081	7.3	84.1	-3.1	34.76
65.	20.3	.911	6.3	81.8	-5.4	40.59
66.	25.0	.894	7.0	91.1	-8.4	50.37
67.	26.0	.785	6.0	82.5	-6.7	56.53
68.	30.1	.767	6.4	84.5	-15.5	90.20
69.	6.3	3.277	21.9	83.2	-9.0	12.47
70.	7.9	2.629	17.5	86.8	-7.9	16.20
71.	4.6	4.577	30.9	79.0	-8.0	8.31
72.	11.4	1.807	12.3	87.7	-11.1	23.78
73.	15.3	1.209	7.9	89.4	-8.4	38.96
74.	25.2	.672	4.5	85.2	-2.3	84.42
75.	25.7	.739	5.4	85.0	-14.2	68.06
76.	39.6	.507	4.4	71.3	-28.7	255.69
77.	5.4	3.857	26.1	75.0	-12.5	14.52
78.	5.5	3.789	25.3	80.0	-10.0	13.47
79.	7.4	2.770	18.3	86.5	-5.1	20.50
80.	8.6	2.383	15.7	89.4	-6.4	24.97
81.	10.7	1.834	11.9	92.4	-6.4	34.34
82.	15.0	1.314	8.8	93.3	-5.7	51.77
83.	17.0	1.078	7.0	93.6	-5.8	65.24
84.	8.8	2.369	15.9	89.4	-8.6	24.97
85.	9.6	2.271	15.7	91.6	-6.2	28.21
86.	10.7	2.175	15.7	92.0	-6.1	30.19
87.	9.0	2.376	16.1	91.9	-6.5	26.30
88.	32.3	.547	3.9	95.5	-4.7	170.59
89.	38.8	.466	3.6	94.3	-6.3	279.32
90.	34.0	.529	3.9	96.2	-4.4	186.88

TABLE 16

DIMENSIONLESS NUMBERS AND FRACTION VAPORIZED AS CALCULATED FROM HEAT TRANSFER DATA

No.	$\frac{N_v}{N_l} \times 10^5$	$Nu_{D,1}$	$Re_D Pr_1$	Re_D	Pr_1	$10^4/T_w$ ($^oK^{-1}$)
1.	1.67	671.1	677.1	318.5	2.13	9.831
2.	1.91	589.9	577.5	272.9	2.12	9.754
3.	2.15	471.9	463.8	229.5	2.02	9.679
4.	6.13	217.4	241.9	115.0	2.10	9.292
5.	10.11	142.4	177.8	84.4	2.11	9.353
6.	12.77	92.0	123.9	64.3	1.93	9.586
7.	1.30	848.2	811.9	380.2	2.14	9.812
8.	2.46	366.7	366.2	188.9	1.94	9.773
9.	2.46	366.2	365.8	190.2	1.92	9.726
10.	3.09	372.7	370.2	175.8	2.11	9.679
11.	3.41	367.6	371.3	172.6	2.15	9.595
12.	2.66	361.0	367.3	185.2	1.98	9.841
13.	14.70	133.9	177.5	85.4	2.08	8.388
14.	.01	*****	173.3	101.4	1.71	7.061
15.	7.15	150.2	175.1	93.7	1.87	9.122
16.	23.48	144.2	180.8	76.3	2.37	8.209
17.	10.78	145.1	177.8	84.3	2.11	9.240
18.	8.45	148.9	175.5	92.1	1.91	8.951
19.	10.59	144.8	178.0	83.9	2.12	9.147
20.	11.34	148.3	178.5	82.4	2.17	9.215
21.	10.14	143.7	178.2	83.2	2.14	9.432
22.	11.67	137.9	176.9	87.3	2.03	8.732
23.	8.94	148.5	178.1	83.4	2.14	9.754
24.	7.20	152.1	176.4	89.0	1.98	9.764
25.	7.25	162.0	176.6	88.3	2.00	9.632
26.	8.09	151.0	177.2	86.3	2.05	9.754
27.	6.99	156.2	176.3	89.4	1.97	9.669
28.	7.38	156.2	176.1	89.9	1.96	9.477
29.	7.15	155.0	175.6	92.0	1.91	9.327
30.	7.89	159.4	176.1	89.9	1.96	9.223

TABLE 16 (Continued)

No.	$\frac{N_v}{N_l} \times 10^5$	$Nu_{D,l}$	$Re_D Pr_l$	Re_D	Pr_l	$10^4/T_w$ ($^oK^{-1}$)
31.	14.27	162.5	178.4	82.6	2.16	8.524
32.	10.43	158.6	176.7	87.8	2.01	8.943
33.	1.63	*****	245.5	30.6	8.03	8.050
34.	4.00	*****	245.5	30.6	8.03	7.374
35.	10.85	133.1	176.7	88.0	2.01	9.040
36.	25.69	117.7	162.8	69.2	2.35	8.437
37.	10.15	151.1	177.1	86.8	2.04	9.232
38.	11.49	159.6	180.2	77.9	2.31	9.397
39.	11.76	149.9	179.1	80.6	2.22	9.283
40.	10.83	152.3	178.6	82.1	2.18	9.249
41.	10.52	163.1	180.2	77.8	2.32	9.669
42.	9.99	149.8	178.5	82.3	2.17	9.549
43.	12.94	127.3	175.4	92.7	1.89	8.169
44.	1.83	749.8	705.8	305.6	2.31	9.669
45.	1.82	842.6	774.3	333.5	2.32	9.679
46.	2.55	584.2	534.1	232.5	2.30	9.745
47.	2.72	395.8	389.1	190.2	2.05	9.735
48.	4.15	249.0	257.5	129.2	1.99	9.688
49.	9.39	148.9	178.5	82.3	2.17	9.707
50.	14.08	99.5	131.0	62.8	2.09	9.675
51.	3.31	312.4	312.8	155.7	2.01	9.710
52.	6.68	188.9	210.0	99.4	2.11	9.720
53.	2.30	496.3	472.1	224.4	2.10	9.697
54.	5.14	200.1	208.0	105.5	1.97	9.697
55.	2.24	732.0	629.6	262.5	2.40	9.669
56.	7.99	158.4	177.1	86.6	2.05	9.441
57.	8.14	152.5	176.4	89.1	1.98	9.223
58.	16.74	147.8	179.0	81.1	2.21	8.575
59.	19.97	153.3	180.5	77.1	2.34	8.256
60.	1.78	684.9	643.2	280.1	2.30	9.783

TABLE 16 (Continued)

No.	$\frac{N_v}{N_l} \times 10^5$	$Nu_{D,l}$	$Re_D Pr_l$	Re_D	Pr_l	$10^4/T_w$ ($^oK^{-1}$)
61.	1.70	680.7	642.3	282.5	2.27	9.831
62.	1.81	691.6	644.2	277.6	2.32	9.726
63.	1.72	688.9	642.4	282.1	2.28	9.735
64.	7.96	178.3	199.7	89.8	2.22	9.679
65.	10.30	161.0	180.2	77.9	2.31	9.568
66.	8.97	152.6	176.2	89.5	1.97	8.717
67.	13.29	151.9	179.9	78.7	2.29	8.943
68.	16.16	161.3	179.0	80.9	2.21	8.346
69.	3.10	634.1	828.6	366.8	2.26	9.773
70.	3.53	480.0	651.9	306.8	2.12	9.735
71.	2.33	975.0	1259.4	520.6	2.42	9.735
72.	5.20	330.1	447.5	214.1	2.09	9.586
73.	7.76	205.4	303.4	149.5	2.03	9.841
74.	17.66	126.5	230.7	105.7	2.18	9.688
75.	16.71	149.5	230.9	105.3	2.19	9.232
76.	44.71	161.5	238.6	87.8	2.72	8.284
77.	4.47	977.4	1738.9	676.0	2.57	9.764
78.	3.70	895.8	1672.0	703.0	2.38	9.783
79.	4.47	541.4	1129.3	529.0	2.13	9.783
80.	4.85	451.1	937.2	461.8	2.03	9.773
81.	5.87	324.4	693.0	361.0	1.92	9.841
82.	8.36	235.1	533.5	282.6	1.89	9.641
83.	10.32	189.7	439.4	233.9	1.88	9.841
84.	4.89	464.7	937.2	461.9	2.03	9.679
85.	4.83	441.7	932.5	477.9	1.95	9.468
86.	5.04	434.4	931.6	481.2	1.94	9.189
87.	4.54	445.5	931.9	480.1	1.94	9.586
88.	23.32	103.7	299.8	165.6	1.81	9.206
89.	35.54	95.9	300.7	162.1	1.86	8.763
90.	24.42	100.3	299.3	167.5	1.79	9.056

APPENDIX H

FILM BOILING ON A VERTICAL FLAT PLATE

An apparatus was constructed and used to investigate forced convection film boiling on a vertical flat plate. An attempt was made to measure heat transfer rates and to correlate the heat transfer data with the wave length and wave frequency at the liquid-vapor interface. Figure 42 is a block diagram of this equipment. A two kilowatt 115 volt heater was used to bring the liquid near to its boiling point and the condenser was used to condense the vapor and cool the liquid permitting it to be pumped by a centrifugal pump. Figure 43 is a diagram of the test section where the boiling occurred. D. C. electric current was passed through the copper and Chromel A strip. The resistance of the copper was sufficiently low that no film boiling took place on the copper portion of the strip. The resistance of the Chromel A was sufficiently high that boiling occurred only on that portion of the strip. The liquid used in this experiment was n-heptane.

An optical system was constructed to measure photoelectrically the wave frequency and wave length at the liquid-vapor interface; however, little success was attained. Edge effects resulting from a meniscus at the quartz wall presented an unsoluable problem. Further problems were caused by a warping of the Chromel strip

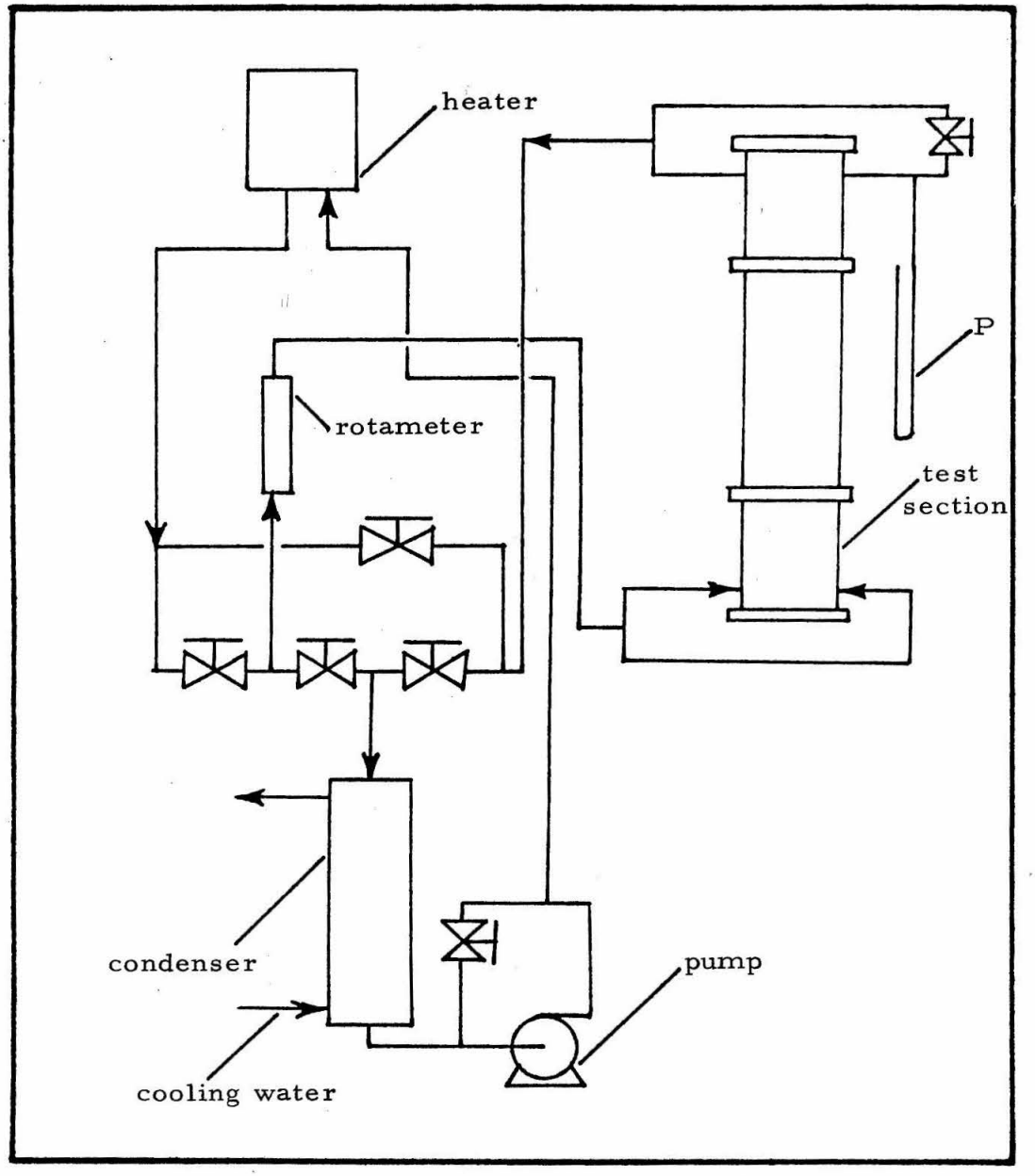

Figure 42. --Apparatus used to observe film boiling on a flat plate.

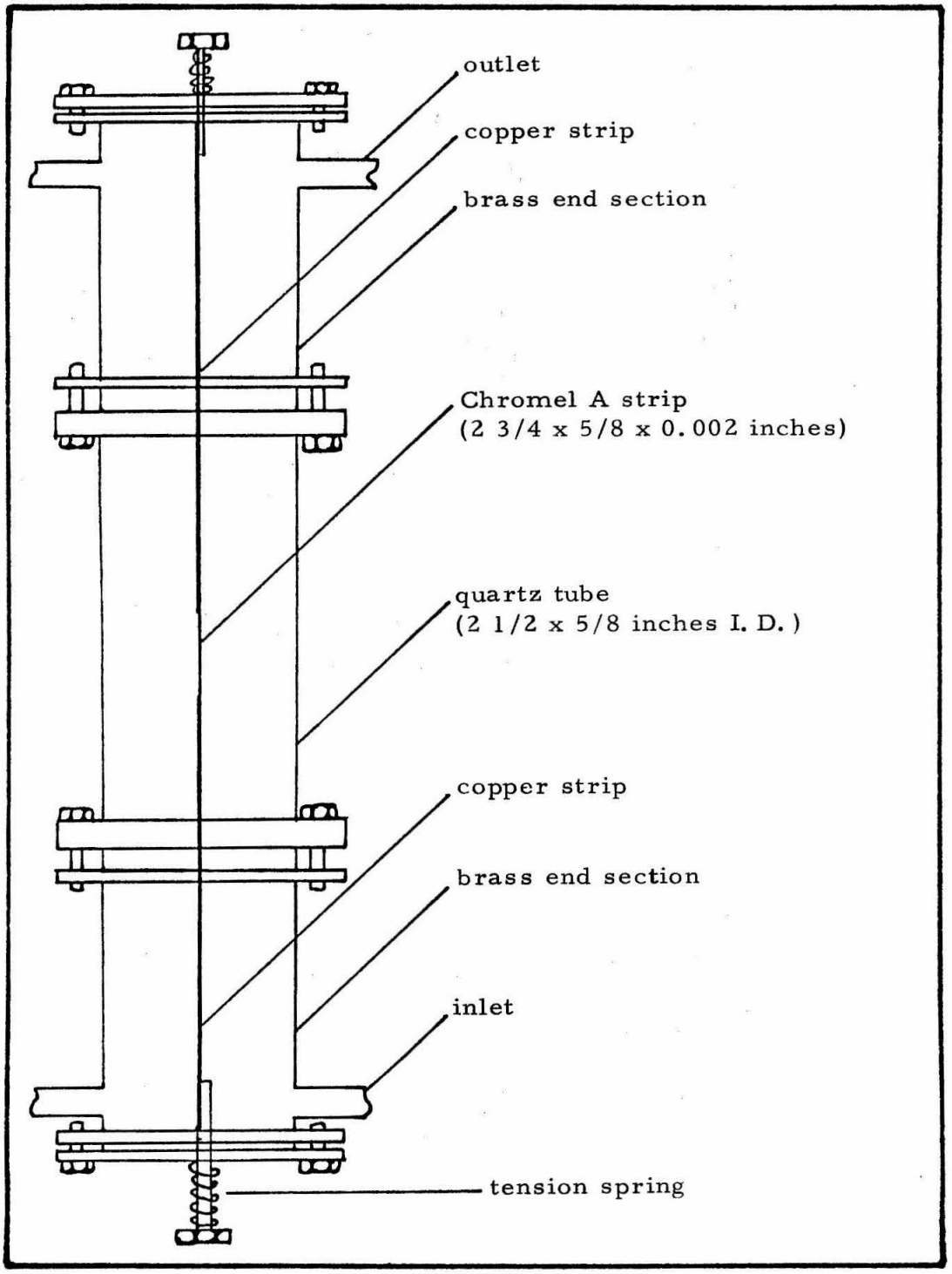

Figure 43. --Flat plate test section.

when heated; the tension springs on the test section could not keep the strip flat.

Some success was achieved in measuring heat transfer coefficients and in exploring the nucleate boiling-film boiling transition point which was described by Kovalev (42). Kovalev found that an equilibrium heat flux exists below which both nucleate and film boiling regimes exist on the same surface. This work confirmed Kovalev's conclusion, but this work was not pursued to the extent at which quantitative results could be obtained.

A Fastex camera was used to photograph an unsteady state situation. Film boiling was begun on the vertical plate and the power then was turned off. The resulting collapse of the film was photographed at 960 frames per second. The film rapidly decreased in thickness and the turbulent nature of the liquid-vapor interface diminished. However, the wave length of the waves still was non-uniform. The frequency was measured at various heights from the lower edge of the 2 22/32 inches by 5/8 inch Cromel strip. The film collapse was noted to be complete in 0.8 seconds. The frequency was determined from the time required for the last 40 cycles prior to complete collapse. The temperature of the incoming n-heptane was 105°F and the temperature of the strip was measured with an optical pyrometer to be 880°C. The power dissipated in the strip

was 560 watts and the liquid flow through the test section was 0.363 gallons per minute, as indicated by the rotameter. Table 17 lists the frequency measured at various distances from the bottom of the strip. It may be seen that the frequency decreased as the measured distance up the strip was increased. The frequencies were of the same magnitude as reported by Bradfield (5) in his investigation of wave generation at a stagnation point during forced convection film boiling on a vertically oriented hemisphere cylinder. In the photographic investigation, it was impossible to measure the thickness of the film because of edge effects resulting from a meniscus at the quartz wall. Therefore, the investigation of the termination of film boiling was stopped at this point.

In conclusion, the work done on the film boiling of n-heptane on a vertical flat plate was unsuccessful. However, work may be continued along one of two paths. The nucleate boiling-film boiling transition interface as a function of the distance from the lower edge of the strip may be investigated, and the effects of the sudden termination of film boiling also may be investigated more extensively.

TABLE 17

FREQUENCY VERSUS POSITION OF INTERFACIAL WAVES

Distance from Bottom of Strip (cm.)	Frequency (Hz.)
6.10	87
5.21	89
4.35	98
3.18	104
2.31	115
1.42	130

APPENDIX I

THE FUTURE OF FILM BOILING

In the past, film boiling has been avoided as a method of heat transfer. However, many practical uses of film boiling now are beginning to appear.

As this investigation has shown, film boiling may be used as a simple means of deaerating water. This process possibly may be used to separate liquid-liquid solutions in which the liquids have widely different volatilities.

Film boiling has been suggested for use in thermal cracking (9). The high temperatures and rapid quenching make this a definite possibility. One of the conclusions reached in Chapter V is that a hetrogeneous chemical reaction may occur at the wall during film boiling. Since virtually any material may be used for this surface, a wide variety of reactions are possible. A sphere made of a catalytic material may be used. The use of film boiling for these heterogeneous reactions has the advantage of rapid quenching.

There are other uses for film boiling which are not related to the experimental investigation. For example, film boiling may be used to obtain very high heat fluxes. Figure 1 indicates that the nucleate boiling has a maximum heat flux beyond which film boiling must be used.

Film boiling has been shown to reduce the friction drag on a body moving through a liquid (6). This phenomena has potential uses in the propulsion of objects through liquids.

Since in film boiling liquid-solid contact does not exist, film boiling may be used in instances in which this contact is not desired. An example is the possibility of the boiling of saline or sugar solutions.

The above practical applications for film boiling indicate that further research still remains to be done on the various aspects of film boiling.

APPENDIX J

FILM BOILING FROM A SPHERE DURING FORCED CONVECTION OF SUBCOOLED WATER

(PRELIMINARY RESULTS)

Reprinted from I&EC FUNDAMENTALS, Vol. 9, Page 183, February 1970

Film Boiling from a Sphere during Forced Convection of Subcooled Water

Forced convection film boiling from a sphere was investigated. The water was subcooled; a vapor film existed in which no net formation of vapor occurred. The resulting rates of heat transfer were considerably greater than that predicted for a saturated fluid or for forced convection from the constant temperature sphere formed by the liquid-vapor interface. If it is assumed that the film does not exist, a poor correlation exists between the experimental and theoretical results; this assumption cannot be justified, since a film was observed in all cases.

FREDERKING and Clark (1963) treated the case of a saturated free convection film boiling from a sphere. Using a boundary layer analysis they found that

$$q = 0.586\left[\frac{h_{fg}gk_v\rho_v(\rho_l - \rho_v)}{D\mu_v(T_w - T_s)}\right]^{1/4}(T_w - T_s) \qquad (1)$$

Witte (1968) presented an analysis for saturated film boiling from a sphere during forced convection. By assuming that the velocity profile is linear and that the interfacial velocity can be determined from potential flow theory, he found that

$$q = 0.698\left[\frac{k_v\rho_v U_\infty h'_{fg}}{D(T_w - T_s)}\right]^{1/2}(T_w - T_s) \qquad (2)$$

Sideman (1966) used potential flow theory and assumed slip at the wall to develop the following equation for nonboiling heat transfer during forced convection flow past a sphere.

$$q = 1.13\left[\frac{U_\infty(\rho kC_p)_l}{D}\right]^{1/2}(T - T_s) \qquad (3)$$

Subcooled forced convection film boiling from a sphere has been investigated experimentally by Witte (1968) and Witte *et al.* (1968). They concluded from a study of liquid sodium that a vapor film does not exist for large degrees of subcooling of the liquid, and that the heat transfer rate may, therefore, be described by Sideman's relationship (1966). However, Witte (1968) suggested that further experiments be performed to verify the absence of a vapor film. It is important to obtain heat transfer data for forced convection film boiling on a sphere under conditions in which the film may be observed.

Apparatus

A Lapel high frequency 5-kw induction heater operating between 2.5 and 5.0 MHs was used to heat the sphere shown in Figure 1. This differs from the experiments of Witte *et al.* (Witte, 1967; Witte *et al.*, 1968) in that the sphere was heated continuously. The liquid used was water and the sphere was steel. A constant fluid velocity was maintained by means of a constant head tank and the flow rate was measured by means of a rotameter. The glass wool was placed in the tube to remove any lateral temperature gradients, and the Lavite disk was used to prevent the hot sphere from touching the glass tube. The hot sphere was supported by the liquid flow itself and was not in contact with the Lavite disk. The temperature of the sphere was determined with a Pyro micro-optical pyrometer. This apparatus permitted film boiling of subcooled liquids and simultaneous visual observation of the film.

Results

Subcooling of the water to between 10° and 50°C resulted in a stable vapor film and no bubbles left the film at flow rates of between 0.4 and 2.7 cc per second. The cool liquid prevented the emission of vapor from the film due to buoyant forces. This greatly simplified the energy balance, since no vapor was present downstream.

The resulting rates of heat transfer were much greater than predicted by Equation 2 for a saturated liquid (Figure 2). This is in qualitative agreement with the theory developed by Cess and Sparrow (1961) for film boiling of a subcooled liquid on a vertical flat plate. Since no net formation of vapor occurs and the vapor-liquid interface is approximately spherical, Sideman's Equation 3 could be expected to apply if T' is set equal to T_s. However, the experimentally measured values are an order of magnitude greater than predicted (Figure 3).

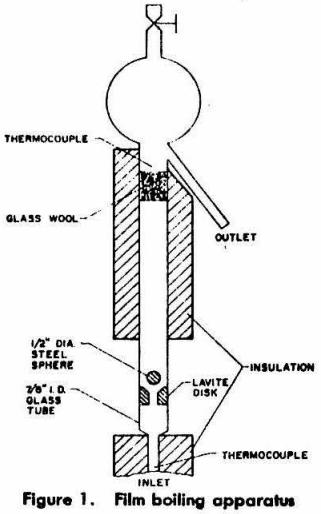

Figure 1. Film boiling apparatus

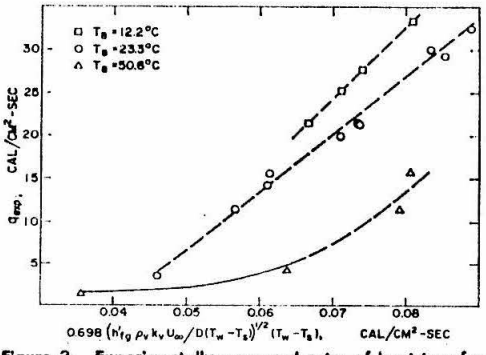

Figure 2. Experimentally measured rates of heat transfer for subcooled water compared to that theoretically predicted for saturated water

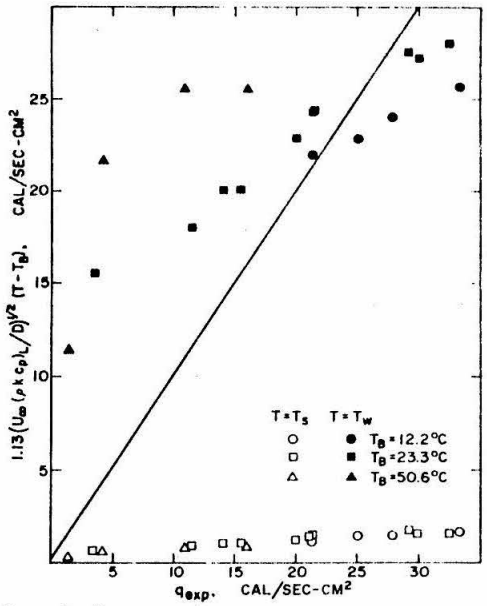

Figure 3. Experimentally measured rate of heat transfer for subcooled water compared to that theoretically predicted by Sideman's Equation 3

Witte *et al.* (1968) concluded from their study of liquid sodium that no film was present, since their data correlated with Sideman's Equation 3 with T set equal to T_w. If these assumptions are made here, a not unreasonable correlation exists, as also shown in Figure 3. However, since a film is visible, this assumption is not justifiable in this case.

In all the cases noted above, the film was visually observed to surround the sphere completely and intermittent liquid-solid contact was not visually apparent. However, by greatly increasing the rate of liquid flow past the sphere, a condition of simultaneous nucleate and film boiling could be made to exist. The nucleate boiling occurred on the downstream side of the sphere, accompanied by a significantly lower surface temperature in the nucleate boiling region of the sphere.

Conclusions

Forced convection film boiling of water subcooled below its boiling point may result in a vapor film in which no net formation of vapor occurs. The resulting rates of heat transfer are considerably greater than that predicted for a saturated liquid and for forced convection from the constant temperature sphere formed by the liquid-vapor interface. If it is assumed that the film does not exist, correlation between experiment and theory is poor; however, this assumption is not justified, since a film was visually observed. A relationship for predicting rates of heat transfer from a sphere to a subcooled liquid during forced convection film boiling remains to be found.

Nomenclature

C_p = specific heat, cal/g-°C
D = diameter of sphere, cm
g = acceleration of gravity, cm/sec²
h_{fg} = latent heat of vaporization, cal/g
h'_{fg} = $h_{fg} + 0.68\ C_p\ (T_w - T_s)$, effective latent heat of vaporization, cal/g
k = thermal conductivity, cal/sec-cm-°C
q = heat transfer rate, cal/sec-cm²
T = temperature, °C
U_∞ = bulk flow rate/annular area between sphere and glass tube, cm/sec
ρ = density, g/cm³
μ = viscosity, g/cm-sec

Subscripts

B = bulk
exp = experimental
l = liquid
s = saturation
v = vapor
w = wall

Literature Cited

Cess, R. D., Sparrow, E. M., *Heat Transfer (Trans. ASME)* **90**, 394 (1961).
Frederking, T. H. K., Clark, J. A., *Advan. Cryog. Eng.* **8**, 501 (1963).
Sideman, S., *Ind. Eng. Chem.* **58** (2), 54 (1966).
Witte, L. C., "Heat Transfer from a Sphere to a Liquid during Forced Convection," Ph.D. thesis, Oklahoma State University, 1967.
Witte, L. C., Ind. Eng. Chem. Fundamentals **7**, 517 (1968).
Witte, L. C., Baker, L., Haworth, R. R., *Heat Transfer (Trans. ASME)* **90**, 394 (1968).

R. N. JACOBSON
F. H. SHAIR

California Institute of Technology
Pasadena, Calif. 91109

Received for review April 11, 1969
Accepted November 28, 1969

PROPOSITION I

A simple photoelectric device may be used to observe the profile of a surface wave and to determine its frequency. For ripples of small amplitude on a deep fluid, the wave profile is a linear reproduction of the original wave.

Light passing through a light absorbing substance will be diminished according to Lambert's law; the intensity of light passing through an absorbing liquid is determined by the depth of the liquid. A periodic surface wave over an absorbing liquid will cause light of periodic intensity to leave the liquid. The light of periodic intensity may be converted to an alternating electrical current by using a phototube. Then, the wave form may be viewed on an oscilloscope, or the wave frequency may be measured by observing the Lissajous diagram produced by the wave form and a calibrated audio oscillator.

This method has been used with infrared light and an electronic linearizing circuit (4). A simpler system has been built by using a standard incandescent bulb as a light source and by adding ink or dye to the liquid. The output is shown to be linear for waves of small amplitude over a deep liquid. The use of an audio oscillator to determine the frequency of a surface wave has not been previously reported.

Apparatus

A periodic surface wave was produced by blowing a jet of air across the surface of a liquid contained in a glass tray. A small quantity of black ink was added to the liquid, water, to absorb light. The apparatus is illustrated in Figure 1.

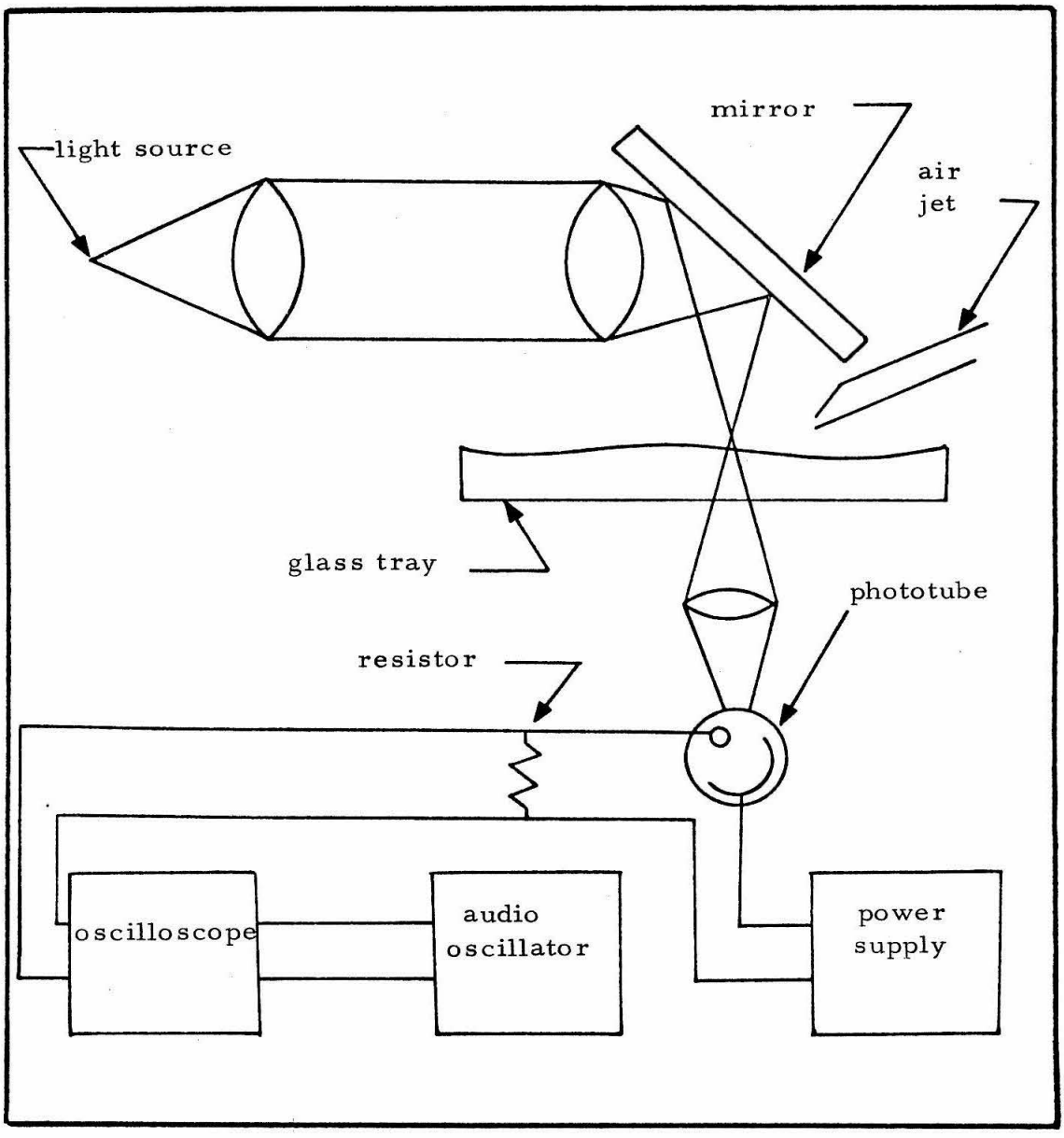

Figure 1. --Apparatus for viewing and measuring the frequency of surface waves.

A tungsten filament bulb fed with direct current was used as a light source. The light was first passed through a collimating lens, then through a focusing lens which focused a small image of the source onto the surface of the liquid. The light which passed through the liquid was focused by a third lens onto a photocell.

The photocell (RCA 922) was connected in series with a 126 megohm resistance and a 200 volt DC power supply. The y axis input of an oscilloscope was connected across the resistor. A Lissajous diagram was produced by an audio oscillator connected across the x input of the oscilloscope.

Conditions of Linearity

Lambert's law may be stated as (1)

$$\log_{10} I_o / I = kd$$

where

I_o = intensity of transmitted light

I = intensity of incident light on surface

k = a constant

d = depth of liquid

This may be rewritten as

$$d = k' \ln I_o/I$$

If the incident light is held constant throughout the experiment, the above may be written as

$$d = k''\ln I_o$$

if

$$I = 1.0$$

Now, if the depth is large in comparison to the wave amplitude and the absorbancy is small, the ratio of I_o/I will be close to unity. The above expression for "d" may be expanded in a Taylor series

$$d = k''\left[(I_o - 1) - (I_o-1)^2/2 + (I_o - 1)^3/3 \ldots\right]$$

In this case, I_o-1 will be small; therefore, only the first term of the Taylor series will need to be considered.

$$d = k''(I_o - 1)$$

$$I_o = d/k'' + 1$$

The photoelectric current will be directly proportional to the illumination of the cathod (3).

$$i = SI_o$$

where "i" is the current, and S is a constant. Then,

$$i = S(1 + d/k'')$$

$$v = RS(1 + d/k'')$$

In the above equation "v" is the voltage across the resistor in series with the phototube, and R is the value of the resistance. If "d" is expressed as an average value, d_{avg}, and a varying value, $\bar{d}$, which represents the waveform

$$d = RS(1 + d_{avg}/k'') + RS\bar{d}/k''$$

Since the oscilloscope may be used to observe only the AC component of its input, then

$$v_{observed} = RS\bar{d}/k'' = k''' \bar{d}$$

Thus, the image observed is the true wave form and the frequency is the true frequency for waves of small amplitude in a deep fluid.

Experimental Results

Figure 2 is a photograph taken directly from the oscilloscope. The sine wave which was produced by blowing a jet of air over the surface of the liquid may be seen. Assuming the original was a sine wave, it can be seen that the linearity is good.

Figure 3 is the Lissajous diagram obtained by placing a 16.0 cycle per second wave across the x input of the oscilloscpoe. The ellipse indicates that the ratio of the two frequencies is one to one (2). In this manner, the frequency of the wave may be determined with a high degree of accuracy.

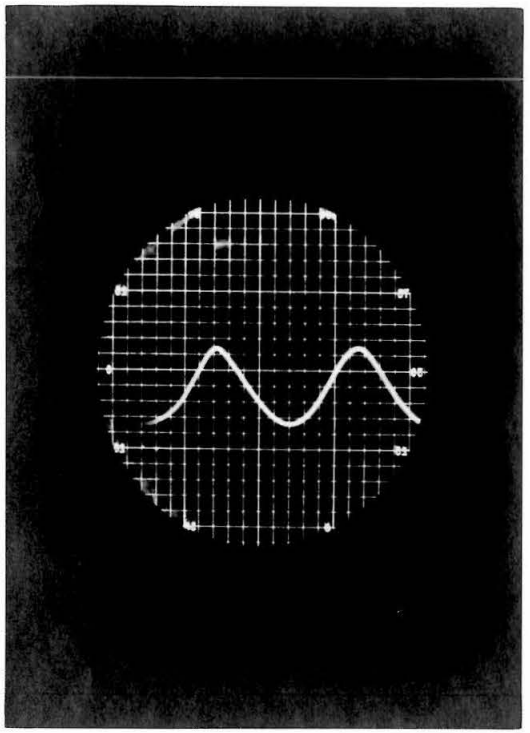

Figure 2. --Surface wave reproduced on oscilloscope screen.

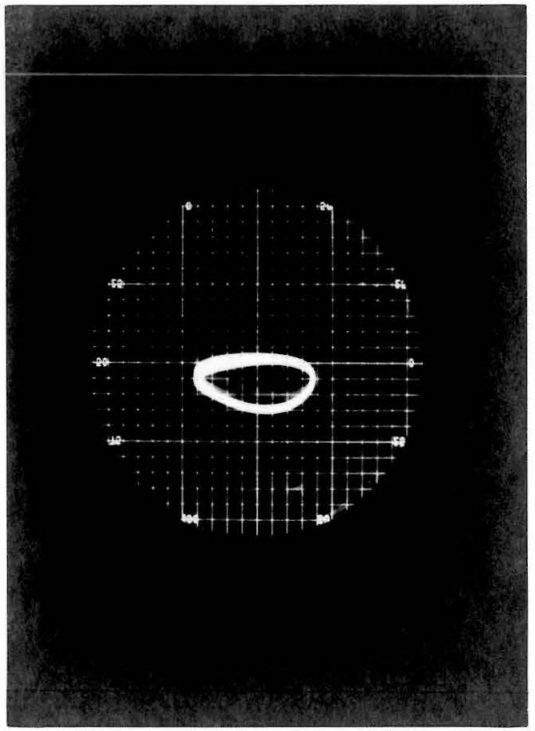

Figure 3. --Lissajous diagram used to determine the frequency of a surface wave.

LIST OF REFERENCES

1. Hamilton, L. F., Simpson, S. G., Calculations of Analytical Chemistry, McGraw-Hill, New York, 1960, p. 254.

2. Holman, J. P., Experimental Methods for Engineers, McGraw-Hill, New York, 1966, pp. 108-109.

3. Lion, K. S., Instrumentation in Scientific Research, Electrical Input Transducers, McGraw-Hill, New York, 1959, p. 235.

4. Sturtevant, B., "Optical Depth Gauge for Laboratory Studies of Water Waves," The Review of Scientific Instruments, 37, 1460-1463 (1966).

PROPOSITION II

The surface concentration of an evaporating binary mixture may vary as a function of relative volatility as well as a function of time, evaporation rate, initial concentration, and diffusivity. An approximate solution to the governing differential equation has been obtained analytically and compared to a numerical solution.

The physical situation is shown in Figure 1; the liquid is of infinite depth and local equilibrium exists at the interface. The entire gaseous phase is assumed to be at a single uniform concentration which varies with time. The rate of evaporation and the diffusivity both are assumed to be constant, and the interface is stationary.

The equations and boundary conditions which describe the concentration as a function of time and position are:

$$\frac{\partial x_a}{\partial t} + \frac{w \partial x_a}{\rho \partial z} = D_{ab} \frac{\partial^2 x_a}{\partial z^2} \qquad (1)$$

$$\text{at } t = 0; \quad x_a = x_{a,o}$$

$$\text{at } z = 0; \quad D_{ab} \frac{\partial x_a}{\partial z} = w (y_a - x_{a,s}) \qquad (2)$$

The $\partial x/\partial z$ term is now omitted from Equation (1) for simplicity even though it may be as important as the other terms in the equation. This omission is made solely to facilitate the solution of Equation (1). The term $wx_{a,s}$ in Equation (2) is not omitted however. At this point, several assumptions are made. The densities of components "a" and "b" are assumed to be equal and not dependent on the concentration. Therefore, there is no hydrodynamic flow in the liquid.

The Fick's diffusion coefficient was used. The definition of this coefficient is

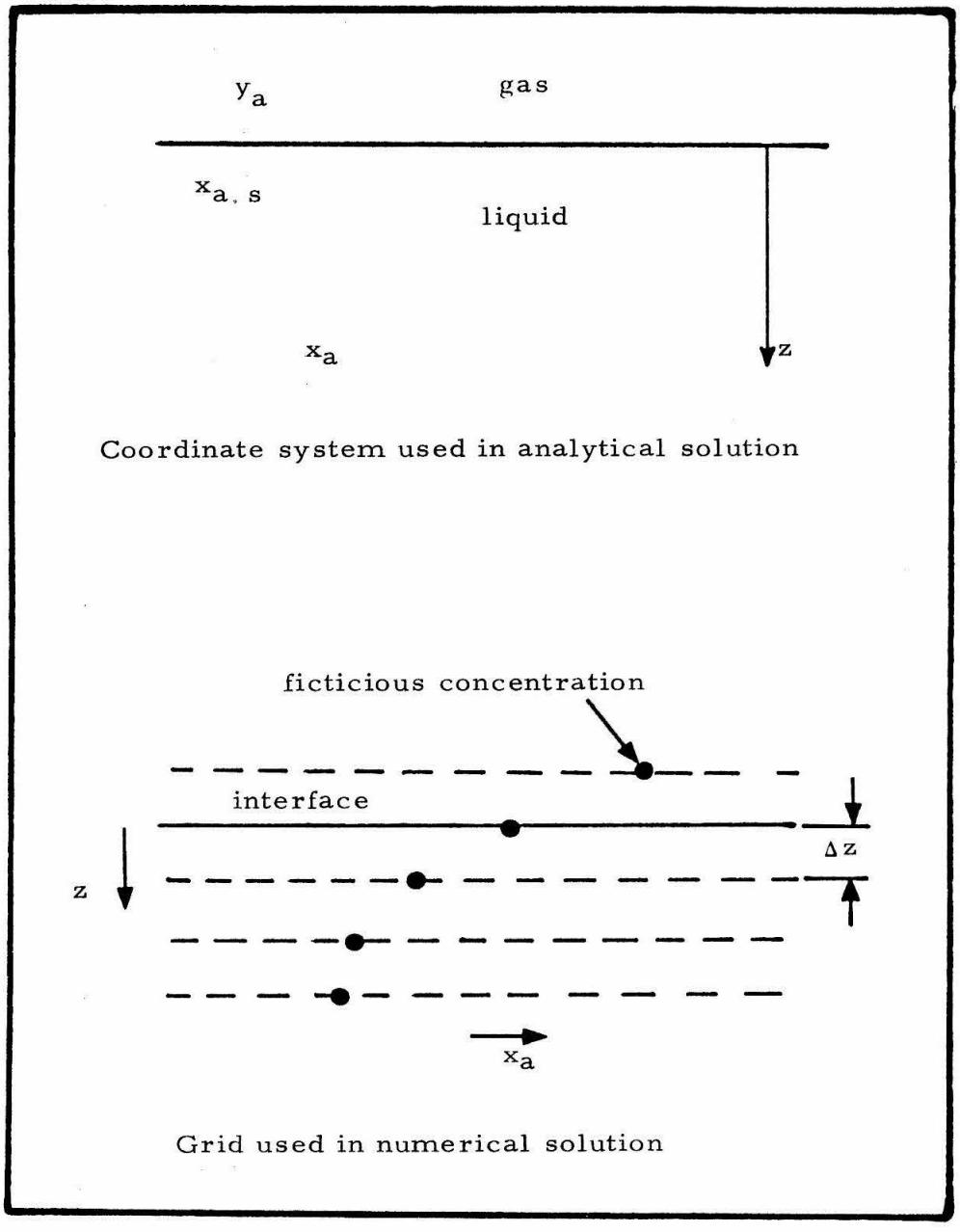

Figure 1. --Coordinate systems used in investigation.

$$D_{ab} = -x_a v_a / \frac{\partial x_a}{\partial z} \tag{3}$$

where v_a is the velocity of component "a" in the liquid (3).

Since the densities of "a" and "b" are assumed to be equal and not dependent on concentration, the Chapman-Cowling and the Fick diffusion coefficients (3) are equal. The Chapman-Cowling coefficient is defined as

$$D_{c,ab} = -\rho_a v_a / \rho \frac{\partial x_a}{\partial z} \tag{4}$$

Further assumptions of constant temperature and constant relative volatility are made to simplify the problem. In addition, the relationship between $x_{a,s}$ and "y" must be found to simplify Equation (2). Because local equilibrium exists at the interface, the following relationship holds:

$$y_a = \frac{\alpha_{ab} x_{a,s}}{1 + (\alpha_{ab} - 1) x_{a,s}} \tag{5}$$

An exact solution of the problem has been obtained (1) (2) for the two limiting cases when the mass balance at the interface is expressed as

$$D_{ab} \frac{\partial x_a}{\partial z} = k\, x_a \tag{6}$$

and

$$D_{ab} \frac{\partial x_a}{\partial z} = k\,(y_a' - x_a) \tag{7}$$

where y_a' is a constant concentration in the atmosphere remote from the interface.

It may be noted that Equation (5) may be rewritten as

$$y_a = \frac{\alpha_{ab}}{\alpha_{ab}-1} \left[(\alpha_{ab} - 1) x_a - (\alpha_{ab} - 1)^2 x_a^2 + (\alpha_{ab} - 1)^3 x_a^3 \ldots \right] \tag{8}$$

where $(\alpha_{ab} - 1)\, x_a < 1$.

In fact, if

$$(\alpha_{ab} - 1) x_a << 1 \tag{9}$$

then

$$y_a = \alpha_{ab} x_a \tag{10}$$

and the mass balance at the interface, Equation (2), becomes

$$D_{ab}\frac{\partial x_a}{\partial z} = w(\alpha_{ab} - 1)x_a \qquad (11)$$

Using the solution to Equation (1) with Equation (11) as a boundary condition, one obtains the following (1):

$$\frac{x_a}{x_{a,o}} = \operatorname{erf}\frac{z}{2\sqrt{D_{ab}t}} + e^{\left[\frac{w(\alpha_{ab} - 1)\, z}{D_{ab}} + \frac{w^2(\alpha_{ab} - 1)^2\, t}{D_{ab}}\right]}$$

$$\cdot\left\{\operatorname{erfc}\left[\frac{z}{2\sqrt{D_{ab}t}} + \frac{w(\alpha_{ab} - 1)\sqrt{D_{ab}t}}{D_{ab}}\right]\right\} \qquad (12)$$

The surface concentration is given by

$$\frac{x_a}{x_{a,o}} = e^{\frac{w^2(\alpha_{ab} - 1)^2 t}{D_{ab}}}\left[\operatorname{erfc}\frac{w(\alpha_{ab} - 1)\sqrt{D_{ab}t}}{D_{ab}}\right] \qquad (13)$$

This relationship has not been stated previously in terms of relative volatility.

Numerical Solution

It is desired to know the variation of surface composition as a function of the following parameters: $x_{a,o}$, α_{ab}, w/D_{ab}, and $D_{ab}t$. A numerical solution will give some indication of the validity of Equation (13). The problem was solved by a digital computer using the Schmidt method (2). A grid with a spacing of 0.01 was used; either cm.-g.-sec. or ft.-lb.-sec. units may be assigned to the numbers obtained since the solution did not consider a specific case. The time increment used was 0.00005.

The boundary condition, Equation (2), requires that the concentration gradient at the interface be related to the current interfacial concentration by the following:

$$\frac{\partial x_a}{\partial z} = \frac{w(y_a - x_{a,s})}{D_{ab}} \qquad (14)$$

This boundary condition is maintained by a ficticious concentration above the interface as shown in Figure 1.

Equation (14) may be expressed in finite difference form to obtain the ficticious concentration, x_a (1).

$$\frac{x_a(2) - x_a(1)}{\Delta z} = \frac{w}{D_{ab}}\left[\frac{\alpha_{ab}\, x_a(2)}{1 + (\alpha_{ab} - 1)x_a(2)} - x_a(2)\right] \qquad (15)$$

A computer program was written to solve the problem for $x_{a,o}$ = 0.01 and several values of w/D_{ab} and α_{ab}. Table I relates the notation used previously with that used within the program. The program is given in Figure 2.

Results of Numerical Computations

Figures 3, 4, and 5 contain results obtained by the computer program. As illustrated by these curves, the surface concentration foes to an asymptote of zero, if α_{ab} is greater than unity. When the relative volatility is less than unity, the surface concentration changes little. This is a consequence of the small initial concentration of x_a, 0.01. If the relative volatility is equal to unity, then the concentrations will not change as a function of time.

Table 2 gives an indication of the size of error to be expected if Equation (13) is used as an approximate solution of the problem. For small values of time a value of $(\alpha_{ab} - 1) x_{a,o}$ close to unity will introduce sizeable errors. In fact, it can be seen that the error is 26% when $(\alpha_{ab} - 1) x_{a,o}$ is equal to 0.99. However, when $(\alpha_{ab} - 1) x_{a,o}$ is equal to 0.09 the error is less than 1%.

TABLE 1

CONVERSION OF NOTATION TO FORTRAN

Notation in Discussion	Notation in Program
w/D_{ab}	WD(M)
$D_{ab}t$	DTIME
D_{ab} t	DDT
x_a	X(I)
$x_{a,o}$	XO
$x_{a,s}$	X(2)
y_a	Y
Δz	DZ
α_{ab}	ALPHA(L)

```
C  ALPHA=RELATIVE VOLATILITY      W=RATE OF VAPORIZATION
C   D=DIFFUSIVITY      WD=W/D      DTIME=(D)*(TIME)
C   X=MOLE FRACTION IN LIQUID   X(2)=MOLE FRACTION IN LIQUID AT INTERFACE
C   Y=MOLE FRACTION IN THE VAPOR
      DIMENSION WD(3)
      DIMENSION XX(1001)
      DIMENSION X(1001)
      DIMENSION ALPHA(8)
    1 FORMAT(5X,5F12.5)
    2 FORMAT(8X,1HY,11X,1HX,11X,5HALPHA,7X,3HW/D,9X,5HDTIME)
    3 FORMAT(1H*)
      WRITE(6,2)
      WD(1)=0.1
      WD(2)=1.0
      WD(3)=0.01
      ALPHA(1)=1.1
      ALPHA(2)=0.9
      ALPHA(3)=0.1
      ALPHA(4)=20.00
      ALPHA(5)=10.0
      ALPHA(6)=100.0
      ALPHA(7)=0.00001
      ALPHA(8)=2.0
      DO 41 M=1,3
      DO 40 L=1,8
      WRITE(6,3)
      DZ=0.01
      DDT=(DZ**2.0)/2.0
      K=0
      N=4
```

Figure 2. --Computer program

```
C       THE INITIAL CONCENTRATION IS SET EQUAL TO 0.01 (MOLE FRACTION)
        XO=0.01
        DTIME=0.0
        DO 9 I=1,1000
        X(I)=XO
      9 CONTINUE
C      THE SCHMIDT METHOD OF ANALYSIS IS USED
        J=0
     10 CONTINUE
        IF(N-999)100,101,101
    100 N=N+1
    101 DO 11 I=2,N
        XX(I)=(X(I-1)+X(I+1))/2.0
     11 CONTINUE
        Y=ALPHA(L)*XX(2)/(1.0+(ALPHA(L)-1.0)*XX(2))
C      A MATERIAL BALANCE IS MADE AT THE INTERFACE
        X(1)=XX(2)-WD(M)*(Y-XX(2))*DZ
        DTIME=DTIME+DDT
        DO 20 I=2,N
        X(I)=XX(I)
     20 CONTINUE
        J=J+1
        IF(J-8*(K+1))10,30,30
     30 K=K+1
        J=0.0
        WRITE(6,1)Y,X(2),ALPHA(L),WD(M),DTIME
        IF(K-15)10,40,40
     40 CONTINUE
C    AT THIS POINT THE PROGRAM IS RERUN WITH NEW VALUES OF ALPHA AND W/D
     41 CONTINUE
     50 STOP
```

Figure 2. --(continued)

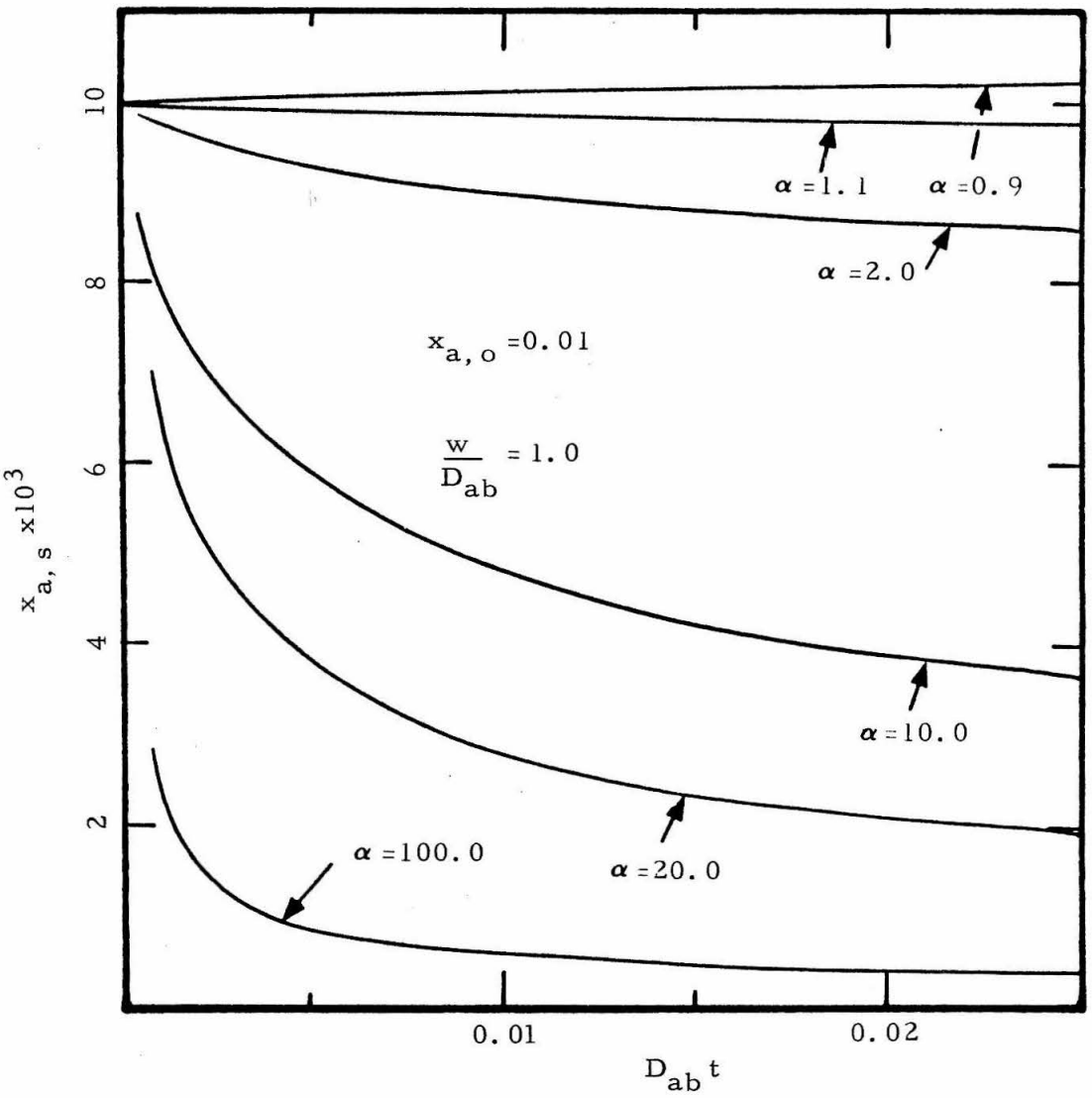

Figure 3. --Surface concentration versus diffusivity-time product.

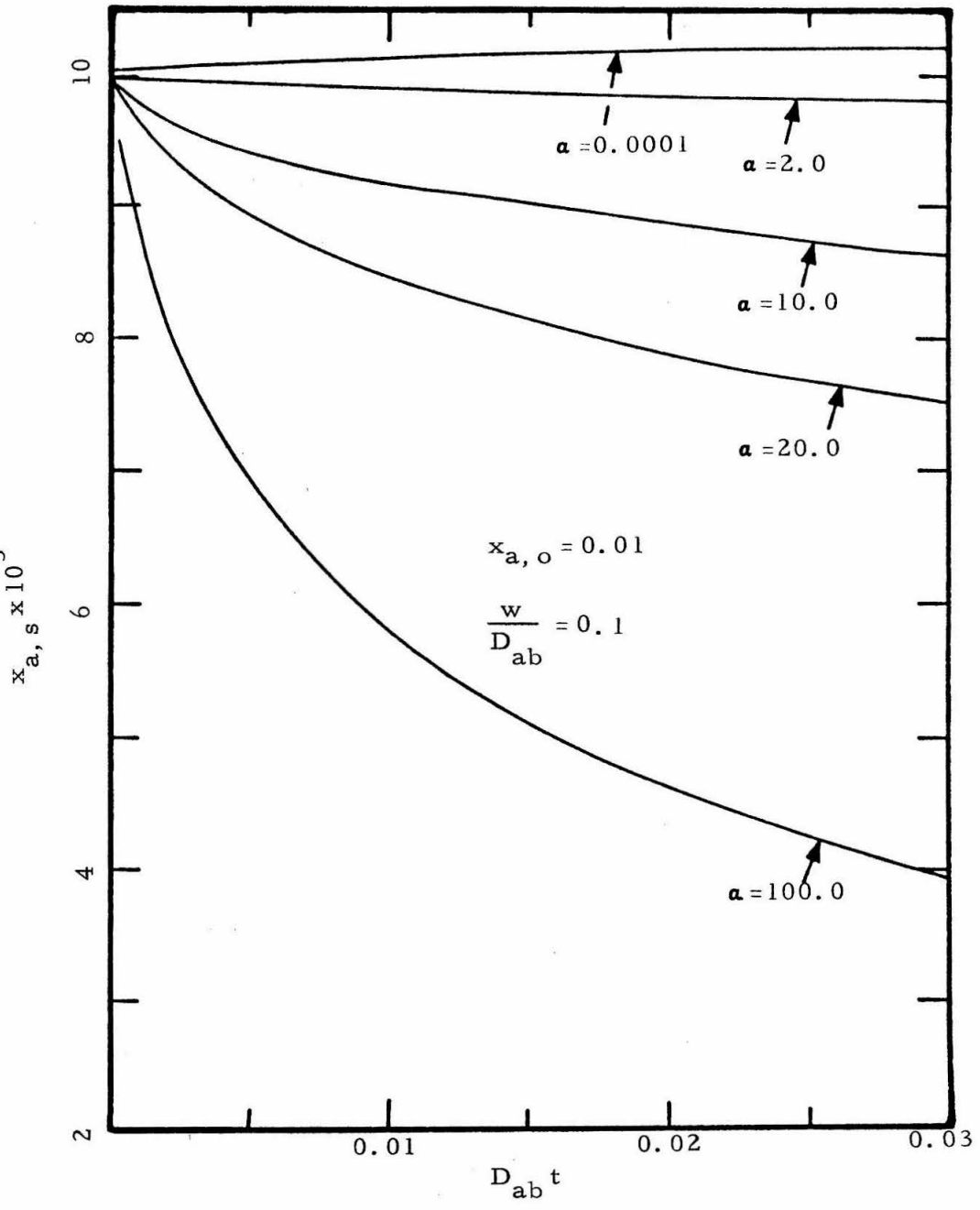

Figure 4. --Surface concentration versus diffusivity-time product.

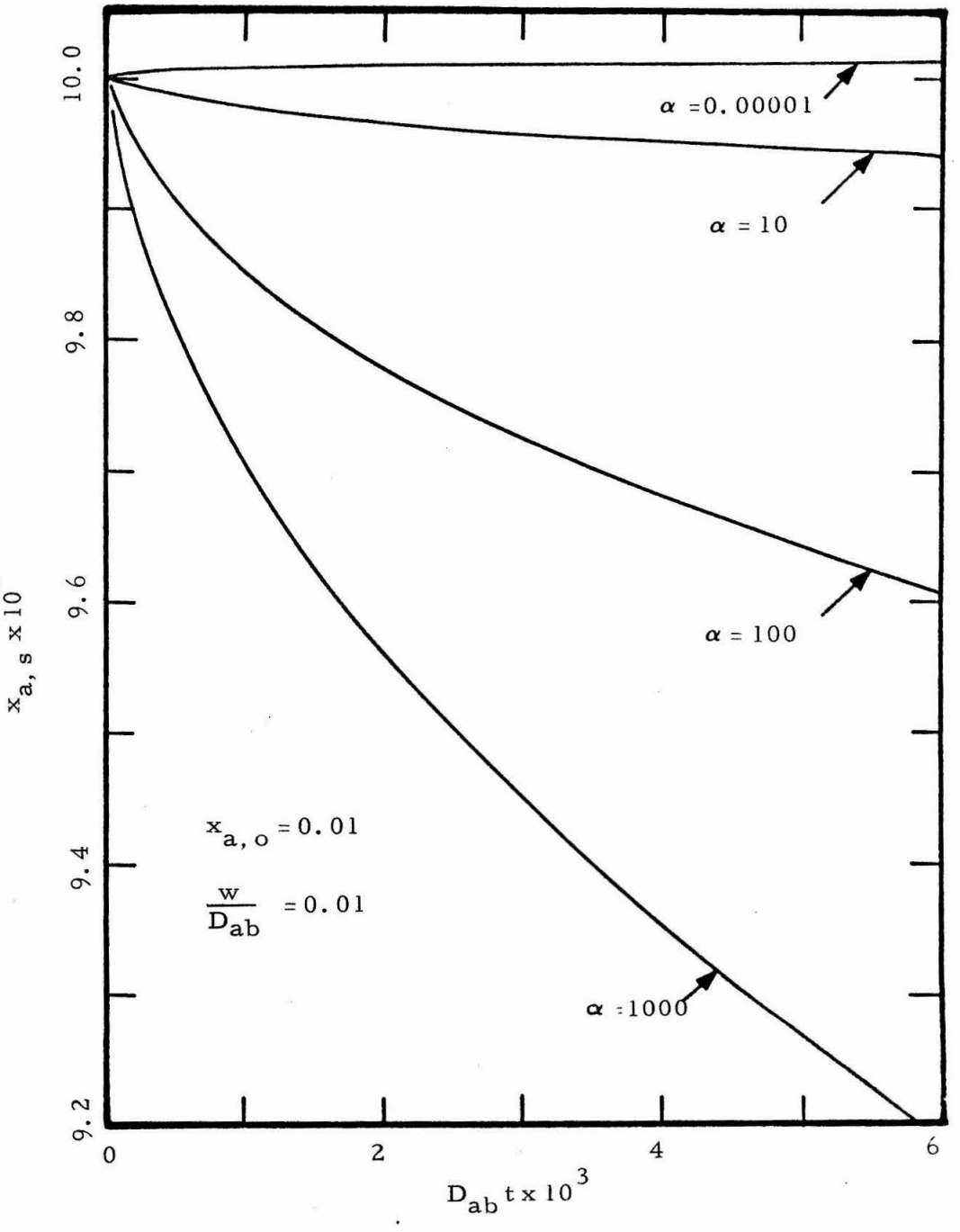

Figure 5. --Surface concentration versus diffusivity-time product.

TABLE 2

REPRESENTATIVE ERROR IN APPROXIMATE SOLUTION

$(\alpha_{ab} - 1)x_{a,o}$	$D_{ab}t$	$x_{a,s}$ (numerical results)	$x_{a,s}$ (approximate result)	% error
0.09	0.022	0.00879	0.00866	0.15
0.99	0.022	0.00442	0.00379	26.3
0.99	0.0012	0.00844	0.00645	23.6
$w/D_{ab} = 0.1$				
$x_a = 0.01$				

Conclusions

The relative volatility has been shown to be an important parameter needed to predict the behavior of evaporating binary mixtures. The problem of an evaporating binary mixture with constant physical properties and a stationary interface has been solved numerically for a gas composition which is at all times in equilibrium with the liquid at the interface. The results compare closely with those of an approximate solution for small values of $(\alpha_{ab} - 1)\, x_{a,o}$.

NOTATION

Symbols

D_{ab}	Fick's binary diffusivity
k	a constant
t	time
v	velocity
w	rate of evaporation
x_a	mole fraction of "a" in the liquid
$x_{a,o}$	initial concentration of "a" in the liquid
$x_{a,s}$	concentratiin of "a" at the interface in the liquid
y_a	mole fraction "a" in the gas at the interface
y_a'	constant concentration in the atmosphere remote from the interface
z	coordinate
α_{ab}	relative volatility
Δt	time increment
Δz	distance increment

LIST OF REFERENCES

1. Carslaw, H. S., Jaeger, J. C., Conduction of Heat in Solids, Clarendon Press, Oxford, 1959, p. 70.

2. Crank, J., The Mathematics of Diffusion, Clarendon Press, Oxford, 1956, pp. 34, 198.

3. Longwell, P. A., Sage, B. H., A. I. Ch. E. J., 11, 46 (1965).

PROPOSITION III

The current selling price of the common shares of a dual closed end mutual fund may be determined by an analysis of current stock market conditions, current rates of interest, the past performance of the fund, and the current net asset value of the fund's investments. An empirical correlation provides the relationship between the past rate of return, current rates of interest, and the required future rate of return.

A closed end mutual fund is a holding company which issues a specific number of shares to obtain capital which in turn is invested in other securities. The shares initially issued by the closed end mutual fund are then traded as the stock of any corporation would be. The current price of these shares does not necessarily equal the current value of the fund's investments, the net asset value. The percentage difference between the value of the fund's shares, P, and the value of the fund's assets, N, is the premium or discount, δ ,

$$\delta = \frac{N-P}{N} \times 100\% \qquad (1)$$

Profits from the fund's assets are either reinvested, or distributed to the holders of the fund's shares.

A dual fund is a closed end mutual fund which enjoys a leverage effect from the existence of preferred shares in addition to the usual common shares. The price of the preferred shares is governed by prevailing interest rates because the preferred shares pay a fixed dividend. However, the current price of the common shares depends on several other factors including the current value of all investments owned by the fund, the current position of the stock market, the expected performance of the fund, the date at which the fund will be dissolved, and the leverage introduced by the preferred shares.

There are seven dual funds presently in existence; all were begun in the spring of 1967 (2). Since then, the common shares of these dual funds usually have been selling at a discount, which has discouraged the creation of more dual funds.

Analysis

Short term stock market effects should be discounted, because the performance of the dual funds depends on the capital appreciation over a long period of time. Market effects may be discounted by multiplying the current total assets of the fund; the sum of the face value of the preferred shares, n, and the common net asset value, N, by the factor

$$\eta = \frac{1}{t_2 - t_1} \int_{t_1}^{t_2} \zeta \, dt / \zeta \qquad (2)$$

where ζ is a measure of the current value of the stock market (Standard and Poor's 500 Stock Average) and $t_2 - t_1$ is an intermediate time interval (2 years). Capital appreciation is based on the total asset value multiplied by the normalizing factor, η

$$\eta (N + n)$$

Since the asset value of the preferred is fixed, the total asset value

introduces leverage into the probable appreciation of the common net asset value. The past rate of return is related to the initial total assets and the current total assets by the following compound interest formula:

$$\left[\eta(N+n) + n\rho(t-t_o)\right] = \left[\eta(N+n)\right]_o (1+R)^{t-t_o} \qquad (3)$$

where R is the past rate of return, $t-t_o$ is the time interval since the fund was introduced, and ρ is the annual rate of interest paid on the preferred shares. It was assumed that no dividends were paid on the common shares. The term

$$n\rho(t-t_o) \ll \eta(N+n) \qquad (4)$$

and represents the total interest paid to date on the preferred shares of the fund. By simplifying Equation (3),

$$R = \left\{\frac{\eta(N+n) + n\rho(t-t_o)}{\left[\eta(N+n)\right]_o}\right\}^{\frac{1}{t-t_o}} - 1 \qquad (5)$$

At some future time, t^*, the fund will be liquidated. The net asset value of the common shares at that time, N^*, will be determined by the appreciation of the assets of both the preferred and common shares. The determination of the appreciation on the assets

of the preferred shares is discussed in the Appendix. If it is assumed that the past rate of return equals the future rate of return, then

$$\text{Appreciation of common assets} = N(1+R)^{t^*-t}$$

$$\text{Appreciation of preferred assets} = n\left\{(1+R)^{t^*-t} - \rho\left[\frac{(1+R)^{t^*-t}-1}{R}\right]\right\}$$

$$N^* = (N+n)(1+R)^{t^*-t} - n\rho\left[\frac{(1+R)^{t^*-t}-1}{R}\right] - n \qquad (6)$$

If the current market price of the dual fund is governed by the estimated value at time, t^*, and the prevailing interest rates for a security with a risk equivalent to that of the fund being considered, r', compounded annualy, then the current price of the common shares, P, is determined by

$$N^* = P(1+r')^{t^*-t} \qquad (7)$$

By combining Equations (6) and (7),

$$P = (n+N)\left(\frac{1+R}{1+r'}\right)^{t^*-t} - \frac{\frac{n}{R}\left[(1+R)^{t^*-t}-1\right] - n}{(1+r')^{t^*-t}} \qquad (8)$$

If the prevailing interest rate for a given group of securities with a common risk is "r", then the interest rate, r', for the dual fund

being considered will be proportional to this interest rate or

$$r' = kr \tag{9}$$

For example, if "r" is determined for a corporate bond rated Baa and a mutual fund is believed to have more risk than a corporate bond rated Baa, then "k" will be greater than unity. The value of "k" can be expected to be related to the past performance of the fund.

The current discount is related to the factor "k", the current interest rate, r, and the other parameters by

$$\delta = \left\{ 1 - \frac{(N+n)}{N} \left(\frac{1+R}{1+kr} \right)^{t^*-t} + \frac{n}{N} \left\{ \frac{\frac{\rho}{R}\left[(1+R)^{t^*-t} - 1\right] - 1}{(1+kr)^{t^*-t}} \right\} \right\} \times 100\% \tag{10}$$

Comparison with Data

A group of five dual purpose funds was chosen for study. The call dates of the funds, the initial asset value of common and preferred shares, and the yield of the preferred shares are presented in Table 1 (2). These funds were examined at five separate dates beginning one year after the initiation of the funds and continuing until two years after the initiation of the funds. The dates and the prevailing interest rates for Moody's Baa corporate bonds on these

TABLE 1

INITIAL DATA ON DUAL FUNDS (2)

Fund	Call Date	Initial N. A.	Preferred Yield
American Dual Vest	6/29/79	$13.80	5.6%
Gemini	12/31/84	11.00	4.7%
Income and Capital Shares	3/31/82	9.15	5.0%
Leverage Fund of Boston	1/4/82	13.73	5.0%
Scudder Duo - Vest	4/1/82	9.15	6.4%

dates are given in Table 2 (1). The values of ζ and η as defined in Equation (2), also are given for each date. The Standard and Poor's 500 Stock Average is used for ζ. The time interval used to determine η is two years (1). The market price of the common shares of each of the five funds as well as their net asset value and their premium have been found for each date (3), (4), (5), (6), and (7). These are presented in Table 3.

To calculate the premium from the preceeding data, one must know the prevailing interest rates, r', for each of the securities. Thus, one must know the value of "k" where

$$r' = kr \tag{9}$$

and "r" is the Moody's Baa bond interest rate.

Thus, Equation (10) may be solved for "k"

$$k = \frac{1}{r}\left\{-1+\left[\frac{1}{1-\frac{\delta}{100}}\left(\frac{N+n}{N}(1+R)^{t^*-t} - \frac{n}{N}\left[\frac{\rho}{R}\left((1+R)^{t^*-t}-1\right)-1\right]\right)\right]^{\frac{1}{t^*-t}}\right\} \tag{11}$$

The past rates of return and the values of "k" have been found for each date from Equations (5) and (11) and are presented in Table 4. The past rate of return has been plotted versus the risk factor in Figure 1, which shows there is a good correlation between the two. This correlation may be expressed as

TABLE 2

DATA ON STOCK MARKET AND INTEREST RATES (1)

Date	Time (years)	Interest Rate, r (Moody's Baa Bond) (%)	ζ	η
3/22/67	0.00	- - -	90	85.2
3/22/68	1.00	6.90	89	88.6
6/21/68	1.25	7.05	100	90.3
9/20/68	1.50	6.80	103	89.5
12/20/68	1.75	7.25	106	93.3
3/21/69	2.00	7.63	100	96.0

TABLE 3

PRICE DATA FOR DUAL FUNDS (3), (4), (5), (6), (7)

Fund	Date	Price	N. A.	Premium (%)
American	3/22/68	$10.25	$12.67	-19.1
Dual Vest	6/21/68	13.875	18.19	-23.7
	9/20/68	15.875	19.73	-19.5
	12/20/68	19.5	22.98	-15.1
	3/21/69	14.5	16.34	-11.3
Gemini	3/22/68	11.375	12.21	- 6.8
	6/21/68	13.0	16.92	-23.2
	9/20/68	15.875	17.75	-10.5
	12/20/68	17.625	19.61	-10.2
	3/21/69	15.50	18.03	-14.0
Income and	3/22/68	9.25	10.65	-13.1
Capital	6/21/68	11.375	14.66	-22.4
	9/20/68	14.5	15.98	- 9.3
	12/20/68	17.125	18.87	- 9.2
	3/21/69	14.5	16.23	-10.7
Leverage Fund	3/22/68	10.0	11.99	-16.6
	6/21/68	10.75	14.57	-26.2
	9/20/68	11.125	15.21	-26.8
	12/20/68	13.0	16.66	-22.0
	3/21/69	11.75	14.99	-21.6
Scudder	3/22/68	7.25	7.88	- 8.0
Duo-Vest	6/21/68	8.375	10.93	-23.4
	9/20/68	8.75	10.56	-17.1
	12/20/68	8.625	11.41	-24.4
	3/21/69	7.75	9.42	-17.7

TABLE 4

CALCULATED PARAMETERS - DUAL FUNDS

Fund	Date	Past Return (R) (%)	k
American Dual Vest	3/22/68	3.99	1.25
	6/21/68	11.6	1.99
	9/20/68	10.5	1,89
	12/20/68	16.3	2.55
	3/21/69	7.03	1.37
Gemini	3/22/68	13.6	2.39
	6/21/68	19.3	2.92
	9/20/68	15.4	2.52
	12/20/68	18.7	2.80
	3/21/69	16.7	2.39
Income and Capital	3/22/68	16.7	2.85
	6/21/68	21.7	3.31
	9/20/68	19.3	3.15
	12/20/68	25.3	3.75
	3/21/69	19.7	2.83
Leverage Fund	3/22/68	1.36	0.83
	6/21/68	1.60	0.65
	9/20/68	0.59	0.52
	12/20/68	4.78	0.98
	3/21/69	4.56	0.93
Scudder Duo-Vest	3/22/68	1.47	0.80
	6/21/68	7.39	1.30
	9/20/68	2.73	0.74
	12/20/68	6.35	1.08
	3/21/69	3.78	0.80

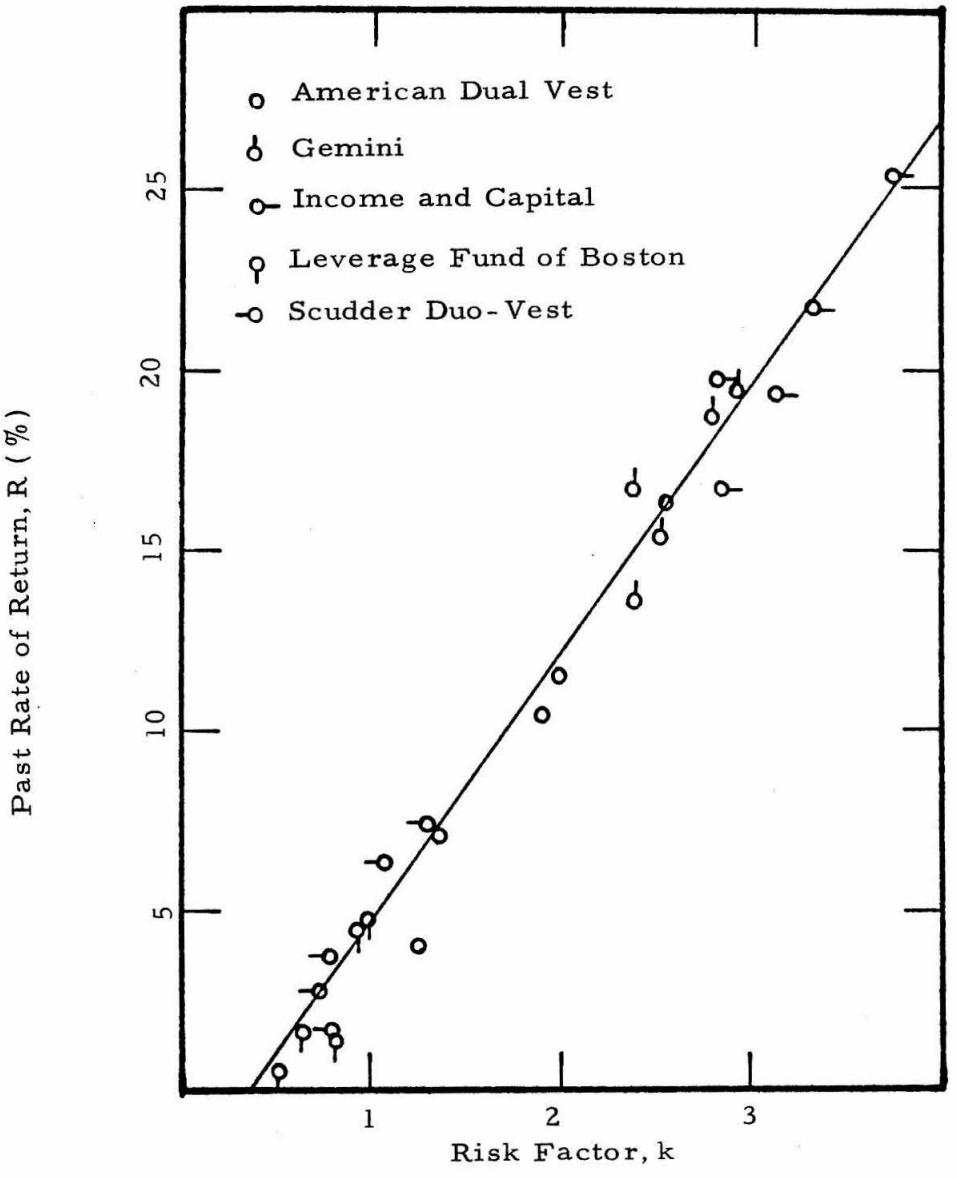

Figure 1. --Correlation between past rate of return and anticipated future rate of return.

$$k = \left(\frac{13.3\ R}{100\%} + 0.43 \right) \qquad (12)$$

Conclusions

The market value of a dual purpose mutual fund may be determined from its past performance, prevailing interest rates, and net asset value. Its past rate of return may be determined from Equation (5). The interest rate to be expected in the future may be determined from Equations (9) and (12). The current price then may be found from Equation (8).

The effects of supply and demand on a commodity in a free market have been reduced to simple mathematical relationships by a correlation between the past rate of return and the expected rate of return.

NOTATION

Symbols

k	risk factor
n	net asset value of preferred shares
N	net asset value of common shares
P	market value
r	prevailing interest rate
r'	expected return on common shares
R	past rate of return
t	time
δ	premium
ζ	Standard and Poor's 500 Stock Average
η	factor to remove effect of stock market
ρ	rate of interest on preferred shares

Subscripts

o	initial

Superscripts

*	call date

LIST OF REFERENCES

1. Federal Reserve Monthly Chart Book, Financial and Business Statistics , (May, 1969), Washington, D. C. : Board of Governors Federal Reserve System, 28, 30.

2. Forbes, (March 15, 1968), 87.

3. Wall Street Journal, Pacific Coast Edition, Volume 78, No. 59. (March 25, 1968), 14.

4. Wall Street Journal, Pacific Coast Edition, Volume 78, No.123. (June 24, 1968), 20.

5. Wall Street Journal, Eastern Edition, Volume 177, No. 59. (September 23, 1968), 33.

6. Wall Street Journal, Eastern Edition, Volume 177, No. 123. (December 23, 1968), 19.

7. Wall Street Journal, Eastern Edition, Volume 178, No. 58. (March 24, 1969), 37.

APPENDIX

The interest on the preferred shares, ρ , and the rate of return, R, on the invested preferred capital effect the preferred assets as follows:

Time	Preferred Assets
Initial	n
1 Year	$n \quad (1 + R - \rho)$
2 Years	$n \left[(1 + R - \rho)(1 + R) - \rho \right]$
3 Years	$n \left\{ \left[(1 + R - \rho)(1 + R) - \rho \right] (1 + R) - \rho \right\}$
...	...

The above may be expressed as

$$\text{Preferred Assets} = n \left[(1 + R)^t - \rho \sum_{1}^{t} (1 + R)^{t-1} \right]$$

or

$$\text{Preferred Assets} = n \left\{ (1 + R)^t - \rho \left[\frac{(1 + R)^t - 1}{R} \right] \right\}$$